Morphological control of self-organized body on supergiant polysaccharides

Kulisara BUDPUD

Japan Advanced Institute of Science and Technology

Doctoral Dissertation

Morphological control of self-organized body on supergiant polysaccharides

Kulisara BUDPUD

Supervisor: Professor Tatsuo Kaneko

Graduate School of Advanced Science and Technology
Japan Advanced Institute of Science and Technology
Materials Science

September 2021

Referee-in-chief: Professor Dr. Tatsuo Kaneko

Japan Advanced Institute of Science and Technology

Referees: Professor Dr. Yoshifumi Oshima

Japan Advanced Institute of Science and Technology

Professor Dr. Kazuaki Matsumura

Japan Advanced Institute of Science and Technology

Associate Professor Dr. Kosuke Okeyoshi

Japan Advanced Institute of Science and Technology

External referee: Associate Professor Dr. Tetsu Mitsumata

Niigata University

Abstract

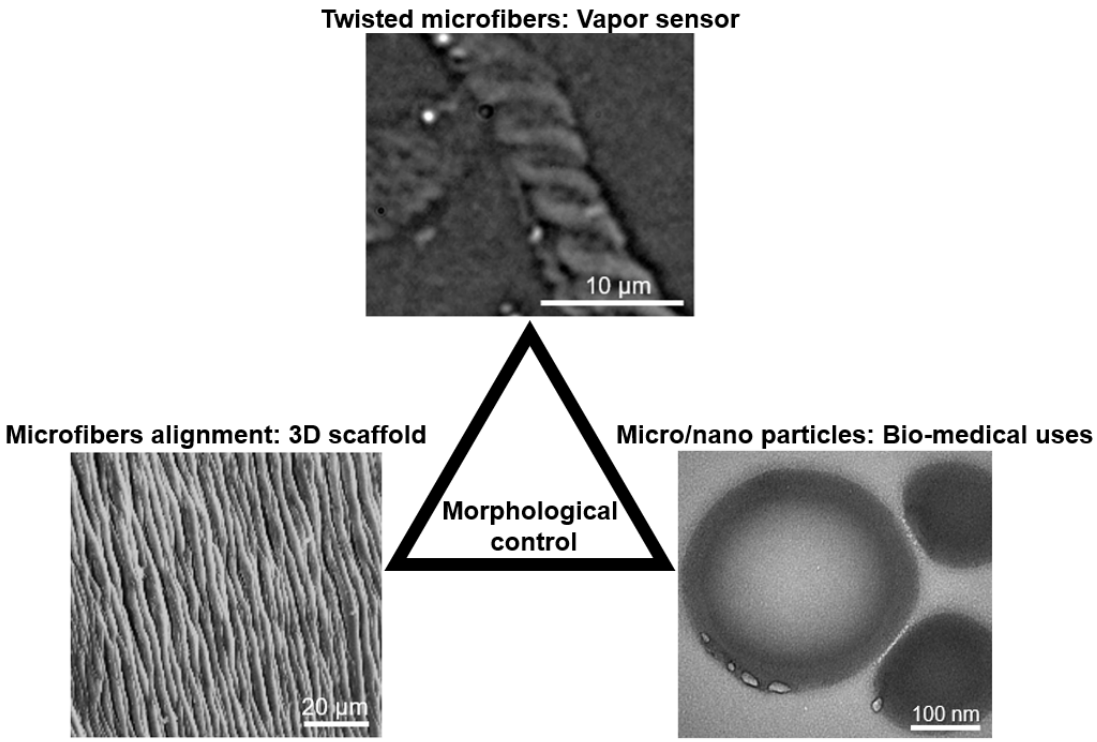

Graphical abstract

In materials design, the relationship between polymer morphology and physical properties is crucial. The researchers are attempting to utilize alternative materials such as natural biopolymers to limit the consumption of non-renewable resources produced by synthetic materials. Because of their biocompatibility, non-toxicity, and some specialized therapeutic properties, polysaccharides, particularly bioactive ones, have attracted attention in recent decades for a variety of novel applications. The biological activities of polysaccharides are strongly affected by their chemical structure and chain conformations. Due to the obvious difficulty in regulating self-assembled structures, morphological regulation of polysaccharides from the nano to micrometer scale has rarely been used in vitro. Herein, it is demonstrated that a cyanobacterial polysaccharide, *sacran*, could hierarchically self-assemble as twisted fibers

from the nanoscale to microscale with diameters of ~1 μm and lengths >800 μm, that are remarkably larger than polysaccharides previously reported. Unlike other rigid fibrillar polysaccharides, the *sacran* fiber was capable of flexibly transforming into two-dimensional (2D) snaking and three-dimensional (3D) twisted structures at an evaporative air-water interface. Moreover, the deformation process of *sacran* microfiber to nano-micro particles was also clarified in vice versa. The interaction between polymer chains is an essential component in studying *sacran* morphological change. The dilution and the salination weakened the intermolecular interaction, leading the microfibers to deform into tiny fragments. Those processes, on the other hand, produced a limited number of particles, which is a problem in terms of production. Therefore, the ultrasonication approach could be able to solve this problem. The polysaccharide chains are cut as a result of the cavitation effect from ultrasonic treatment. The shock wave may cause *sacran* microfibers to change to a *sacran* spherical shape from micro to nanometer scale.

In this research, the morphological changes of *sacran*, a novel self-organized supergiant polysaccharide has been investigated. This clarification leading not only to understand the fundamental of anionic polysaccharide self-assembling/disassembling but also developing in a new material such as humidity-sensitive actuator, a micropattern cell scaffold, and a super-moisturizing microparticle.

Keywords: Polysaccharides, self-assembly, fibers, particles, drying.

Acknowledgements

First and foremost, I want to convey my gratitude to Professor Tatsuo Kaneko and Dr. Maiko Okajima my respected advisors, for their kind support at both for their professional and personal encouragement during my PhD study at JAIST.

I also want to express my appreciation to the committee members: my advisor for minor research *Professor Kazuaki Matsumura*, *Associate Professor Kosuke Okeyoshi* for well-supervised since my master course, *Professor Yoshifumi Oshima* at JAIST and *Associate Professor Tetsu Mitsumata* from Niigata University, for their time and valuable advice during the defense.

I am very grateful to my second supervisor *Associate Professor Toshiaki Taniike* and *Assistant Professor Kenji Takada* for their suggestions and kind support throughout my research in JAIST. My sincere thanks also extend to all Kaneko lab colleagues who have assisted and encouraged me over the past three years.

I would like to acknowledge Mr. Nobuaki Ito and Ms. Shoko Kobayashi (JAIST, Center for Nano Materials and Technology) for their helpful discussion on the SEM and TEM observations.

I would like to give thanks to all of my Thai friends with whom I have experienced a tough moment and spent priceless time. I would not be much as pleasurable without them.

Importantly, I would like to thank you from the bottom of my heart to my parents and my family for their care and encouragement. Thank you for always being by my side.

September 2021

Kulisara Budpud

Contents

Pages

Abstract I

Acknowledgements III

CHAPTER I GENERAL INFORMATION 1

1.1 Polyion/polyelectrolyte self-assembly 1

1.2 Polysaccharides 5

1.3 Sacran supergiant polysaccharide 10

1.4 General Purpose 14

1.5 References 15

CHAPTER II POLYSACCHARIDE FIBERS 19

WITH SELF-ASSEMBLING TWISTED MICROSTRUCTURES 19

2.1 Introduction 20

2.2 Materials and methods 23

2.3 Results and discussion 24

2.3.1 Application section I 37

2.3.2 Application section II 43

2.4 Conclusion 47

2.5 References 48

CHAPTER III SUPER-MOISTURIZING MATERIALS FROM MORPHOLOGICAL TRANSFORMABLE SUPERGIANT POLYSACCHARIDE 51

3.1 Introduction 52

3.2 Materials and Methods 55

3.3 Results and discussion 58

3.3.1 Dilution/concentration effect 58

3.3.2 Salination/desalination effect 63

3.3.3 Sonication effect 71
3.4 Conclusion 82
3.5 References 84
CHAPTER IV GENERAL CONCLUSION 87
LIST OF PUBLICATIONS 89

CHAPTER I

GENERAL INFORMATION

1.1 Polyion/polyelectrolyte self-assembly

Macromolecules carrying multiple charges (polyion or polyelectrolyte) are ubiquitous in nature and include nucleic acids, proteins, or polysaccharides.[1] The physical features of these biopolymers, such as self-assembly and solubility in a physiological environment, are frequently dictated by the presence of these charges. More crucially, charge-charge interactions frequently mediate essential biological processes, ranging from the packaging of DNA around histones[2] to microbe adherence to surfaces and hosts.[3] To explain the mechanism of polyion complex formation, ideas based on electrostatic forces and Flory-Huggins mixing free energies of polyelectrolytes have been presented.[4][5][6] The backbones of the two polymers are generally incompatible and repel each other; however, the charge fraction of the polymers affects the type of interaction. When the charge fraction is low, the polymer backbone repulsion (Flory interaction parameter) is prioritized, and the solution splits into two phases, each containing mostly one of the polymers. The favorable electrostatic interactions between the polymers dominate at high charge fractions, and they precipitate to form a complex. The equilibrium state in an intermediate range of charge fraction can be a meso phase, in which the two polymers only separate microscopically. Depending on the stoichiometry of the mixture (relative concentrations, chain lengths, and charge densities), one can see either a macroscopic phase separation between the solvent and the polymers or a partial aggregation of the polymer chains.[7] It is no surprise that scientists have attempted to mimic these fundamental polyionic interactions in order to create synthetic systems that can interact with biology. Various works about polyionic complex have been investigated as novel platforms to stabilize and deliver

drugs,[8][9] proteins,[10][11] or nucleic acids.[12][13][14] Based on electrochemistry, they are classified as polyacids/polyanions, polybases/polycations and polyampholytes. Some of the important polyelectrolytes are exemplified in **Table 1.1.**

Table 1.1 Some of the important polyelectrolytes[15]

Name	Category (based on the charge type)
Natural Polyelectrolytes	
Nucleic acids	Polyanion
Poly (L-lysine)	Polycation
Poly (L-glutamic acid)	Polyanion
Carrageenan	Polyanion
Alginates	Polyanion
Hyaluronic acid	Polyanion
Chemically modified biopolymers	
Pectin	Polyanion
Chitosan (deacetylation of chitin)	Polycation
Cellulose - based	Polyanion or polycation
Starch - based	Polyanion or polycation
Dextran - based	Polyanion or polycation
Synthetic polyelectrolytes	
Poly (vinylbenzyl trialkyl ammonium)	Polycation
Poly (4-vinyl-N-alkyl-pyridimiun)	Polycation
Chemically modified biopolymers	
Pectin	Polyanion
Chitosan (deacetylation of chitin)	Polycation
Cellulose - based	Polyanion or polycation
Starch - based	Polyanion or polycation
Dextran - based	Polyanion or polycation

As shown in **Figure 1.1**, The formation process involved mainly three steps. The first step is primary complex formation, which is controlled by Coulomb forces. The formation process within intracomplexes is the second step. It includes the construction of new bonds and/or the correcting of polymer chain distortions. The third step is intercomplex aggregation, which includes secondary complexes aggregating mostly through hydrophobic interactions.[15]

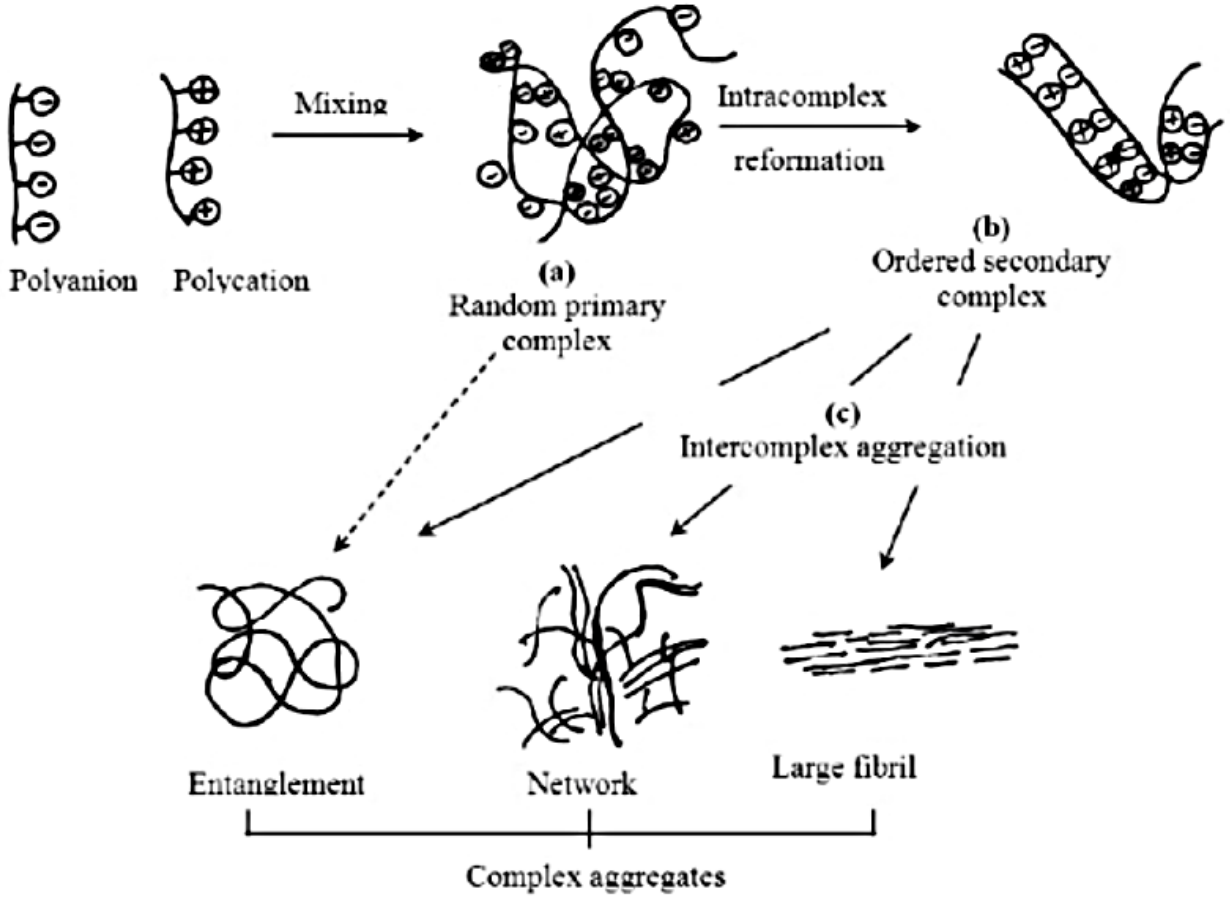

Figure 1.1 Schematic representation of the formation and aggregation of polyelectrolyte complex. a. Primary complex formation. b. Formation process within intracomplexes. c. Inter complex aggregation process.[15]

A number of parameters are known to influence the formation of polyelectrolyte complex.[16] These are ion site, charge density, polyelectrolyte concentration, pH, ionic strength, solvents and temperature. Therefore, many of the applications are based on the functional properties of the polyelectrolyte. The functional applications of polyelectrolyte complex are summarized in **Table 2.1**.[15]

Table1.2 Practical application of polyelectrolyte complexes.

Functional property	**Application**
Interaction with counter ions	Support of filtration process - removal of counter ions
	Gelation process - bridging with multivalent counter ion
	Analytical methods - counter ion exchange
Interaction with surfactants	Insoluble polyion surfactant complex for low energy surface modification
	Highly ordered structures (micelle) formation
Interaction with charged low molar mass molecules	Polyion drug complexes - soluble or insoluble
Interaction with charged particles	Floculation - waste water treatment
	Dewatering - sludge, pulp and paper production
	Flotation - mining
	Retention - paper production
Interaction with charged surfaces	Displacement chromatography - separation and concentration of biomolecules
	Modification of surfaces and interfaces - coating (antistatic, sensors, multi-layer)
	Additive (cosmetics, detergents)

Polyelectrolytes and polyelectrolyte complexes are the subjects of substantial investigation. They have a lot of potential in ecology, biotechnology, medicine, and pharmaceutical technology, which is an excellent option for designing novel material in various applications.

1.2 Polysaccharides

Polysaccharides consist of multiple monosaccharide or disaccharide units that are linked by glycosidic bonds. Their function in living organisms is both structure and storing energy in the body system. Many polysaccharide chains can assemble as ordered helical in secondary structures. A regular repeating sequence of sugar residues may terminate the secondary structure. Hence, the mechanism by which native polysaccharides may link up to form three-dimensional networks such as biological tissues and gel formation, which lead to adaptation in a variety of applications.[17] The concept of self-assembled polymers covers large polymerlike structures designed by reversible or nonreversible aggregation of monomers, oligomers, and polymer segments driven by chemical reactions or noncovalent interactions, such as hydrogen (H) bonding, π–π stacking, van der Waals forces, and hydrophobic and host-guest interactions.[18][19] In general, self-assembled polysaccharide systems are stable, meaning they have a low Gibbs free energy and thus a thermodynamic state that is closer to equilibrium. As a result, self-assembled polysaccharides on the macromolecular surface prefer to release energy or reduce overall energies.[20] Due to its adaptability in terms of morphological variations, hierarchical features, number of utilized, and stabilizing effects, polysaccharide self-assembly has been manipulated marvelously for a great number of applications in recent decades, as shown in **Figure 1.2a-d**.[21]-[25] Apart from self-assembling ability, polysaccharides provide many benefits from their bioactive functional group, which is summarized in **Table1.4**.[27] Polysaccharides, on the other hand, can have a wide range of molecular weights and their chemistry can be quite variable. As a result, predicting or limiting the possible use in drug administration is difficult.[26] The alternative material or technique is still required to be developed for more advanced material design.

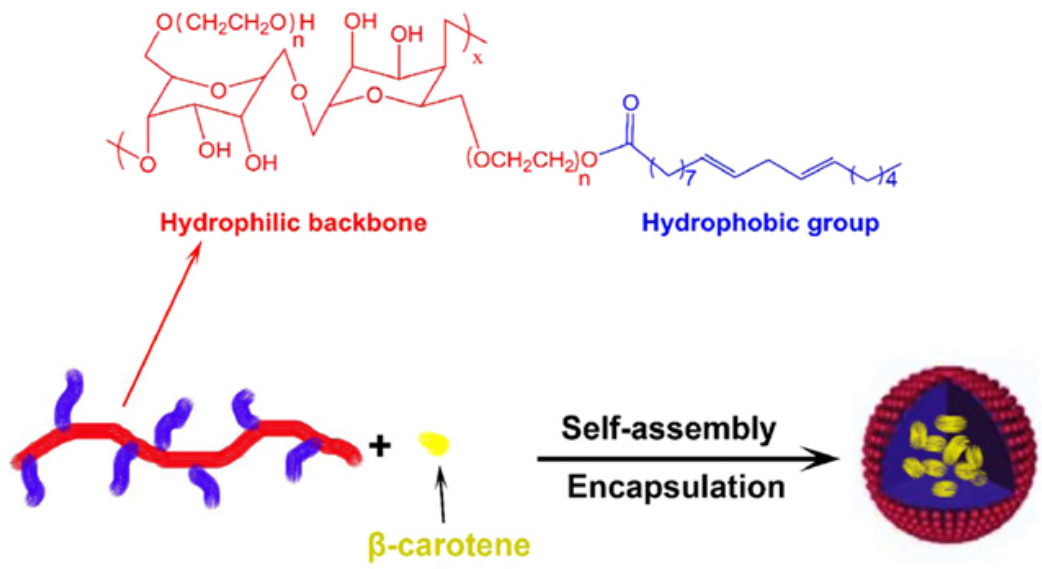

Figure 1.2 a. Schematic illustration for self-assembly of hydroxyethyl cellulose-linoleic acid copolymer into nanomicellar structures.[21]

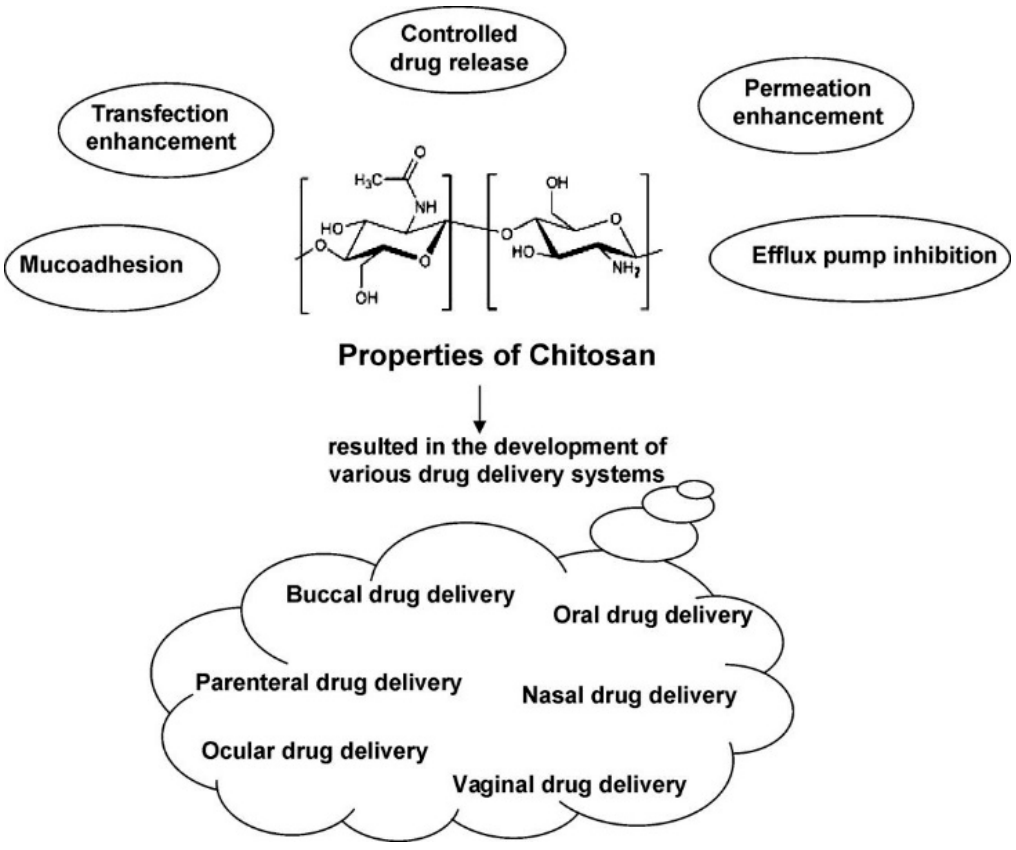

Figure 1.2 b. Potential use of Chitosan in drug delivery applications.[22]

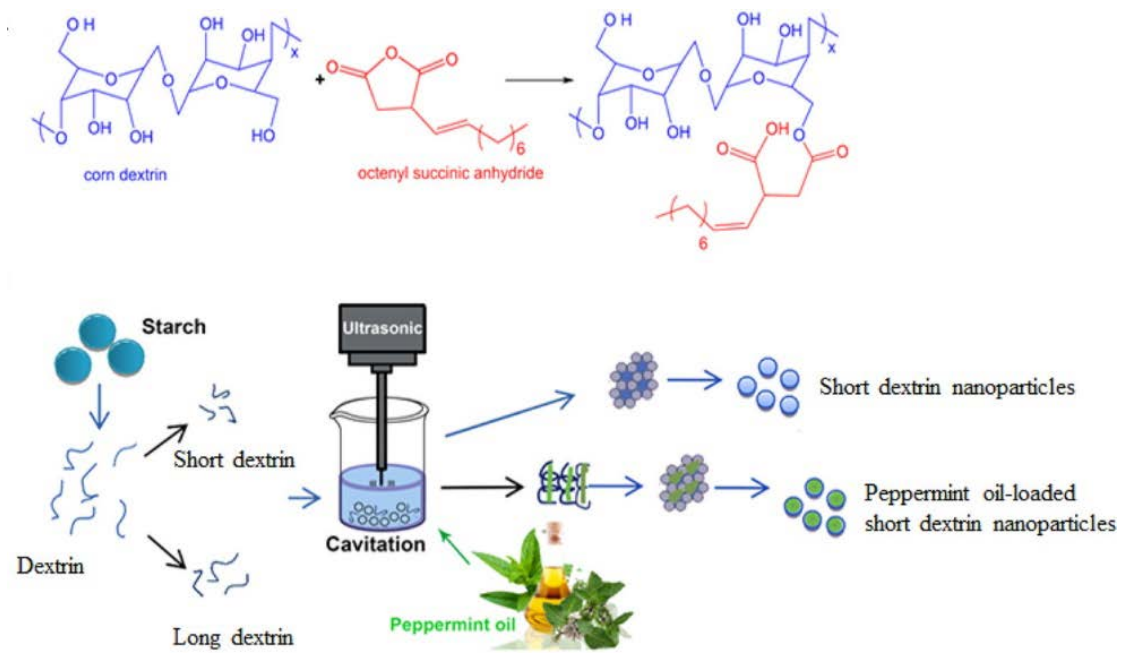

Figure 1.2 c. The construction of short dextrin nanoparticles and peppermint oil-loaded.[23]

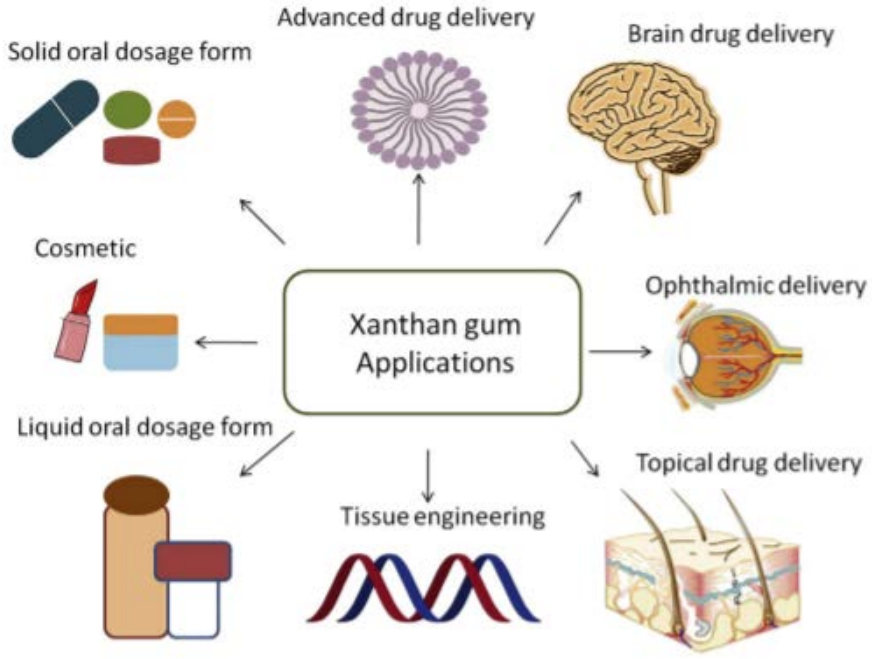

Figure 1.2 d. Potential role of xanthan gum in healthcare systems.[24][25]

Table1.4 A brief summary of bioactive polysaccharides from different sources.[27]

Type	Name	Composition	Sources	Physiological effects
Dietary fiber	Cellulose	β-(1→4) linked-D-glucopyranose, linear and homopolysaccharides	Grains, fruit, vegetables, nuts	Increase stool bulk and help to regulate bowel movement
	Hemicelluloses	Four classes of structurally different cell-wall polysaccharides including xylans, mannans, β-glucans with mixed linkages and xyloglucans	Vegetative and storage tissues of annual and perennial plants, fruit, legumes, and nuts	Immunomodulating activity, antithrombotic activity, free radicals eliminating activity, antioxidant activity, bowel movements regulating and cholesterol lowering effect
	Pectins	α-(1→4)-D-Galacturonic acid and rhamnose backbone, arabinose, galactose, xylose side chains, partially O-methyl/acetylated	Plant primary cell wall, soft tissues of fruit and vegetable	Intestinal immune system modulating activity, cholesterol lowering effect, decrease gastric emptying and small intestine transit time
	β-Glucans	β-(1→4)-D-Glucose and β-(1→3)-D-glucose	Oats, barley grains	Cholesterol lowering effect, control of blood glucose level and lipids; reduction of hypertension, stimulation of immune system
	Resistant starch	α-(1→4) and/or (1→6) linked D-glucopyranosyl	Cooked and cooled potatoes, rice, green bananas, legumes, food containing modified starch	Prevention of colonic cancer, hypoglycemic and hypocholesterolemic effects, role as prebiotic, inhibition of fat accumulation, enhance the absorption of minerals
	Gums	Galactan, xylan, xyloglucan, glucuronic mannan, galacturonic rhamnosan type	Locust bean gum, gum arabic, and guar gum which are exudates of trees or isolated from seeds	Hypocholesterolemic and hypotriglyceridemic effects, influence on postprandial glycemia, lipemia, and lipoprotein composition, gel-forming to increase satiety, slow gastric emptying

Table1.4 (continue) A summary of bioactive polysaccharides from different sources.[27]

Type	Name	Composition	Sources	Physiological effects
Algae and lichens	Green algae sulfated polysaccharides	(1→3(6))-Linked galactose, (1→3(4))-linked arabinose, (1→4)-linked glucose and terminal, (1→4)-linked xylose residues. Sulfations occur on O_6 of galactose and O_3 of arabinose. Sulfate ester content: 9%	Green algae, *Caulerpa racemosa*	Antiviral activity (herpes simplex virus type 1 and 2)
	Brown algae sulfated polysaccharides	Fucan: (1→3)-linked α-L-fucopyranosyl backbone, mostly sulfated at C_4, and branched at C_2 with non-sulfated fucofuranosyl and fucopyranosyl units, and 2-sulfated fucopyranosyl units. Galactan: D-galactopyranose units linked on C_3 and C_6, and sulfation mostly on C_4. Sulfate ester content: 30–34%/21–24%	Brown algae, *Adenocystis utricularis*	Antiviral activity (herpes simplex virus type 1 and 2), Antiretroviral activity (HIV-1)
	Red algae sulfated polysaccharides (porphyran)	Backbone of alternating β-(1→3)-linked D-galactosyl units and α-(1→4)-linked L-galactosyl, (1→6)-sulfate or 3,6-anhydro-α-L-galactosyl units. Sulfate ester content: 17%	Red algae, *Porphyra haitanensis*	Antioxidant activities, anticoagulant activities
	Green algae sulfated rhamnan	(1→2)-Linked L-rhamnose residues with sulfate groups substituted at positions of C_3 and/or C_4. Sulfate ester content: 23%/25%	Green algae, *Monostroma latissimum*	Anticoagulant activity
	Algal fucoidan	Fucose, galactose. Sulfations occur on position-2 and -3. Sulfate ester content: 41–92%	Brown algae, *Ecklonia cava*	Anti-inflammatory activity
	Brown algae sulfated polysaccharides	Mainly composed of fucose (82%), galactose (14%), and small amounts of xylose and mannose Sulfate ester content: 92%	Brown algae, *Ecklonia cava*	Antiproliferative activity, anticancer activity
		Galactofuranomannans, β-glucan lichenan		
		Galactofuranomannans, β-glucan	Lichen *Thamnolia vermicularis var. subuliformis*	Immunomodulating activity

1.3 Sacran supergiant polysaccharide

Cyanobacteria is one of the oldest and most important groups of bacteria on earth which live in the water and obtain their energy by photosynthesis. Cyanobacteria have been essential in evolution and ecological change all over the earth. One of the most beneficial of cyanobacteria is they are the origin of eukaryotic mitochondrion throughout the endosymbiosis process. Moreover, many cyanobacteria can produce mucus polysaccharide, which is released into the medium of cell. These released polysaccharides (RPSs) are created for the purposes of adhering to the surface, keeping moisturizer and protecting themselves from host's immune system.[28]-[30] RPSs consist of numerous number and types of monosaccharides. Cyanobacteria are an abundant source of diverted polysaccharides which are complex anionic heteropolymers.[31] Most of it contains non-saccharide components such as peptidic moieties, acetyl and sulfate group. Following those constituents, cyanobacterial RPSs could play important roles for instant thickening or suspending agents, emulsifying or cation chelating compounds and residual capsulated biomass. Owing to their advantages, cyanobacterial RPSs have attracted researcher's interest in various fields.

Aphanothece sacrum (Sur.) is one of cyanobacteria (**Figure 1.3, 1.4**) and produces jellylike matrix for their own cell colony which contains a plenty number of polysaccharides. They naturally grow in the spring river around the middle region of Kyushu island in Japan. Aphanothece sacrum is only 5-6 species out of 2500 species in the world that are edible. In addition, RPSs from the matrix have high water content and high-performance hydration behavior. So, Okajima M. et al.[28] has studied and successfully extracted cyanobacterial polysaccharide, which is called *sacran* from *Aphanothece sacrum.*

Figure 1.3 Picture of *Aphanothece sacrum* [32]

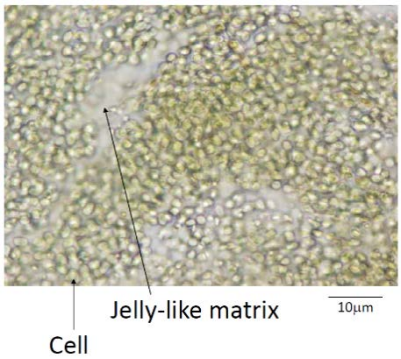

Figure 1.4 Optical micrograph of *Aphanothece sacrum* [32]

Sacran (**Figure 1.5, 1.6**) is one of the fascinating anionic polysaccharides (polyion) which was reported in various valuable properties, for example, metal adsorption,[33] anti-inflammatory [34] and transdermal drug carrier.[45] It shows incredibly high molecular weight over 10^7 g/mol, which is an enormous number compared with other extracted microorganism polysaccharides reported so far. The characterization of *sacran* structure was also studied by the same research group. The partial structure of *sacran* (**Figure 1.7**) composes of more than ten sugar residues such as hexoses, pentoses, deoxyhexoses, uronic acid, sulfated muramic acid, etc. From previous research, *sacran* is plant-derived functional materials and shows self-orientation, which could have formed a bundle with twisted morphologies in 3 μm in length, as shown in **Figure 1.8**.

Figure 1.5 Polysaccharides extracted from *Aphanothece sacrum* in acetone [32]

Figure 1.6 Polysaccharides extracted from *Aphanothece sacrum* in dry state [32]

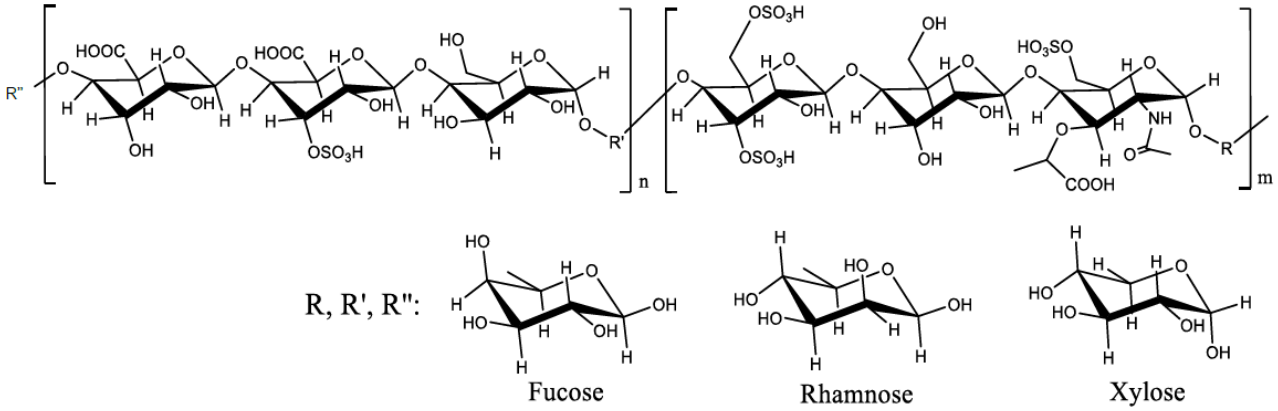

Figure 1.7 Partial structure of *sacran* [32]

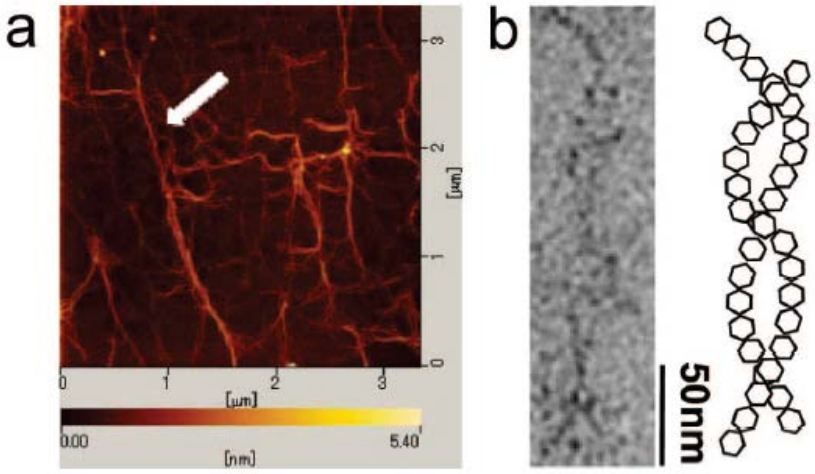

Figure 1.8 Microscopic images of *sacran* chains. a. Atomic force microscopic (AFM) images of *sacran* chains dried from very dilute solutions on mica substrates (arrow: a representative bundle of *sacran* chains). b. Transmission electron microscopic (TEM) images of specimens dried on a carbon-coated Cu grid. Illustration: the helical form of *sacran* chains speculated as to the basis of TEM images.[30]

Moreover, the study about ionic state and chain conformation of *sacran* aqueous solution was clarified (**Figure 1.9**). It can be concluded that *sacran* aqueous solution has overlap concentration (c^*) ≈ 0.004 wt% and entanglement concentration (c_e) ≈ 0.015 wt%.[36]

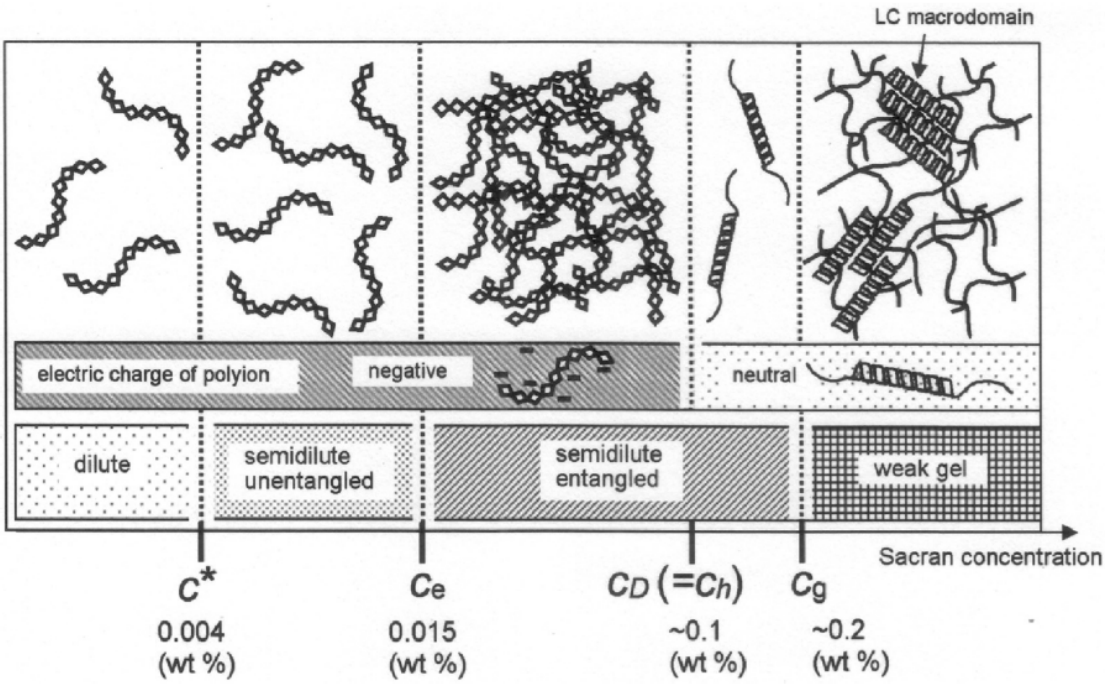

Figure 1.9 Schematic illustrations representing the chain conformation of *sacran* in salt-free solutions [(c^*) overlap concentration, (c_e) entanglement concentration, (c_D) critical polyelectrolyte solution, (c_h) helix transition concentration, (c_g) gelation concentration].[36]

From the previous researches, it can be said that *sacran* could self-assembled to form twisted structures from nanometer scale to micrometer scale under mild conditions and without any modification. In the range of concentrations between 0.02 and 0.09 wt%,[36] *sacran* chains have many opportunities to overlap each other but do not show associations. When the concentration is more than 0.09 wt%, *sacran* chains form double-helical and rigid structures. At 0.25 wt%, the aqueous *sacran* solution shows a sol-gel critical state phase because of an increase in chain entanglement and fractions. The nematic LC phase seems to form at ~0.5 wt%.[38]

Recently, a rigid rod-like microdomain from the drying record of *sacran* was observed by optical microscope (**Figure 1.10**).[37] The microdomains which could be observed presented rigid character, which is likely to relate with its twisting structure. This is a result of self-assembly in water, and they easily orient on a drying interface. Comparing with other polysaccharides such as cellulose or xanthan gum, the *sacran* microfiber has a remarkably large self-assembled structure. The microfiber also could easily disassemble into fiber bundles ~50 nm in diameter by adding NaCl, $CaCl_2$ and, HCl.[39]

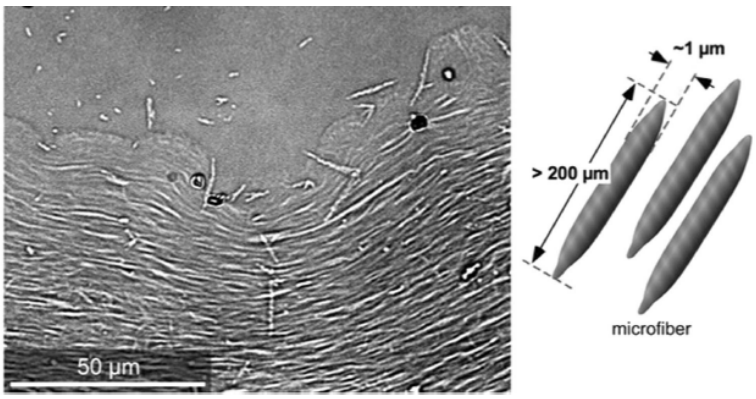

Figure 1.10 Optical microscopic images of *sacran* after drying the aqueous solution.[37]

1.4 General Purpose

Sacran has remarkable self-assembling/disassembling capabilities that allow it to generate morphologies of varied sizes. Additionally, the biological features of *sacran* may ignite our curiosity in learning more about it and developing it further. As a result, the morphological regulation of self-organized *sacran* will be defined in this study, and it will be utilized as new advanced material.

1.5 References

[1] I. Insua, A. Wilkinson, F. Fernandez-Trillo, *Eur. Polym. J.* **2016**, *81*, 198.

[2] K. Luger, A. W. Mäder, R. K. Richmond, D. F. Sargent, T. J. Richmond, *Nature* **1997**, *389*, 251.

[3] A. M. Krachler, K. Orth, *Virulence* **2013**, *4*, 284.

[4] G. Joshi, K. Okeyoshi, T. Mitsumata, T. Kaneko, *J. Colloid Interface Sci.* **2019**, *546*, 184.

[5] A. R. Paredez, C. Somerville, D. Ehrhardt, *Science (80-.).* **2006**, *312*, 1491.

[6] J. Mehringer, E. Hofmann, D. Touraud, S. Koltzenburg, M. Kellermeier, W. Kunz, *Phys. Chem. Chem. Phys.* **2021**, *23*, 1381.

[7] C. Hollitt, A. Deeb, *Determining Image Orientation Using the Hough and Fourier Transforms*, **2012**.

[8] V. Vergaro, F. Scarlino, C. Bellomo, R. Rinaldi, D. Vergara, M. Maffia, F. Baldassarre, G. Giannelli, X. Zhang, Y. M. Lvov, S. Leporatti, *Adv. Drug Deliv. Rev.* **2011**, *63*, 847.

[9] M. Müller, *Adv. Polym. Sci.* **2014**, *256*, 197.

[10] C. L. Cooper, P. L. Dubin, A. B. Kayitmazer, S. Turksen, *Curr. Opin. Colloid Interface Sci.* **2005**, *10*, 52.

[11] A. B. Kayitmazer, D. Seeman, B. B. Minsky, P. L. Dubin, Y. Xu, *Soft Matter* **2013**, *9*, 2553.

[12] C. M. Jewell, D. M. Lynn, *Adv. Drug Deliv. Rev.* **2008**, *60*, 979.

[13] M. Soliman, S. Allen, M.C. Davies, C. Alexander. *Chem. Commun.,* **2010,** *46,* 5421-5433.

[14] H. Yin, R. L. Kanasty, A. A. Eltoukhy, A. J. Vegas, J. R. Dorkin, D. G. Anderson, *Nat. Rev. Genet.* **2014**, *15*, 541.

[15] Lankalapalli S, Kolapalli VR. Polyelectrolyte complexes: a review of their applicability in drug delivery technology. *Indian J Pharm Sci*. **2009**, *71(5)*

[16] M. M. Caruso, D. A. Davis, Q. Shen, S. A. Odom, N. R. Sottos, S. R. White, J. S. Moore, Chem. Rev. **2009**, *109*, 5755.

[17] Monika S. Layered polyelectrolyte complexes: Physics of formation and molecular properties. *J Phys Condens Matter.* **2003**, *15*, 1781–808.

[18] Rees, D. and Welsh, E. Secondary and tertiary structure of polysaccharides in solutions and gels. Angewandte Chemie International Edition in English, **1977**, *16(4)*, 214-224.

[19] G. A. Valencia, E. N. Zare, P. Makvandi, T. J. Gutiérrez, *Compr. Rev. Food Sci. Food Saf.* **2019**, *18*, 2009.

[20] Huang, F., Reilly, R. O., & Zimmerman, S. C. Polymer self-assembly: A web themed issue. Chemical Communications, **2014**, *50(88)*, 13415–13416.

[21] G. A. Valencia, E. N. Zare, P. Makvandi, T. J. Gutiérrez, *Compr. Rev. Food Sci. Food Saf.* **2019**, *18*, 2009.

[22] A. Bernkop-Schnürch, S. Dünnhaupt, Eur. J. Pharm. *Biopharm.* **2012**, *81*, 463.

[23] Yan, L., Wang, R., Wang, H., Sheng, K., Liu, C., Qu, H., Zheng, L. *Food Hydrocolloids*, **2018,** *84*, 450–457.

[24] G. Singhvi, N. Hans, N. Shiva, S. Kumar Dubey, *Academic Press*, **2019**, 121–144.

[25] Hamilton, I. E., & Norton, I. T. *Food Hydrocolloids*, **2016**, *55*, 220–227.

[26] Y. Wen, J. K. Oh, *Macromolecular Rapid Communications*, **2014**, *3*, 1819–1832.

[27] J. Liu, S. Willför, C. Xu, *Bioact. Carbohydrates Diet. Fibre* **2015**, *5*, 31.

[28] Okajima MK, Ono M, Kabata K, Kaneko T. *Pure Appl. Chem.* **2007**, *79*, 2039–46.

[29] Okajima MK, Bamba T, Kaneso Y, Hirata K, Fukusaki E, Kajiyama S, et al. *Macromolecules.* **2008**, *41*, 4061–4.

[30] Okajima MK, Kaneko D, Mitsumata T, Kaneko T, Watanabe J. *Macromolecules.* **2009**, *42*, 3057–62.

[31] Tamaru, Y., Takani, Y., Yoshida, T., Sakamoto, T. T. *Appl. Environ. Microbiol.* **2005**, 7327-7333.

[32] Okajima, M. K., studies on extraction of cyanobacterial polysaccharides (*sacran*) from *Aphanothece sacrum* and its structure and properties. Ph.D. Dissertation, Tokyo Institute of Technology, Japan, 2009.

[33] Okajima, M., Higashi, T., Asakawa, R., Mitsumata, Kaneko, D. T., Kaneko, T., Ogawa, T., Kurata, H., Isoda, S. *Biomacromolecules,* **2010**, *11*, 3172–3177.

[34] Kawashima, H., Atarashi, K., Hirose, M., Hirose, J., Yamada, S., Sugahara, K., Miyasaka, M. *Journal of Biological Chemistry.* **2002,** *277,* 12921–12930.

[35] Motoyama, K., Tanida, Y., Hata, K., Hayashi, T., Higashi, T., Ishitsuka, Y., Kondo, Y., Irie, T., Kaneko, S., Arima, H. *Chem Pharm Bull.*, **2014**, *62(7),* 636-41.

[36] Mitsumata, T., Miura, T., Takahashi, N., Kawai, M., Okajima, M. K., & Kaneko, T. S*oft Matter Physics*, **2013**, *87(4),* 1–9.

[37] Okeyoshi, K., Okajima, M. K., & Kaneko, T. *Biomacromolecules*, **2016,** *17(6)*, 2096–2103.

[38] K. Okeyoshi, M. K. Okajima, T. Kaneko, *Polym. J.* **2021**, *53*, 81.

[39] K. Budpud, K. Okeyoshi, M. K. Okajima, T. Kaneko, *Small* **2020**, *16*, 2001993.

CHAPTER II

POLYSACCHARIDE FIBERS

WITH SELF-ASSEMBLING TWISTED MICROSTRUCTURES

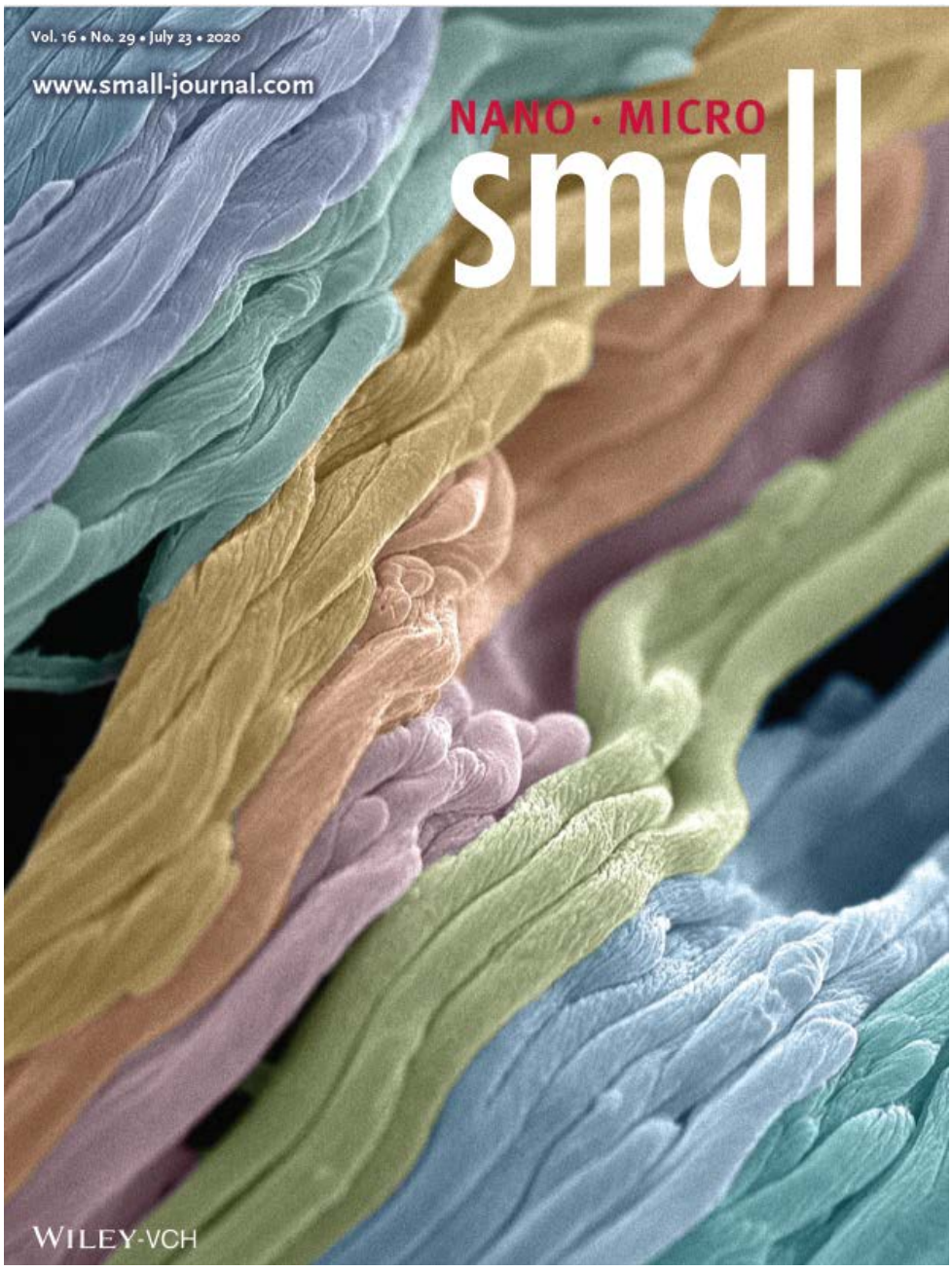

2.1 Introduction

Polysaccharides are natural products that have attracted significant attention owing to their environmental adaptivity, their biocompatibility with commercial products such as foods[40][41] and cosmetics,[42][43] and their suitability for medical applications.[44][45][46] Recently, various kinds of advanced soft materials have been designed using polysaccharide nanoarchitecture, such as pullulan, which is used in a drug delivery system, and cellulose nanofibers, which have been used to engineer flexible paper devices.[47][48][49] Moreover, in consequence of biochemical polymerization from the various saccharides and the arrays, various architectures of self-assembled polysaccharides at nano- and submicrometer scales have huge potentials in material fields. However, the original hierarchical structures of polysaccharides are rarely utilized because of the difficulties involved in regulating their self-assembled structures on the micrometer scale. In contrast, many types of bio-inspired materials have been fabricated using synthetic polymers, such as soft actuators that respond to environmental changes, including temperature, charge, and humidity,[50]-[59] and the responsiveness of these materials has been amplified and diversified through the immobilization of functional molecules or functional nanoparticles into polymer networks.[60]-[67] Here, considering the origin of polysaccharides and the habitat environments, the polymers should have significant potential for use not only in water but also in humid environments. If the self-assembled structures of these natural polysaccharides can be reconstructed in vitro, it will lead to a better understanding of the morphological changes that occur during polysaccharide self-assembly in water, as well as the development of a new class of bio-inspired materials with regulated nanoscale structures. *Sacran* is a natural polysaccharide that is extracted from the freshwater cyanobacteria Aphanothece sacrum.[68] This polysaccharide has unique properties such as its megamolecular weight (10^6–10^8 g mol^{-1}) and a composition consisting of more than ten types of sugars. On the molecular scale, *sacran* contains rigid rod bundles with helical structures, similar to other

polysaccharides.[69] In the extracted state, it exhibits stable polymeric liquid crystallinity (LC) even at relatively low concentrations (>0.5 wt%).[68] Remarkably, unlike typical "microfibrils" that have diameters of ≈5 nm and lengths <1 μm, such as those seen in cellulose nanofibers, *sacran* is capable of self-assembling into very large fibers with diameters of ≈1 μm and lengths >200 μm.[70],[71] It is remarkable that a cyanobacterium with a diameter of only ≈5 μm can produce such a large polysaccharide fiber as an extracellular matrix. Although the unique polymeric properties have been revealed, the fiber's microstructures, microscopic morphologies, and transformations have been unknown. In this study, a method for inducing the self-assembly of a polysaccharide-based on an evaluation of its morphological properties is demonstrated (**Figure 2.1**). First, micrometer-scale morphological changes in the self-assembled microfiber at the evaporative air–LC interface were determined in vitro. The self-assembly/disassembly of large fibers was then studied under controlled salt conditions. This is first reported that the polysaccharide can form unique twisted fibers in nanometer scale and micrometer scale. The air-water interface and capillary forces drive the geometric deposition of microfibers during the drying process. Focusing on the effect of the capillary force, the deposition behaviors of assembled fibers and the single fiber are studied. A cross-linked polysaccharide film was made and the impacts of the microfiber's spring behaviors in an environment with a humidity gradient were presented to indicate the possible usage for vapor sensitive materials.

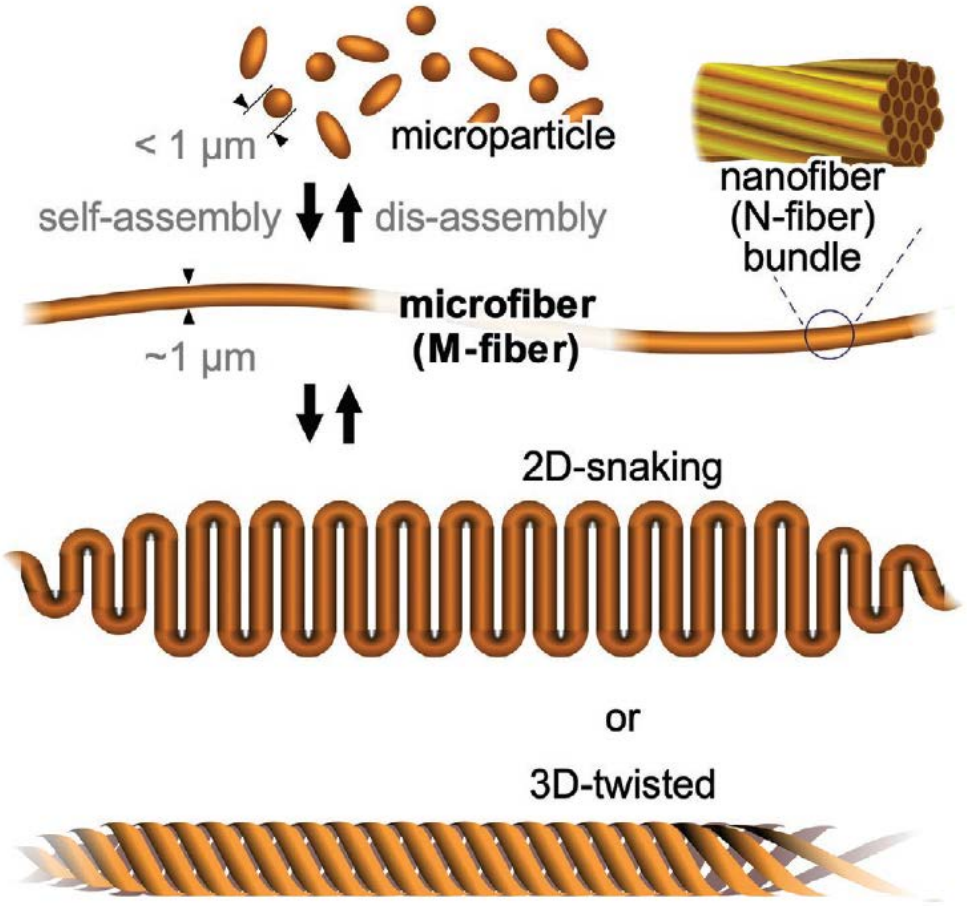

Figure 2.1 Schematic illustration of *sacran* fiber morphological changes. The upper section of the figure illustrates particle shapes with ≈1 μm diameter at low concentration and self-assembled microfiber with ≈1 μm diameter at high concentration, as well as the micrometer-scale fiber (M-fiber) as a bundle of nanometer-scale fibers with ≈50 nm diameter (N-fiber). The lower section of the figure illustrates the transformation of the M-fiber into 2D snaking and 3D twisted structures upon drying.

2.2 Materials and methods

2.2.1 Materials

Sacran was extracted from *Aphanothece sacrum* and purified following a previously described procedure.[68] The average molecular weight of *sacran* used in the experiment was measured by size exclusion chromatography with multi-angle light scattering: Mn = 3.23 × 10^6 g/mol, Mw = 3.45 × 10^6 g/mol (Mw/Mn = 1.04). TEMPO-cellulose nanofiber (TEMPO-CNF), used as a polysaccharide control, was purchased from Oji Holding Co. Analytical-grade HCl, NaCl, and CaCl2 were supplied by Kanto Chemical Co. and used without further purification.

2.2.2 Preparation of polymer solutions

The *sacran* solution was obtained by dissolving the appropriate amount of *sacran* in deionized water at room temperature (~25 °C). To study ionic effects, 1 mM aqueous solutions of HCl, NaCl, and $CaCl_2$ were used instead of deionized water to make the *sacran* solution. The *sacran* solutions were homogenized using a mechanical stirrer, and at least 6 h was allowed to elapse before use.

2.2.3 Microscopy observations

The *sacran* solutions (1–3 μL) were dropped onto a non-modified glass slide and dried at ~25 °C and 1 atm. The drying process was observed and recorded using a polarized optical microscope (IX73, Olympus), with a first-order retardation plate (λ = 530 nm) in the light path. The size and the bending degree of the fibers were analyzed by ImageJ software. The dried polymer depositions were observed at the submicron scale with a field emission scanning electron microscope (FE-SEM, S-5200, Hitachi). The samples were prepared for FE-SEM by dropping each solution onto a carbon-coated copper grid and then drying. The samples were then coated with platinum-palladium at 5 mA for 100 s. Scanning was performed under a high vacuum at an ambient temperature (~25 °C) with a beam voltage of 10 kV.

2.3 Results and discussion

Sacran was extracted from *Aphanothece sacrum* and observed using a variety of microscopy techniques.[72] **Figure 2.2a** shows super-resolution confocal microscopy images of a 0.5 wt% aqueous solution of *sacran* dyed with fluorescein isothiocyanate. This clearly indicates that *sacran* exists in water primarily as a microfiber, with a diameter of 0.5–1 μm. Optical microscopy images of dried *sacran* reveal a fibrous structure with a length of hundreds of micrometers (**Figure 2.2b**).

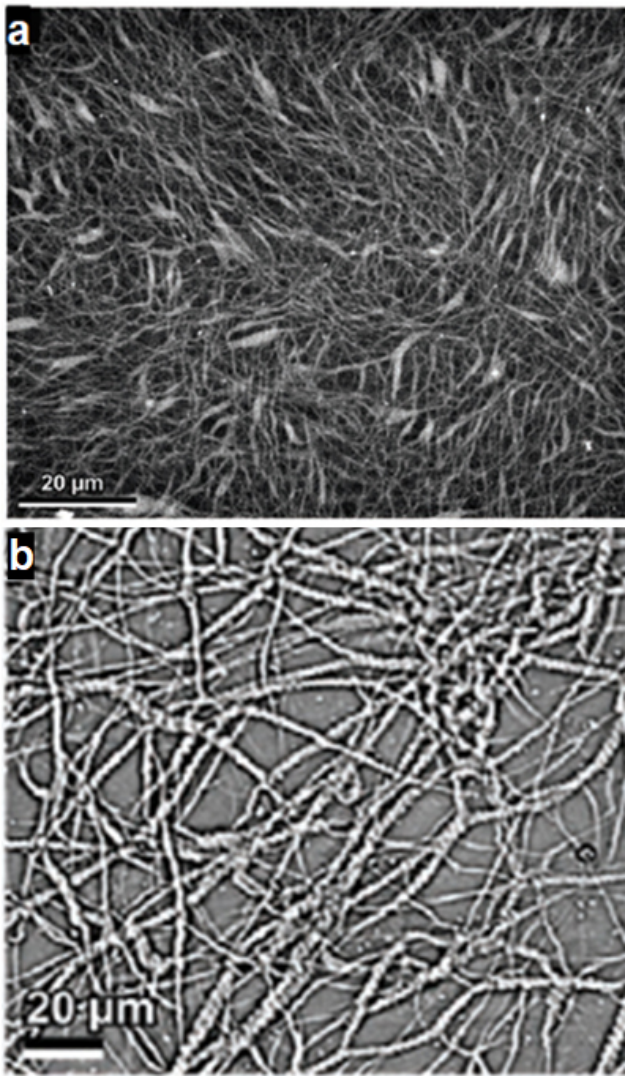

Figure 2.2 Self-assembly/disassembly of *sacran* microfibers. a. Super-resolution confocal microscopy image of an aqueous solution of dyed *sacran*. b. Optical microscopy images of dried *sacran* showing the microfiber.

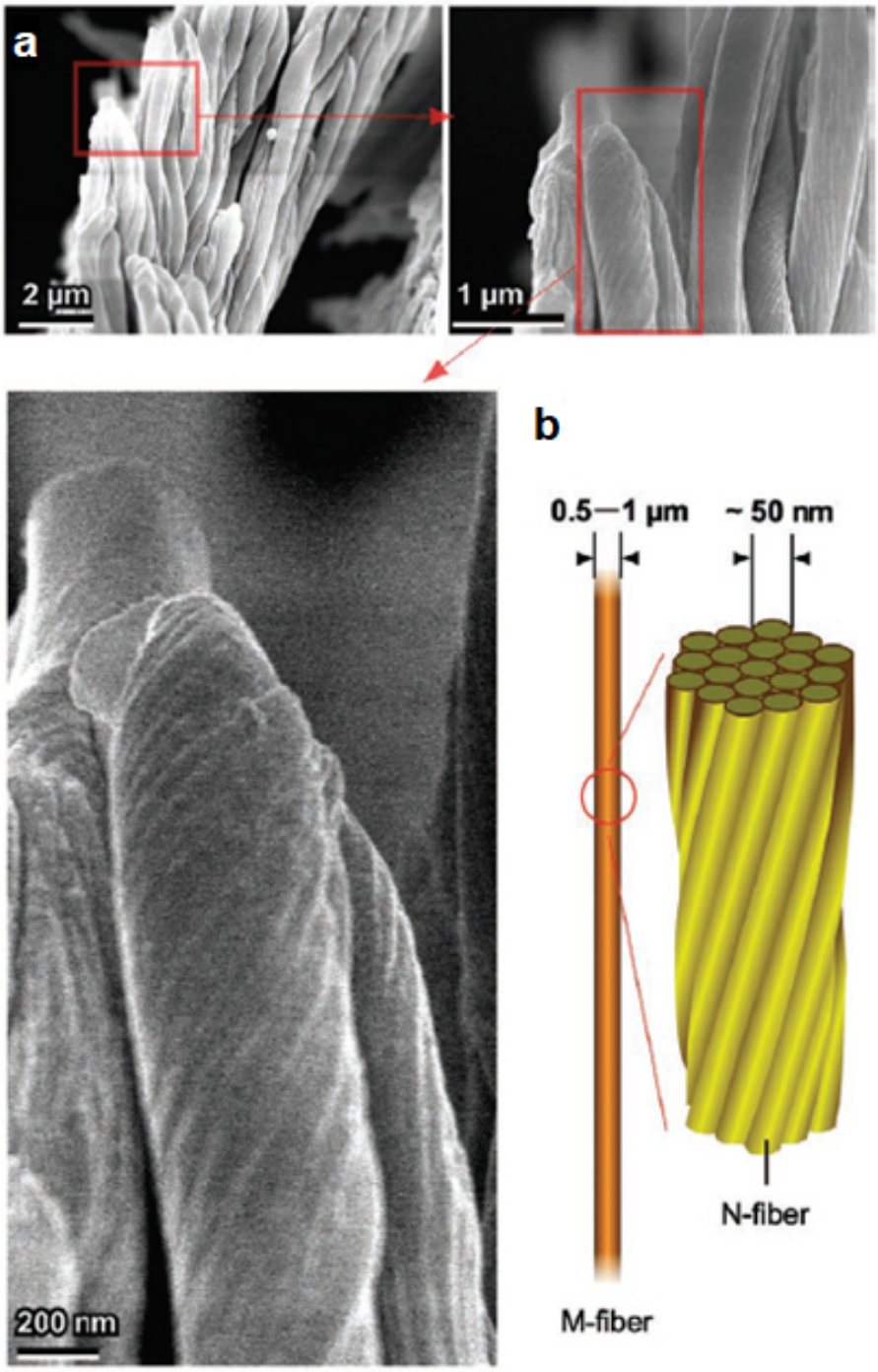

Figure 2.3 a. SEM images of *sacran* microfibers. b. Schematic illustration of fibers with diameters in the micrometer scale (M-fiber) and nanometer-scale (N-fiber).

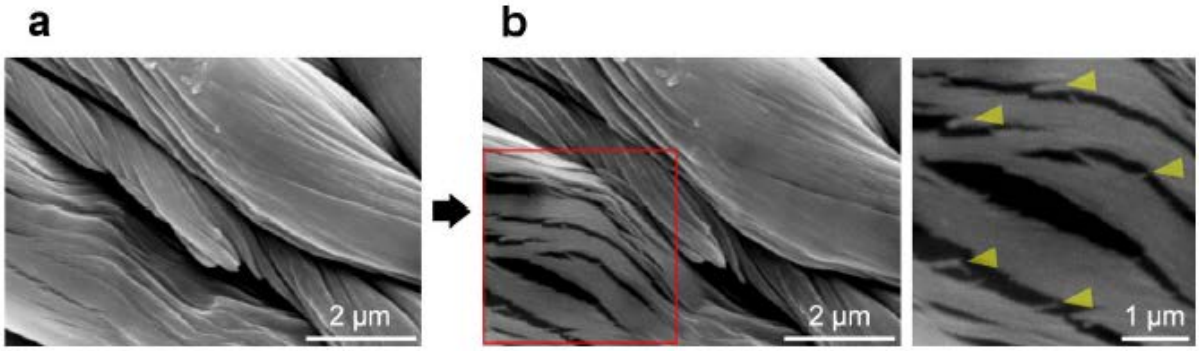

Figure 2.4 FE-SEM images of a dried *sacran* sample. a. Image just after being focused. b. Image ~10 s after being focused. The moment that the M-fiber was damaged by the electron beam during FE-SEM observation was captured; N-fibers can be seen around the edge of the cracked M-fiber (yellow arrows).

Figure 2.3a shows field emission scanning electron microscope (FE-SEM) images of the M-fibers. Each M-fiber is composed of torsional nanometer-scale fibers (N-fibers) with diameters of ≈50 nm (**Figure 2.3b**). This N-fiber is of a similar scale to the microfibrils in cellulose nanofibers. Such an N-fiber assembly could also be seen as a result of damage from the electron beam during SEM analysis (**Figure 2.4**). Thus, the M-fiber is torsional self-assembly of N-fibers. To examine the macroscopic structure of the M-fibers, a dried droplet of the aqueous solution was observed using several types of microscopy. **Figure 2.5a** shows a polarized optical microscopy image of the dried droplet through a retardation plate (λ = 530 nm). The blue and yellow parts around the edge indicate the orientation along the circular arc. The optical microscopy image from the edge to the center, as shown in **Figure 2.5b**, clearly indicates that the M-fibers orient along a circular arc around the edge with >200 μm length in the radius direction. The SEM image clearly shows that the M-fibers on the edge are in a densely packed orientation (**Figure 2.5c**), but the density is relatively lower in the center. These results indicate that the M-fibers integrate and deposit along the contact line during the initial water evaporation stage.[34] At this point, the capillary force should enhance the integration of the fibers on the moving interface (**Figure 2.5d**).[74]-[77]

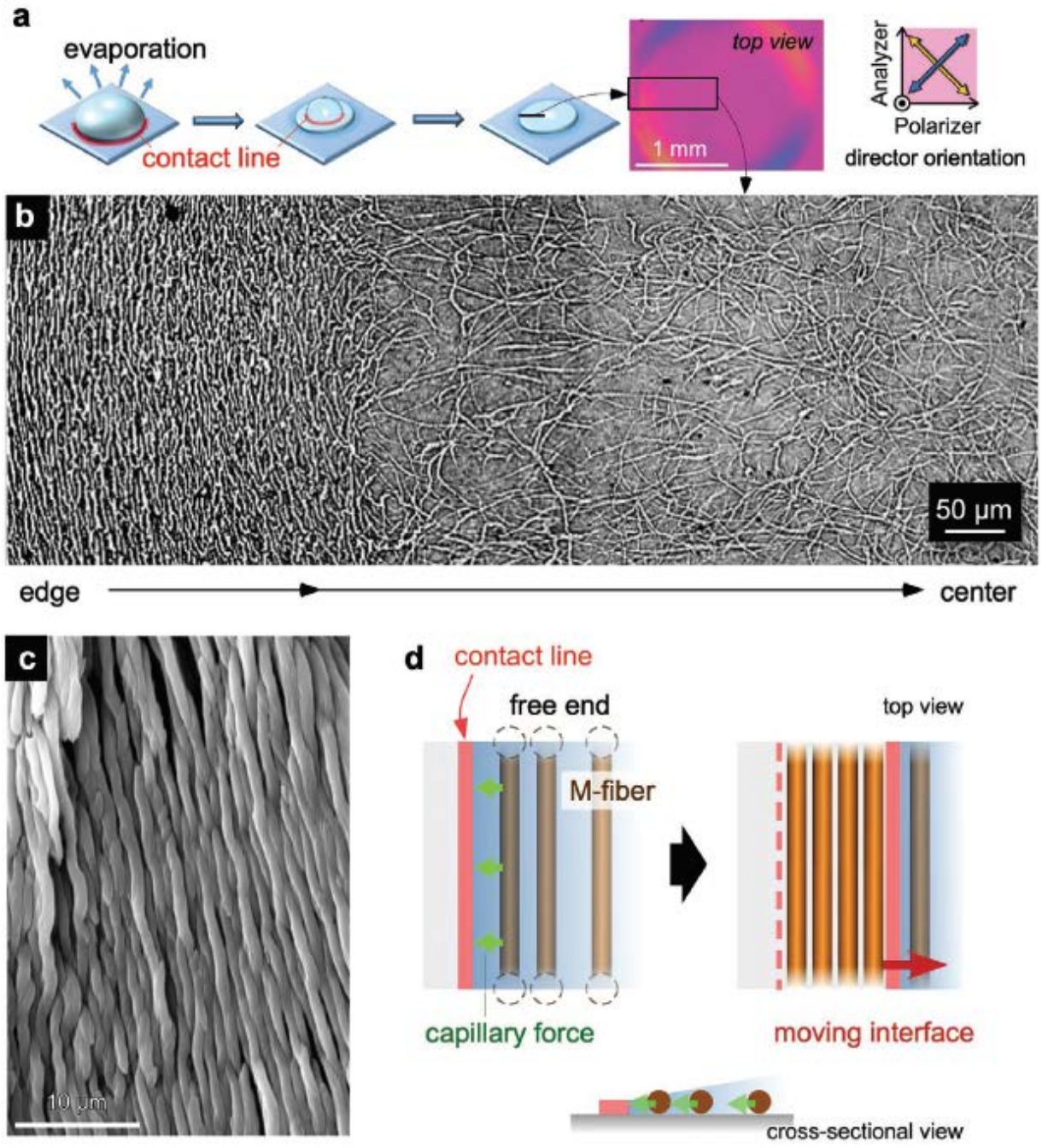

Figure 2.5 Effect of interfacial contact line on *sacran* microfibers. a) Schematic illustration of a drying droplet on the substrate and polarized optical microscopy image through a first order retardation plate ($\lambda = 530$ nm). b) Drying record of a droplet from edge to center. c) SEM image of microfibers. d) Mechanism of microfiber integration parallel to the contact line. Initial concentration of *sacran*: 5×10^{-2} wt%. Drying temperature: ≈25 °C.

The transformation of M-fibers into 2D snaking and 3D twisted structures was clearly observed on the inner side of the dried droplet (**Figure 2.6a,b**). The snaking structures have a width of ≈5 μm and length of >50 μm. Most of the snaking structures are aligned in a similar direction, perpendicular to the circular arc of the contact line (**Figure 2.6a**). **Figure 2.7** shows the formation of snaking structures during interface movement. It can be seen from these images that the M-fiber exhibits sufficient flexibility to conform to the shape of the moving contact line, positioning itself in parallel to the contact line. The moving velocity of the contact line, V was estimated as follows: $V = \Delta r/\Delta t$ (where $\Delta r = r_{i+1} - r_i$ = displacement (μm), and $\Delta t = t_{i+1} - t_i$ = time change (s)). By estimating the change of the contact line position from the images (**Figure 2.7**), the velocities (V) at regions I, II, and III were calculated to be 17.5, 26.7, and 28.5 μm/s, respectively. The pitch (P) of the snaking fiber (**Figure 2.7**, 3 s, yellow highlight in the image) in regions 1, 2, and 3, which was measured using ImageJ software, was calculated to be 3.2, 2.3, and 1.9 μm, respectively. These values are analyzed in light of the images taken. As V increased, P decreased in combination with a transformation from snaking structures to twisted structures (**Figure 2.9c**). In fact, the M-fiber is capable of forming an immediate U-turn while maintaining its diameter (**Figure 2.6a**). Such a U-turn can occur during the slow movement of the contact line because of the capillary forces among the M-fibers (**Figure 2.8**).

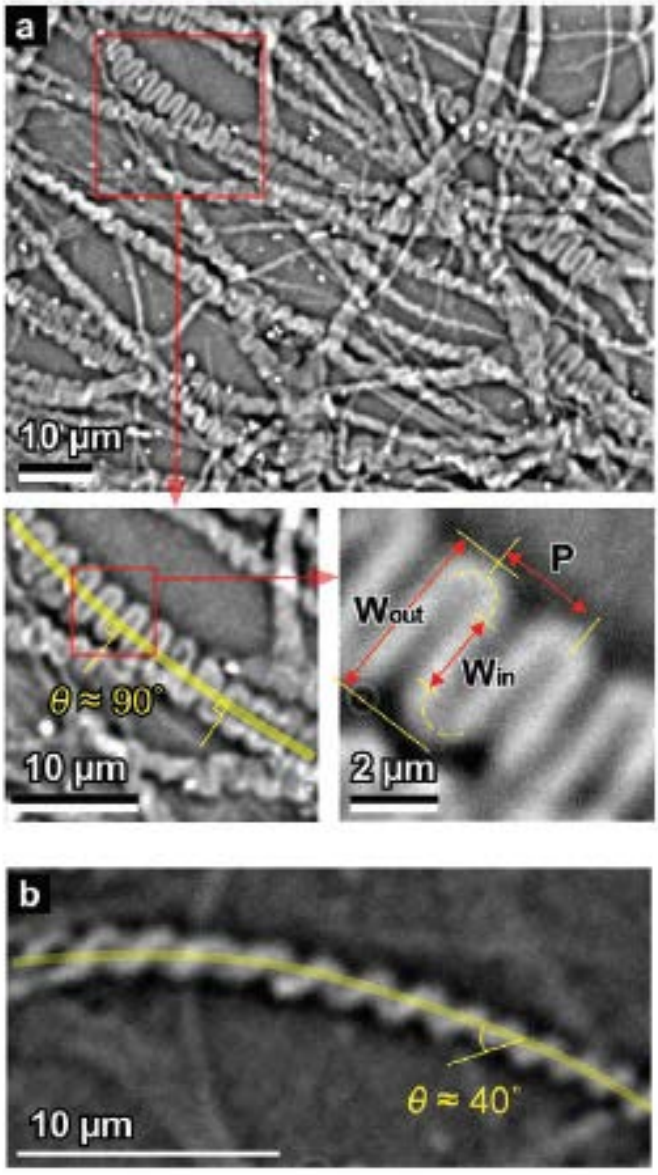

Figure 2.6 Snaking and twisted structures of M-fibers. Optical microscopy images of a) snaking M-fibers and b) twisted M-fibers.

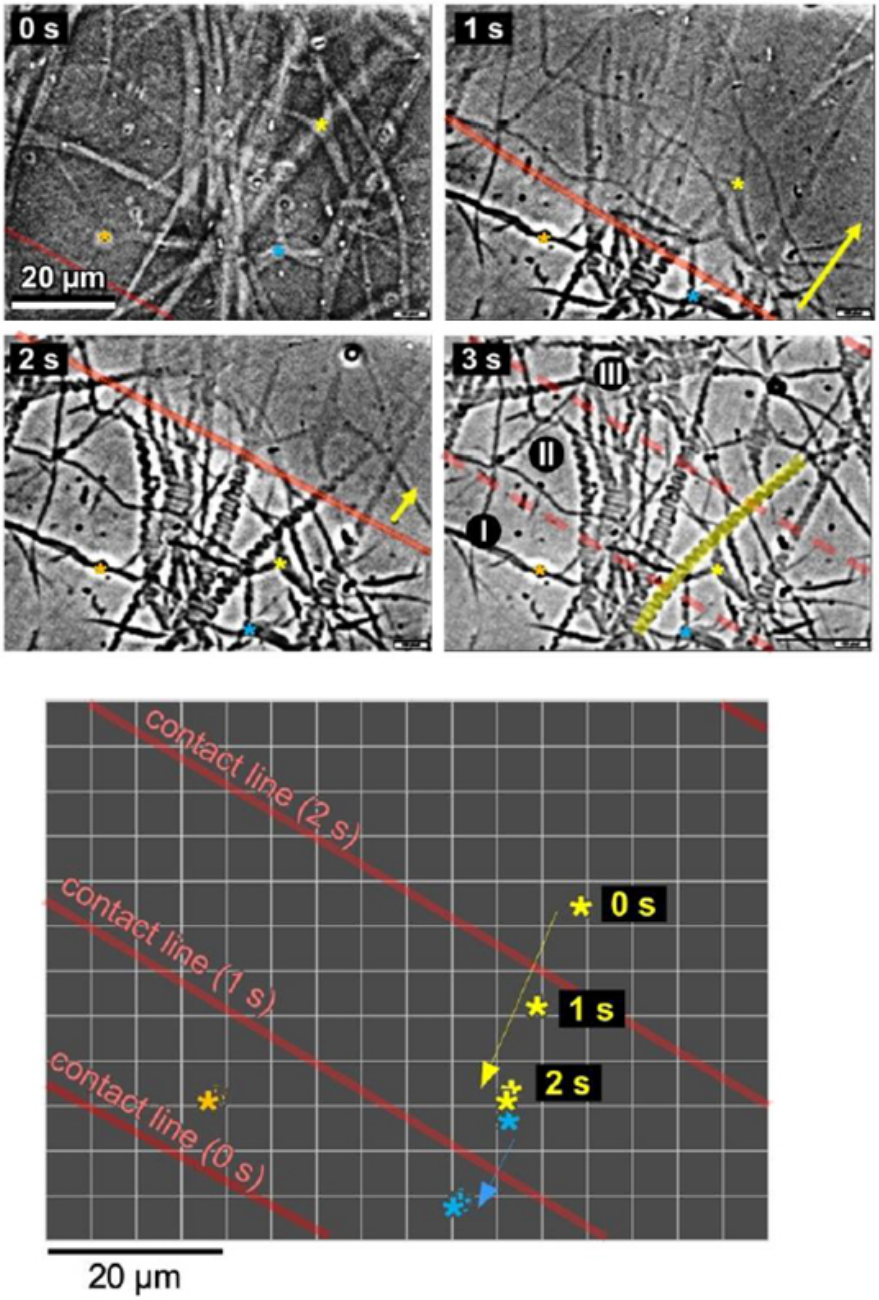

Figure 2.7 Formation of snaking structures at the contact line over time. Yellow arrows indicate the direction of the moving interface.

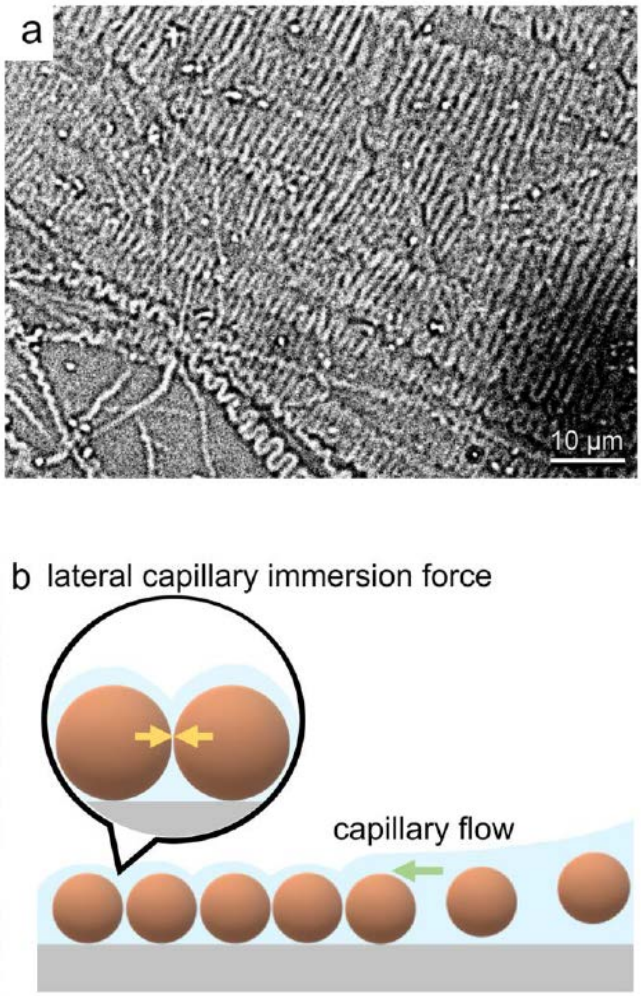

Figure 2.8 2D-snaking structures formed under action of capillary force. a. Optical microscopy image of the packed snaking M-fibers. Initial concentration of *sacran*: 5×10^{-2} wt%. Drying temperature: ~25 °C. b. Schematic illustration for a cross-section of the droplet edge and M-fiber deposition under the action of capillary force.

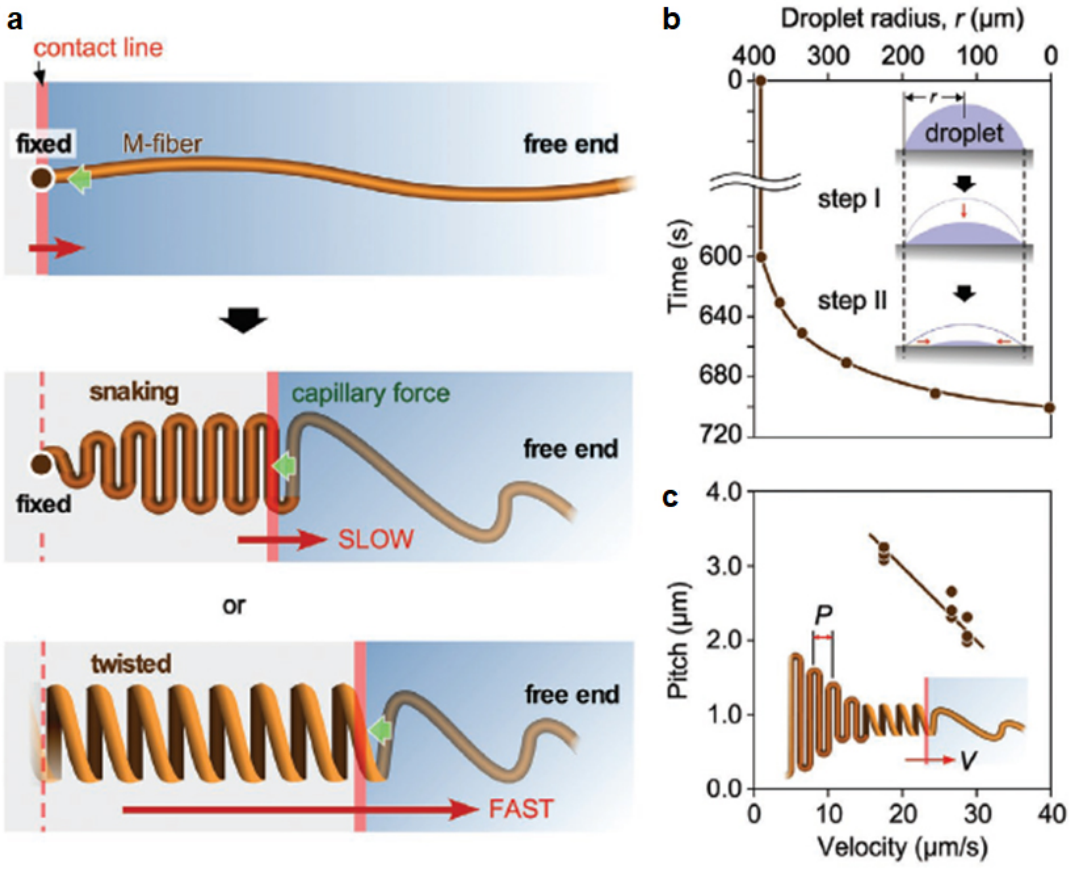

Figure 2.9 a) Transformation mechanism of M-fibers based on correlation between direction of contact line and long axis of M-fibers. b) Time-dependent change in drying droplet radius. c) Pitch in snaking form as a function of velocity of moving interface

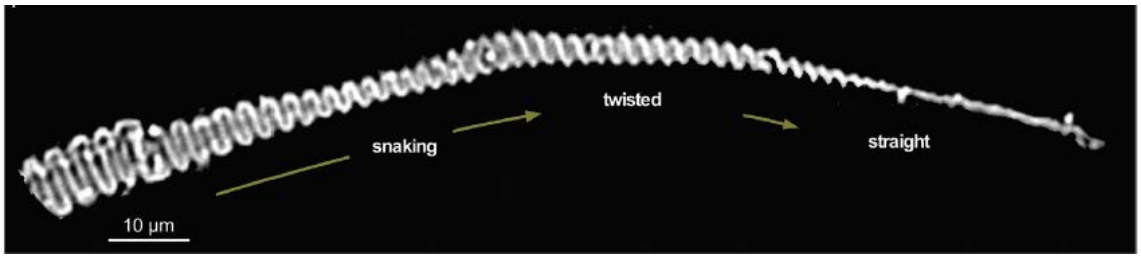

Figure 2.10 Optical microscopy image of a single M-fiber in snaking, twisted, and straight structures. Initial concentration of *sacran*: 5×10^{-2} wt%. Drying temperature: ≈25 °C.

Similarly, twisted structures with a width of ≈5 μm and a twist angle of ≈40° were observed (**Figure 2.6b**). Capillary forces and the velocity of the contact line are the dominant factors in creating these formations (**Figure 2.9a**). When one end point of the M-fiber is pinned on the substrate side, the fiber transforms into snaking structures when the contact line motion is slow and twisted structures when the contact line motion is rapid. As the droplet radius dried over time, the shape of the droplet changed in two steps: (I) the height of the droplet decreased, and (II) the radius of the droplet decreased (**Figure 2.9b**). During step I, the radius showed only a slight change, and the M-fibers gradually positioned themselves parallel to the contact line. In step II, not only was the radius reduced but the speed of the contact line motion was also accelerated. In fact, the pitch in the snaking structure reduced as the velocity of the contact line motion increased (**Figure 2.9c**). This acceleration induced a twisting transformation toward a thinner width. **Figure 2.10** shows a series of optical microscopy images demonstrating the transformation of a single M-fiber into snaking, twisted, and straight structures. Considering that the M-fiber is estimated to have a length of ≈800 μm, the aspect ratio of these self-assembled structures is remarkably high. Twisted multiple M-fibers were also confirmed by microscopy observations. **Figure 2.11a** shows a structure with a tightly twisted part and a loosely twisted part; **Figure 2.11b** shows the optical microscopy images of double and triple M-fibers in a twisted state; and **Figure 2.11c** is an FE-SEM image of a twisted structure with more than five M-fibers. These images clearly show that the M-fibers have a strong tendency to form twisted structures when induced by the motion of the interface. Similar to the formation process of single twisting structures, multiple straight M-fibers in a parallel orientation transform into a twisted structure parallel to the direction of contact line travel (**Figure 2.11d**). Given that the M-fiber is composed of torsional N-fiber bundles, the formation of these micrometer-scale twisted structures shows that this material has a self-similar relationship at the nanometer and micrometer scales.

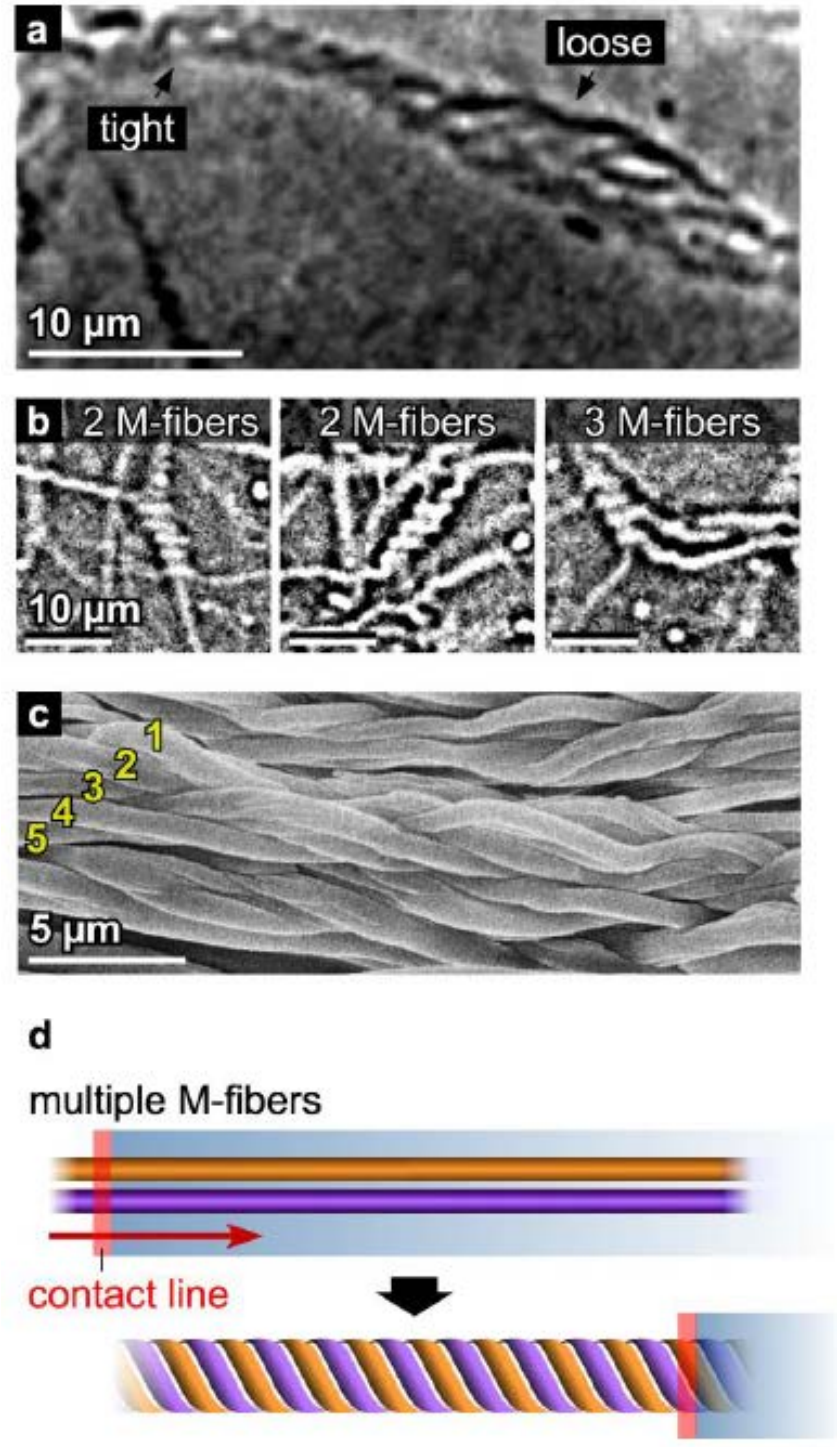

Figure 2.11. Multiple twisted structures of M-fibers. a, b. Optical microscopy images. **c.** FESEM image. **d.** Schematic illustration of twisting formation induced by contact line motion. Initial concentration of *sacran*: 5×10^{-2} wt %. Drying temperature: ~25 °C.

Such a self-assembled microfiber is extremely unique. The microfiber (M-fiber) is capable of disassembling into submicrometer-scale particles in aqueous NaCl solution. This is because the sodium cations displace the protons of carboxylic acid groups, breaking the intermolecular hydrogen bonds. This ionic effect was confirmed by mixing HCl, NaCl, or $CaCl_2$ into the *sacran* solution (**Figure 2.12**).[72] In cases of HCl and NaCl having monovalent cation, the microfibers were disassembled into small fragments in the concentration of 1×10^{-3} M. In contrast, the microfiber maintained their structure in 1×10^{-3} M $CaCl_2$ solution. This difference should be because that the divalent cation Ca^{2+} is capable of binding with the carboxylate groups as a crosslinker. In the aqueous solutions with more than 10×10^{-3} M $CaCl_2$ (**Figure 2.12b**), it showed the disassembled small fragments, similar to the result in the cases of 1×10^{-3} M NaCl. In the existence of the excess divalent cation, the Ca^{2+} would displace the protons of carboxylic acid groups on one-on-one level, similar to the case of monovalent cation. This supports the proposition that hydrogen bonding of the carboxylic acid groups is what makes it possible for the M-fibers to form a stable, self-assembled structure in pure water.

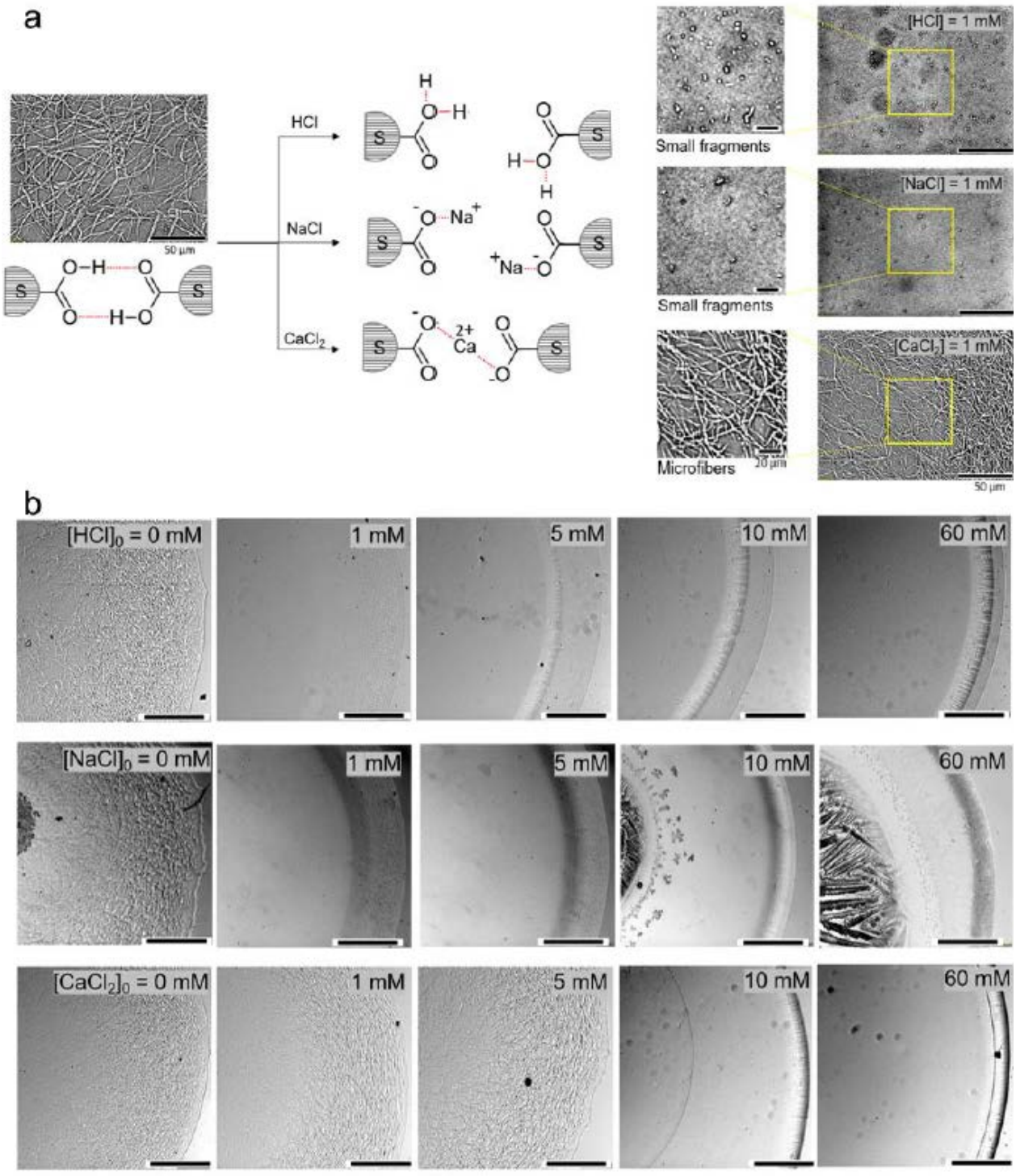

Figure 2.12 Ionic effect on assembly/disassembly of *sacran* M-fibers. a. Optical microscopy images of deposited polymers in hydrochloric acid, sodium chloride, and calcium chloride solutions and hypothesis of the binding mechanism. Initial concentration of *sacran*: 5×10^{-2} wt %. Drying temperature: ~25 °C. $[HCl]_0$, $[NaCl]_0$, $[CaCl2]_0$ = 1 mM. b. Optical microscopy images of given ionic concentrations. $[HCl]_0$, $[NaCl]_0$, $[CaCl2]_0$ = 0, 1, 5, 10, 60 mM.

2.3.1 Application section I

By utilizing the polymeric network formed by the M-fibers, a dried film was prepared and used as a vapor sensor.[71] The film used for the vapor sensor was cut from the area of the dried film having M-fibers in random directions (see **Figure 2.5**) and the thickness of the dried film was typically ~13 μm. Physical crosslinking could be introduced into the film by annealing at 100 °C to make multiple hydrogen bonds among the sacran chains and ester bonds between the carboxylic acid and hydroxyl groups.[76] As shown in **Figure 2.13** and Movie S2, when a water drop approached the flat film, the film immediately showed repulsive bending. When the water drop was kept at a distance of ~500 μm or more, the film reversibly returned to a flat state through evaporation of water. Spatio-temporal analysis of the motion indicated that the film reversibly switched between flat and bent states within 300–800 ms (**Figure 2.13**). The snaking and twisting structures of the M-fiber are responsible for the film's repulsive motion. The M-fiber on the damp side of the flat film can extend the network like an uncoiled spring when it absorbs moisture.The force and repulsive motion generated by the extension of the fiber when moisture is introduced can be explained using Hooke's Law, as illustrated in **Figure 2.14**. Hooke's law is represented by the equation F = –kX, which states that the extension of a spring (X) is linearly proportional to the force (F), with a variable corresponding to the spring constant (k). The transformation of the M-fiber from a tightly twisted state to a snaking state was proceeded by an increasing water content, and corresponded to an increase in length on the long axis of ~1.5 times its original length (see also **Figure 2.15** and Movie S3). From Hooke's law, it can be seen that the restoring force should act in the opposite direction of the displacement. In agreement with this, when the moisture source was removed, the film immediately reverted to its previous position. These results support the theory that the snaking and twisted structures act as micro-springs within the film. Such a repulsive motion was not observed in the case of a film made of TEMPO-oxidized cellulose nanofibers (TEMPO-CNF),

which was prepared under the same conditions and with a similar thickness. In the CNF network, the rigid bundles of microfibrils apparently restricted the extension of the network. This theory is supported by a comparison of the swelling kinetics from the dried state to the wet state between the *sacran* film and the CNF film (**Figure 2.16**). Whereas the CNF film only swelled to ~110% in length, the *sacran* film swelled drastically to ~135%. By performing the motion test under different solvent vapors of various relative permittivities, it was confirmed that the film motion was caused by hygroscopicity and not by an electrostatic force (see Movie S4 and **Table 2.1**). **Figure 2.17** shows a schematic illustration of the bending motion of the *sacran* film upon sensing local humidity. The water-approaching side of the film adsorbs moisture and the snaking/twisted M-fibers immediately extend. In contrast, the other side of the film remains dry for a short time, which causes no extending. Similarly, the film depicts a quick reaction to the water drop receding, moving from the bent to the flat state. The network could swiftly release water by shrinking because the expanded M-fibers had extension stress like a spring. As a result, the twisted film immediately flattens. Thus, the snaking and twisted M-fiber network enables millisecond bending and stretching responses to changes in local humidity.

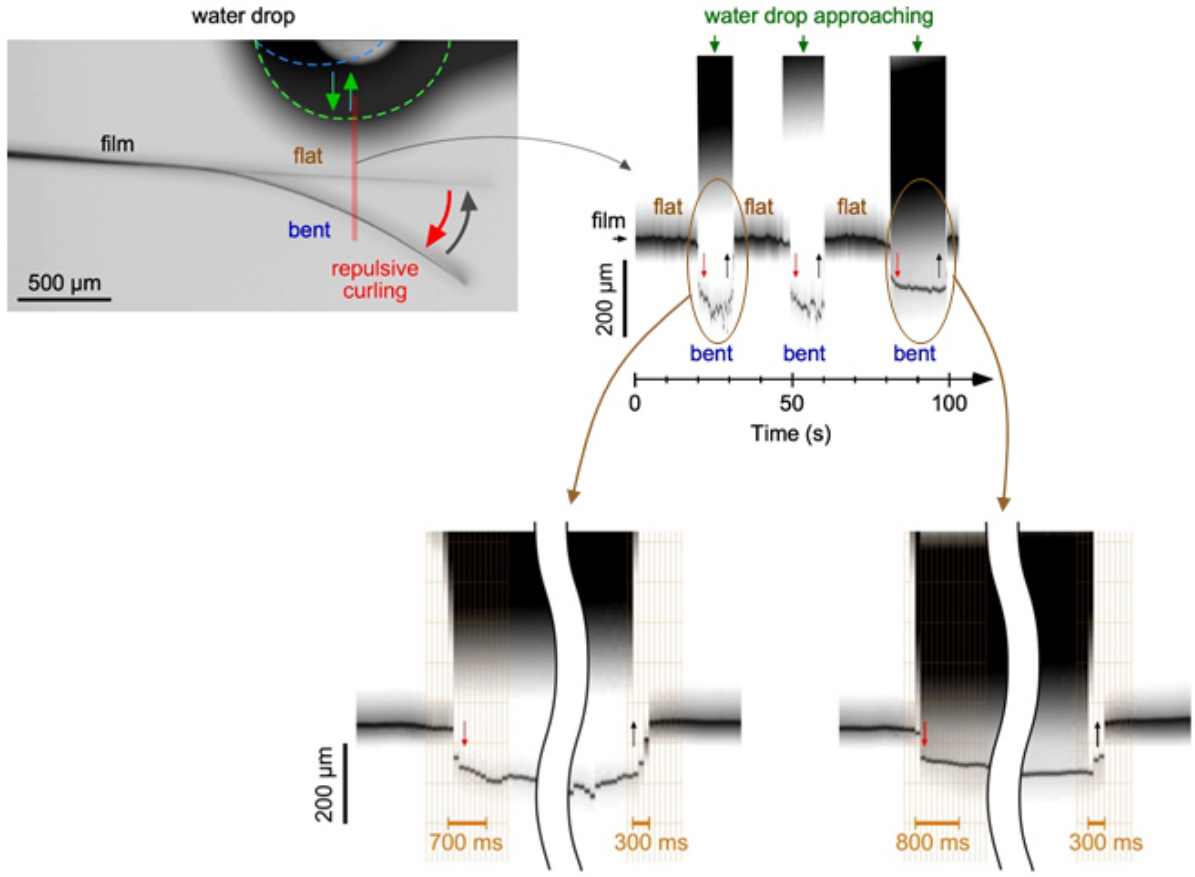

Figure 2.13 Humido-sensitive polysaccharide film. Repulsive motion against water drop approach and stacked images of the selected line showing the mechanical responsiveness to the water drop approach. Radius of water drop: ~1 mm.

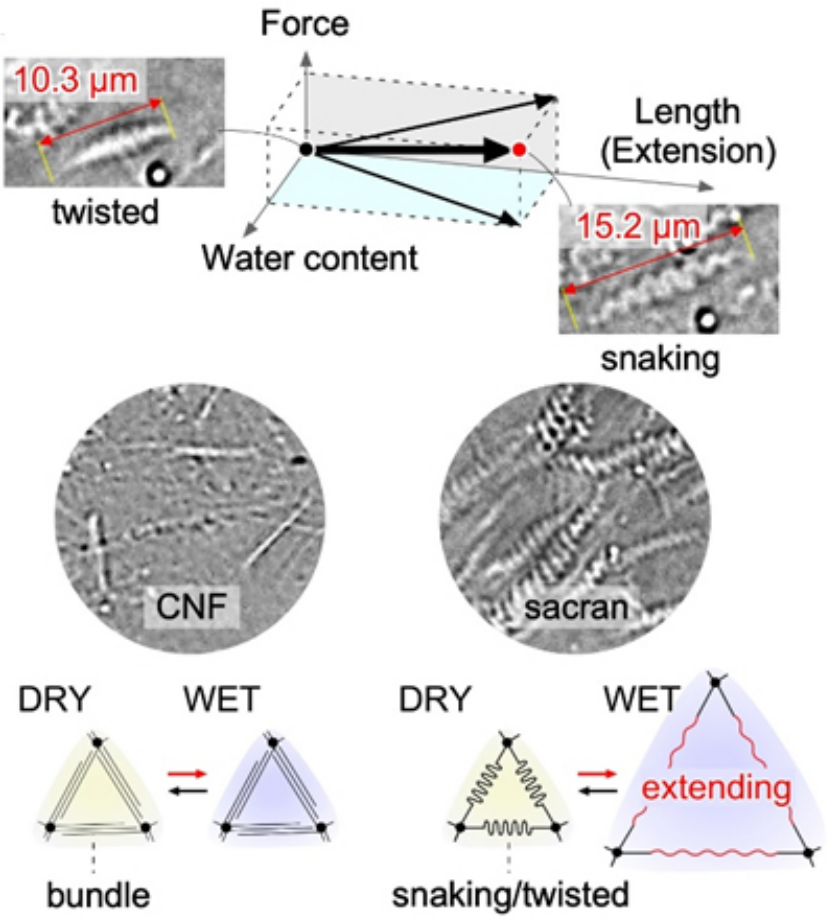

Figure 2.14 Microscopy images of CNF and *sacran* films (viewed from above) and network models. The CNF film is composed of rigid microfibril bundles, and the *sacran* film is composed of snaking/twisted M-fiber networks.

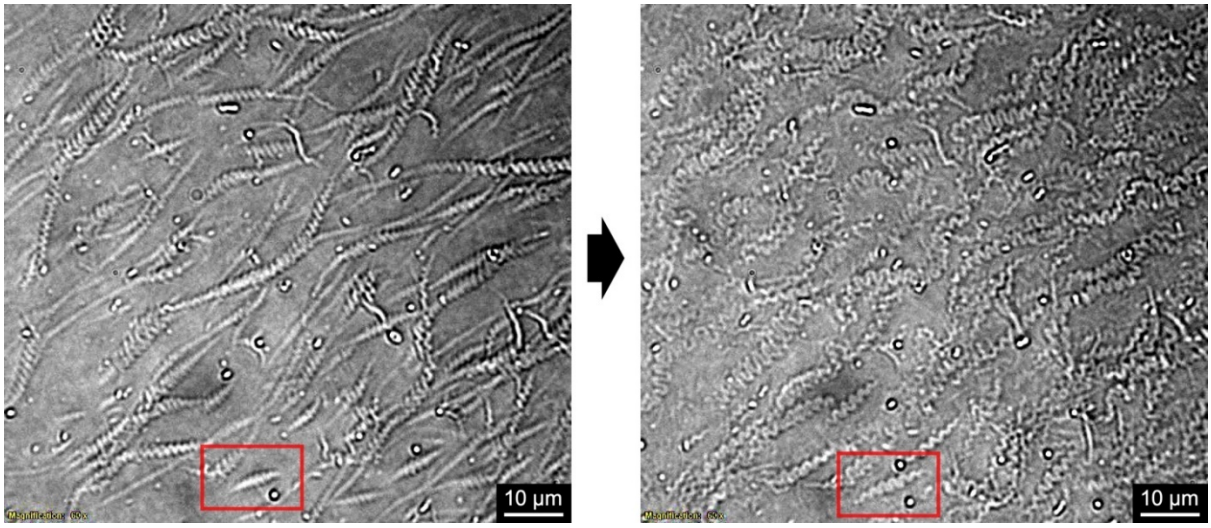

Figure 2.15 Optical microscopy images of twisted M-fibers transformed into snaking M-fibers at the same position. Initial concentration of *sacran*: 5×10^{-2} wt %. Drying temperature: ~25 °C. See also Movie S3.

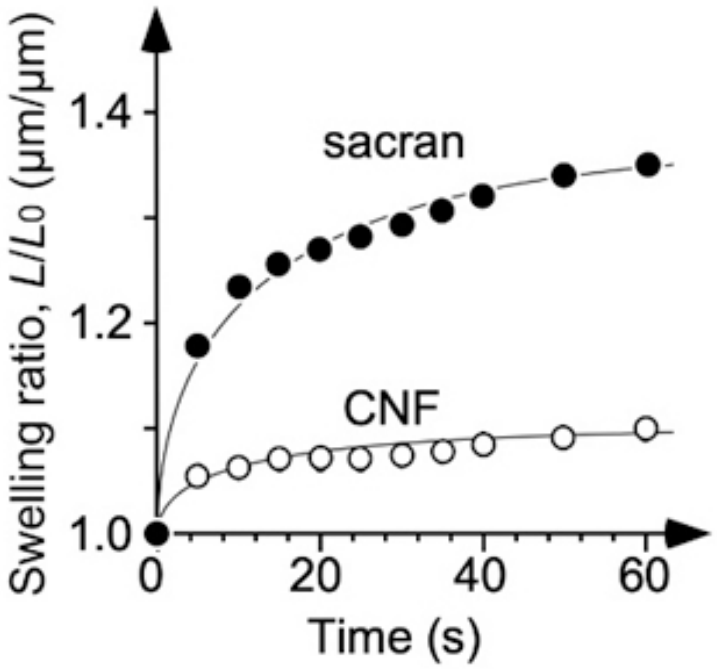

Figure 2.16 Swelling kinetics of the films from the dried state to the wet state in pure water.

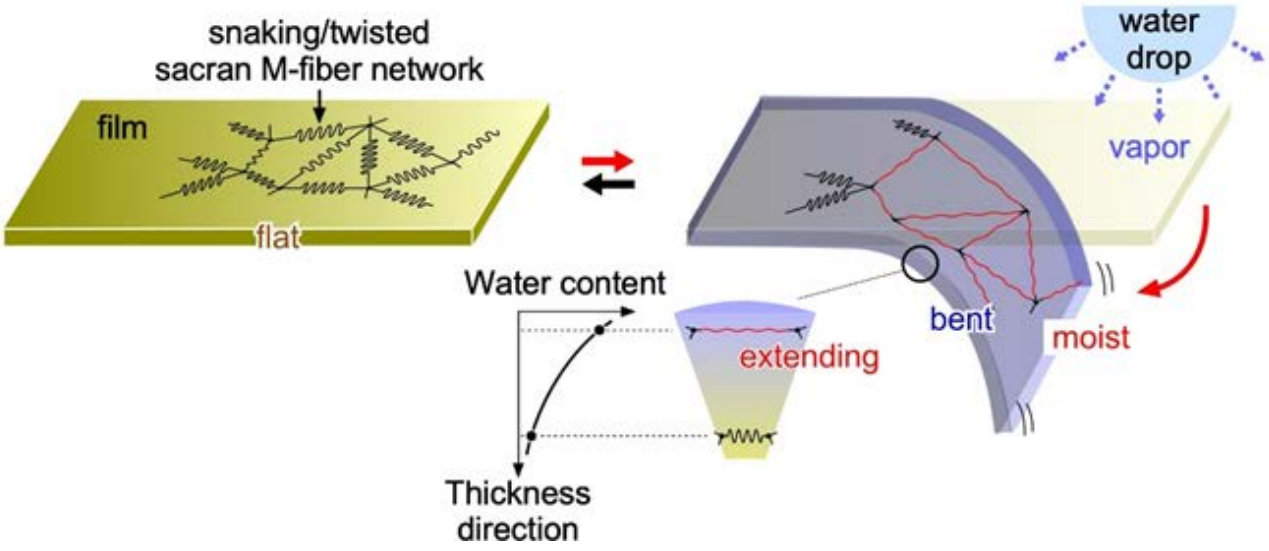

Figure 2.17 Schematic illustration of the humido-sensitive film composed of a snaking/twisted M-fiber network.

Table 2.1 Response of film to solvent vapors.

Solvent	water	formic	ethanol	acetic	hexane	acetic pH2	ammonia pH12
Relative permittivity (Fm^{-1})	80	58	24	6.2	2.0	mixed solvent	mixed solvent
Response	++	+++	+	+	–	++	++

Symbols indicate the speed at which the film responded to the vapor: very fast (+++), fast (++), slow (+), and no response (–).

2.3.2 Application section II

The M-fiber not only could use as a humido-responsive material but also could adapt to use as a micropattern scaffold for controlling cell orientation. Because of its unique ability to form hierarchical twisted fiber in the nano-micro scale, the micro-alignment surface was successfully prepared. This study was well supported by Matsumura Laboratory. Under mild conditions, this material could be created by a natural drying process. The deposition from a solution 5×10^{-1} wt%, rigid fibers were observed with high orientation around the droplet edge (**Figure 2.18**). To prepare the sacran oriented fibers as a scaffold, the *sacran* sample is annealed at a high temperature to maintain its micro pattern fibers under a wet environment in the form of a hydrogel. The human mesenchymal stem cells (hMSC) were loaded to *sacran* hydrogel. After 6 days, a number of cells could grow in the whole area. This indicated that *sacran* hydrogel is cell compatible. Furthermore, the cell showed orientation according to the microfiber's alignment around the edge area (**Figure 2.19**). The optimized condition is at 5×10^{-1} wt% with the initial cell density 100,000 cells/ mL. The main factors that affected cell attachment, shape and, orientation on *sacran* hydrogel substrate are 1) the softness of hydrogel and, 2) the roughness of micropattern. So, the results supported the hypothesis that *sacran* microfiber's alignment could control the cell orientation, which would affect to the cell function and differentiation. This research will help to better understand how cells respond to polysaccharide micropattern and will aid to the development of a new straightforward cell orientation.

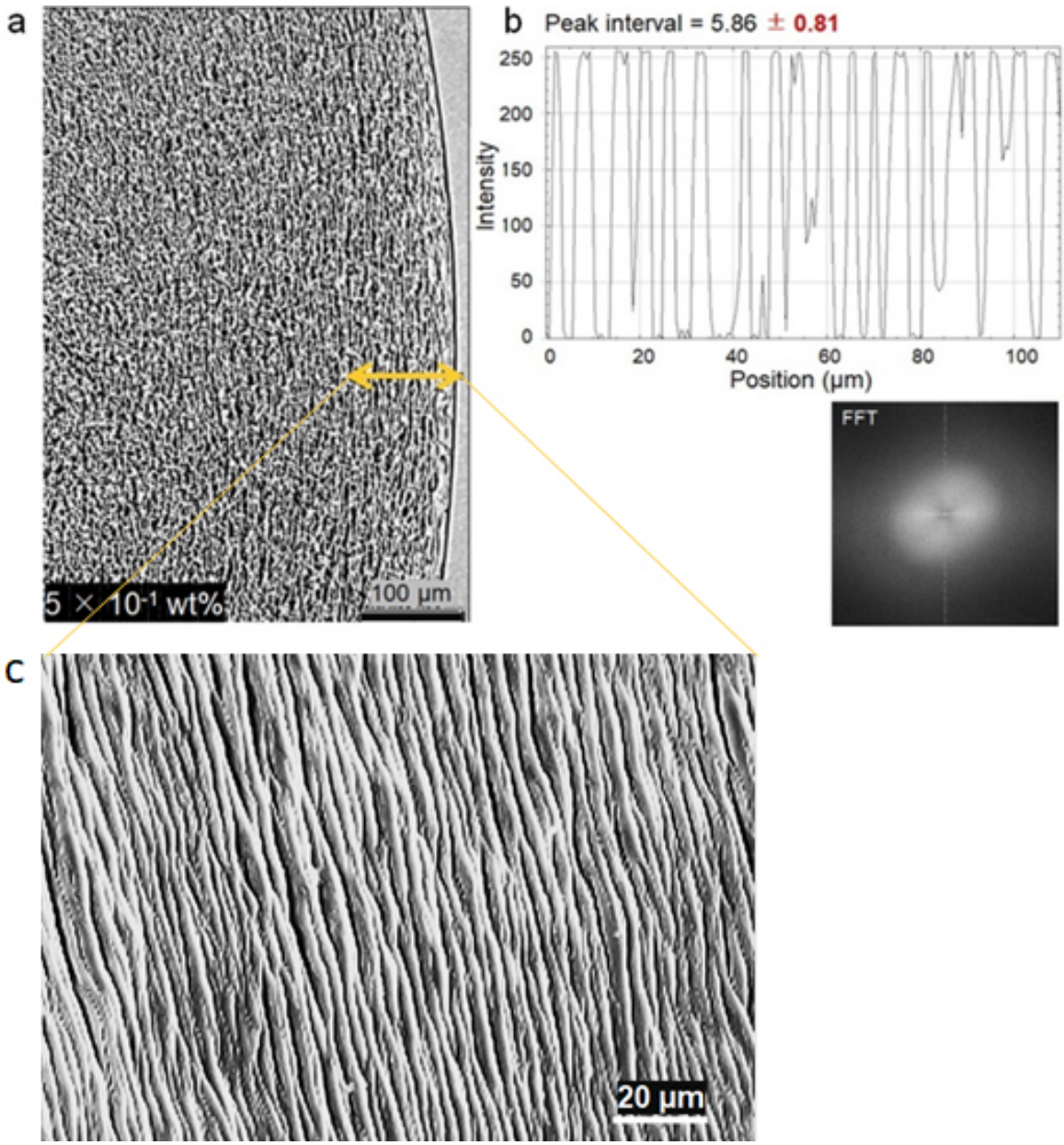

Figure 2.18 a. Optical microscopic images at the edge of the droplet drying record, b. the evaluation of the orientation, FFT means *fast Fourier transform.* c. SEM image of oriented microfibers at initial concentration of sacran: 5×10^{-1} wt%, drying temperature ~25 °C.

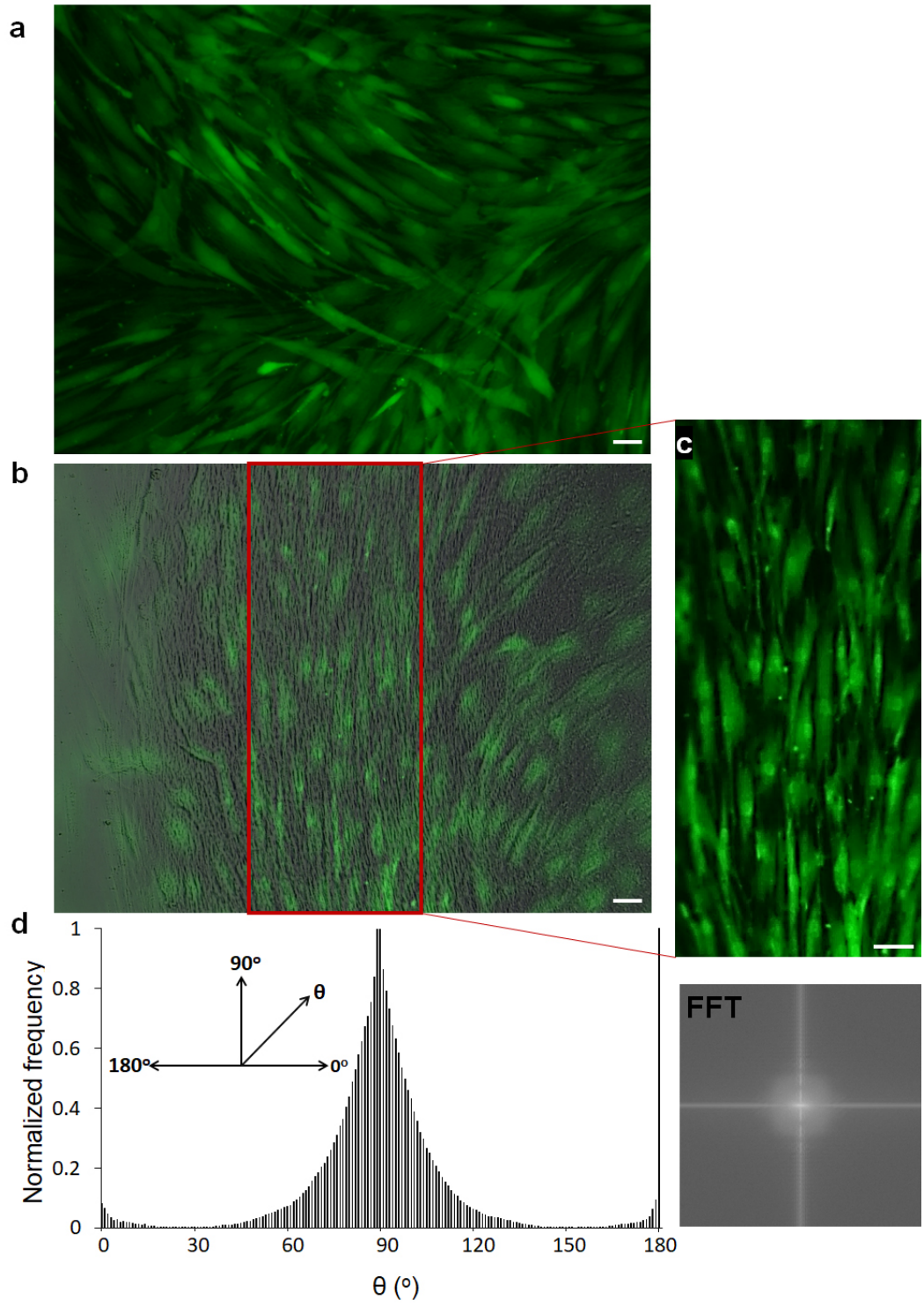

Figure 2.19 a. fluorescent images of hMSCs with the cells density 100,000 cells/mL seeded on on the polystyrene substrate for 6 days. b. the cells seeded on sacran dried droplet 5×10^{-1} wt% for 6 days. hMSCs were stained by Calcein-AM. All scale bars are 100 µm. c. zoom in oriented cells at the edge area. d. histogram data of the distribution of angle θ, of the extended cell along with the sacran orientation pattern around the edge. FFT means *fast Fourier transform of* area c.

Other Supplementary Materials for chapter 2 include the following:

Movie S1. Snaking structure formation.

Structure formation in the direction of the moving interface. See also Figure 2.7.

Movie S2. Water vapor sensing demonstration.

Actual speed. See also Figure 2.13.

Movie S3. Transformation from twisted M-fibers to snaking M-fibers.

See also Figure 2.17.

Movie S4. Effect of solvent vapor on film motion.

The film was exposed to a vapor environment of water, concentrated acetic acid, concentrated formic acid, ethanol, hexane, diluted acetic acid (pH2), and diluted ammonia (pH12) at ~25 °C and atmospheric pressure.

2.4 Conclusion

The polysaccharide *sacran* was studied morphologically as a self-assembling microfiber and used in the preparation of a humidity-sensitive actuator. It was determined that the microfiber had a diameter of ~1 μm and formed of a torsional self-assembled structure of nanofibers with diameters of ~50 nm. This structure was stable in pure water. Upon adding monovalent cations such as Na+ from NaCl, the microfiber is capable of disassembling into submicrometer-scale particles. The microfibers tended to integrate into a uniaxially oriented state along the contact line of the evaporative air-water interface. When one side of the microfibers was fixed, they drastically transformed into 2D snaking and 3D twisted structures. The velocity of the contact line movement during drying affected the structure formed because of the capillary forces at work between the microfibers. The evaporative air-water interface also induced multi-twisted structures to form from multiple microfibers, thereby showing that this material has self-similar nano and microstructures: the snaking and twisted fibers made possible a film exhibiting millisecond-response repulsive motion to water vapor. It would be feasible to produce a variety of soft actuators responding to various changes in the external environment, such as light, pH, and temperature, by inserting functional molecules into the microfiber. This study's method for creating vapor sensors not only advances our understanding of how self-assembled structures respond to stimuli, but it also aids in the development of environmentally adapting materials with a high potential for long-term use. We envision that this approach is capable of reconstructing additional natural materials towards developing advanced microsensors. Moreover, the scaffold of highly oriented M-fibers was successfully prepared. This could be a excellent place to start looking into cell orientation in relation to M-fibers for the new material design.

2.5 References

[40] E. D. Sonnenburg, H. Zheng, P. Joglekar, S. K. Higginbottom, S. J. Firbank, D. N. Bolam, J. L. Sonnenburg, Cell 2010, 141, 1241.

[41] R. A. A. Muzzarelli, J. Boudrant, D. Meyer, N. Manno, M. Demarchis, M. G. Paoletti, Carbohydr. Polym. 2012, 87, 995.

[42] M. Rinaudo, Prog. Polym. Sci. 2006, 31, 603.

[43] B. H. A. Rehm, Nat. Rev. Microbiol. 2010, 8, 578.

[44] J. K. Francis Suh, H. W. T. Matthew, Biomaterials 2000, 21, 2589.

[45] R. D. Astronomo, D. R. Burton, Nat. Rev. Drug Discovery 2010, 9, 308.

[46] Z. Wang, Z. Wang, W. W. Lu, W. Zhen, D. Yang, S. Peng, NPG Asia Mater. 2017, 9, e435.

[47] Z. Liu, Y. Jiao, Y. Wang, C. Zhou, Z. Zhang, Adv. Drug Delivery Rev. 2008, 60, 1650.

[48] A. Isogai, T. Saito, H. Fukuzumi, Nanoscale 2011, 3, 71.

[49] Y. Hashimoto, S. Mukai, S. Sawada, Y. Sasaki, K. Akiyoshi, ACS Biomater.

Sci. Eng. 2016, 2, 375.

[50] G. M. Whitesides, B. Grzybowski, Science. 2002, 295, 2418.

[51] T. Tanaka, Phys. Rev. Lett. 1978, 40, 820.

[52] Y. Osada, H. Okuzaki, H. Hori, Nature 1992, 355, 242.

[53] R. Yoshida, K. Uchida, Y. Kaneko, K. Sakai, A. Kikuchi, Y. Sakurai, T. Okano, Nature 1995, 374, 240.

[54] H. Okuzaki, T. Kuwabara, K. Funasaka, T. Saido, Adv. Funct. Mater. 2013, 23, 4400.

[55] H. Zhang, L. Li, M. Möller, X. Zhu, J. J. H. Rueda, M. Rosenthal, D. A. Ivanov, Adv. Mater. 2013, 25, 3543.

[56] L. T. De Haan, J. M. N. Verjans, D. J. Broer, C. W. M. Bastiaansen, A. P. H. J. Schenning, J. Am. Chem. Soc. 2014, 136, 10585.

[57] H. Arazoe, D. Miyajima, K. Akaike, F. Araoka, E. Sato, T. Hikima, M. Kawamoto, T. Aida, Nat. Mater. 2016, 15, 1084.

[58] K. Matsumoto, N. Sakikawa, T. Miyata, Nat. Commun. 2018, 9, 2315.

[59] Y. Hu, Z. Li, T. Lan, W. Chen, Adv. Mater. 2016, 28, 10548.

[60] Y. Yu, M. Nakano, T. Ikeda, Nature 2003, 425, 145.

[61] A. Sidorenko, T. Krupenkin, A. Taylor, P. Fratzl, J. Aizenberg, Science 2007, 315, 487.

[62] Y. Takashima, S. Hatanaka, M. Otsubo, M. Nakahata, T. Kakuta, A. Hashidzume, H. Yamaguchi, A. Harada, Nat. Commun. 2012, 3, 1270.

[63] M. Ma, L. Guo, D. G. Anderson, R. Langer, Science 2013, 339, 186.

[64] P. Egan, R. Sinko, P. R. Leduc, S. Keten, Nat. Commun. 2015, 6, 7418.

[65] L. Ionov, Langmuir 2015, 31, 5015.

[66] G. M. Whitesides, Angew. Chem., Int. Ed. 2018, 57, 4258.

[67] K. Kumar, C. Knie, D. Bléger, M. A. Peletier, H. Friedrich, S. Hecht, D. J. Broer, M. G. Debije, A. P. H. J. Schenning, Nat. Commun. 2016, 7, 11975.

[68] M. K. Okajima, M. Ono, K. Kabata, T. Kaneko, Pure Appl. Chem. 2007, 79, 2039.

[69] K. Okeyoshi, G. Joshi, S. Rawat, S. Sornkamnerd, K. Amornwachirabodee, M. K. Okajima, M. Ito, S. Kobayashi, K. Higashimine, Y. Oshima, T. Kaneko, Langmuir 2017, 33, 4954.

[70] K. Okeyoshi, M. K. Okajima, T. Kaneko, Biomacromolecules 2016, 17, 2096.

[71] K. Okeyoshi, M. K. Okajima, T. Kaneko, Sci. Rep. 2017, 7, 5615.

[72] Materials and methods are available as supplementary materials at Page 22.

[73] M. C. Cross, P. C. Hohenberg, Rev. Mod. Phys. 1993, 65, 851.

[74] P. A. Kralchevsky, N. D. Denkov, Curr. Opin. Colloid Interface Sci. 2001, 6, 383.

[75] R. D. Deegan, O. Bakajin, T. F. Dupont, G. Huber, S. R. Nagel, T. A. Witten, Nature 1997, 389, 827.

[76] P. J. Yunker, T. Still, M. A. Lohr, A. G. Yodh, Nature 2011, 476, 308.

[77] P. G. de Gennes, F. Brochard-Wyart, D. Quere, Capillarity and Wetting Phenomena: Drops, Bubbles, Pearls, Waves, Springer, New York 2003.

[78] M. K. Okajima, R. Mishima, K. Amornwachirabodee, T. Mitsumata, K. Okeyoshi, T. Kaneko, RSC Adv. 2015, 5, 86723.

CHAPTER III

SUPER-MOISTURIZING MATERIALS FROM MORPHOLOGICAL TRANSFORMABLE SUPERGIANT POLYSACCHARIDE

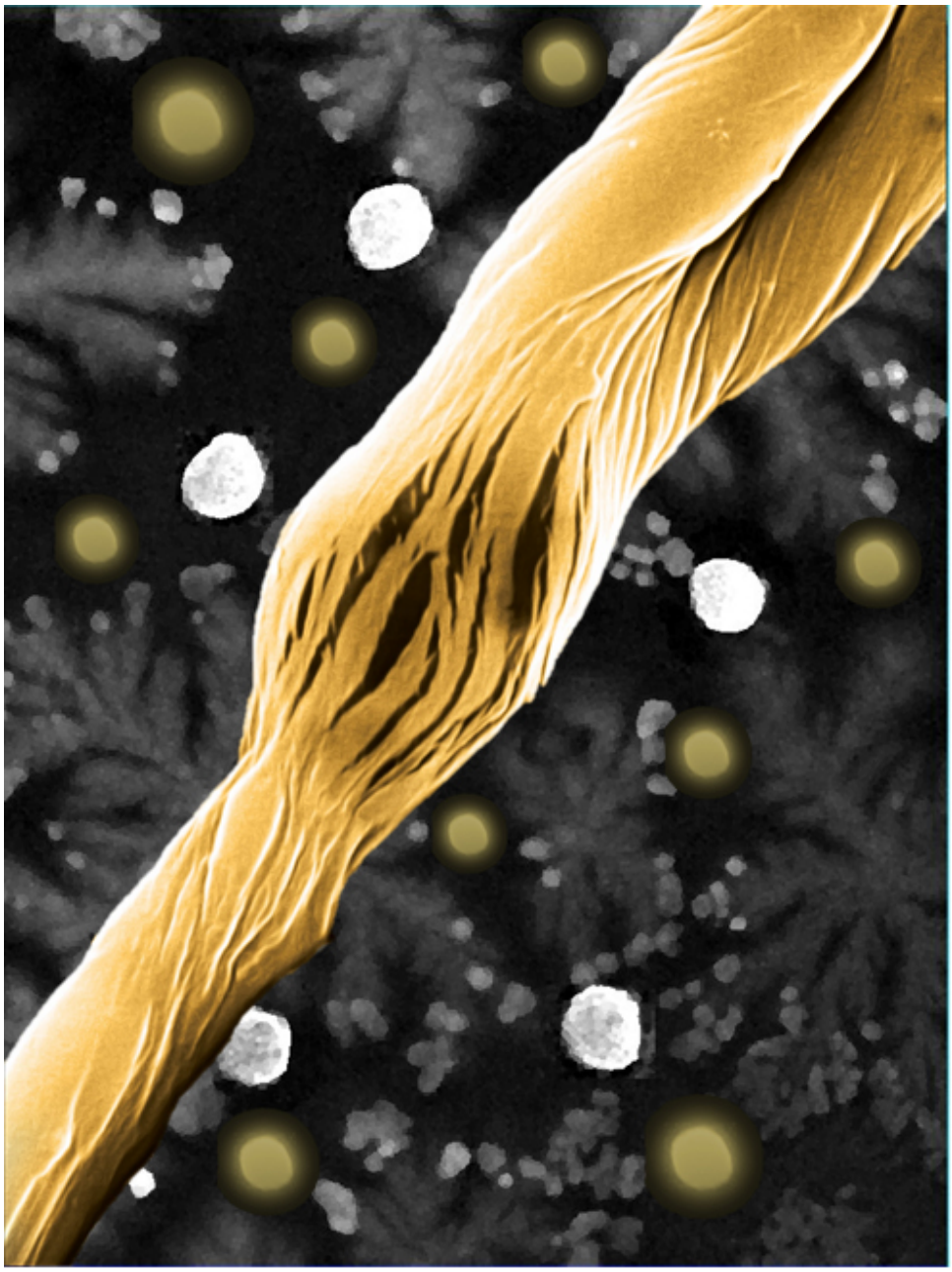

3.1 Introduction

Polysaccharides are biopolymers made up of monosaccharides linked by glycosidic bonds that are extracted from plant, animal, microbial, and algal sources. They are frequently found in high abundant, water soluble, and easily processed biomaterials that are fairly affordable cost.[79],[80] Because of the diversity of polysaccharides and their natural sources, they can produce biocompatible and biodegradable systems with a wide range of biological and chemical functionality that is useful for drug delivery applications. Drugs can be absorbed onto surface compartments or bonded to the external surface when utilizing polysaccharides as particles.[81] This can improve the drug's aqueous solubility and the stability of drugs and other unstable therapies like proteins.[82]-[86] In particular, drug carrier material is frequently done in nanoparticle formTheir small size helps them to cling to mucosal surfaces for oral or nasal delivery, after which they are delivered to cells via intracellular transport. [87]-[91] However, polysaccharides may have broad and/or mixed molecular weights and, that some polysaccharide chemistry is extremely changeable. As a result, it difficult to predict or limits the potential use in drug administration.[92] *Sacran* polysaccharide could be extracted with a low polydispersity index of the molecular weight. It also has beneficial properties for use with living organisms, including cell compatibility, anti-inflammatory properties, and water solubility. As a respect, it could be an excellent option for developing a novel polysaccharide nano-micro carrier.

In this study, the morphological change from a polysaccharide microfiber to micro-nano particles is studied under controlled polymer concentration, salt addition and, sonication (**Figure 3.1**). Firstly, the reversible self-assembly/disassembly of micrometer-scale fibers are determined in vitro depending on the dilution/concentration effect. The *sacran* microfibers are able to transform into small fragments on a nanometer scale due to the diluted state of the polymer concentration. Secondly, a method for inducing the morphological transformation from microfibers to microparticles based on a salination effect is also demonstrated. The *sacran* microfibers are capable of disassembling on a nanometer-scale fragments in NaCl aqueous solution. According to a high salt concentration, this could be further proceeded to form microparticles through the self-organization of polysaccharides. Dilution and salination could reduce entangle ability of the polymer chain. Hence, the interaction between polymer chains is the main factor that caused the morphological transformation of the microfibers. Lastly, the sonication effect is considered, the polysaccharide chains are cut due to a cavitation effect from the sonication process. The shock wave could induce the morphological change of *sacran* microfibers to *sacran* spherical shape in the nanoscale to a micrometer. On account of the facile and non-organic solvent of the particle preparation, this material could be the alternative option in the green chemistry and medical material field.

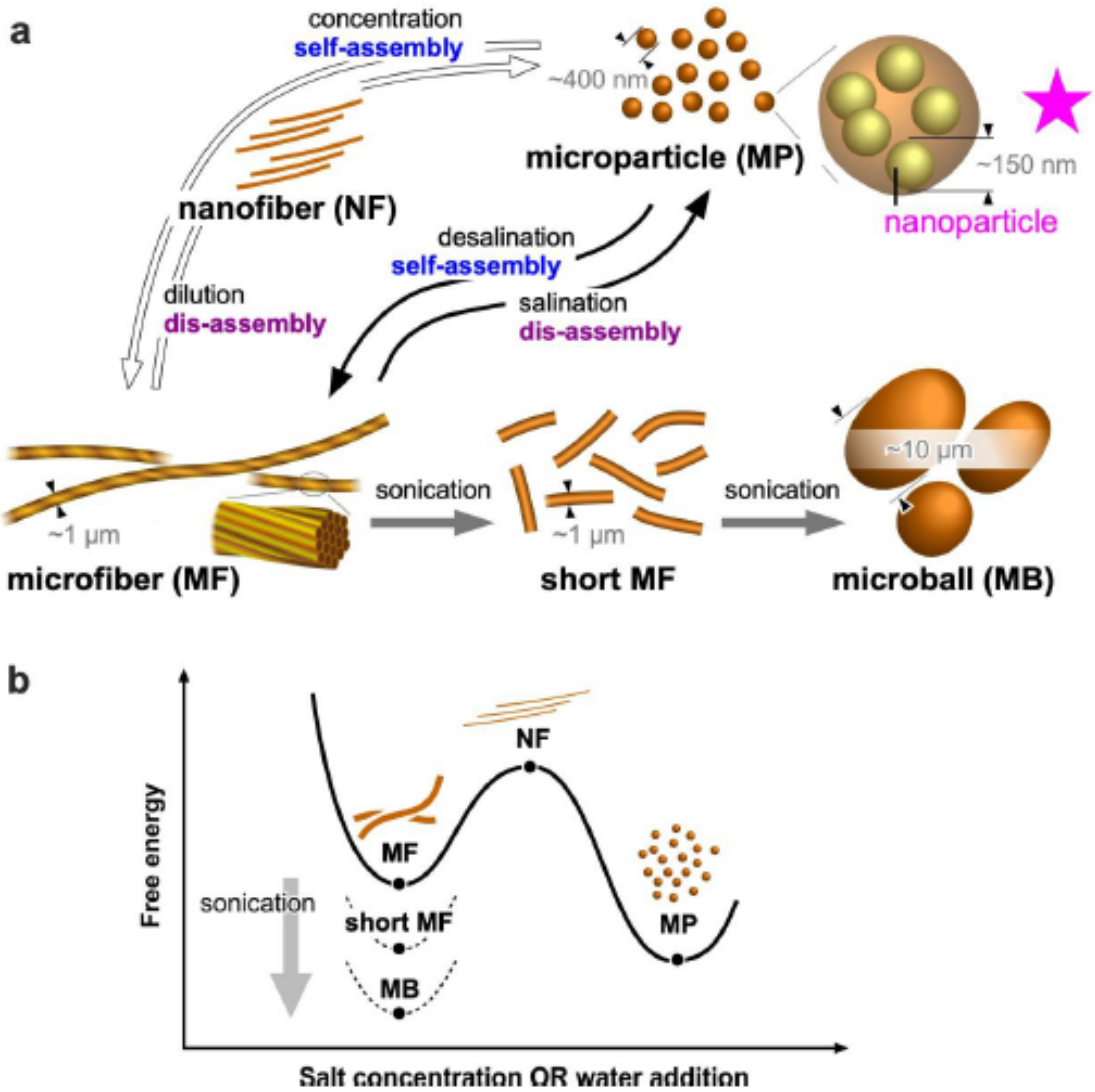

Figure 3.1 The hypothesis of morphological instability of polysaccharides, *sacran*.

a. Schematic illustration of morphological changes under the control of polymer concentration, salt concentration, and sonication.

b. Correlation of underwater environment and metastable morphological states.

3.2 Materials and Methods

3.2.1 Materials

The average of *sacran* initial molecular weight used in the experiment was measured by size exclusion chromatography with multi-angle light scattering: M_n = 5.327×10^6 g/mol, M_w = 5.418×10^6 g/mol (M_w/M_n = 1.017). NaCl was provided by Kanto Chemical Co. and used without further purification.

3.2.2 Dilution and concentration study

The *sacran* solution was prepared by dissolving the appropriate amount of *sacran* in deionized water at room temperature (~25 °C). Then it was homogenized using a mechanical stirrer, and at least 6 h was allowed to elapse before use. To study the dilution effect, deionized water was added in appropriate amount to the solution. After that, the solution was homogenized by vortexing. To study the concentration effect, the Amicon® Ultra filter device with Ultracel™-PL regenerated cellulose membranes MWCOs 100 kDa was used to remove water from the initial solution.

3.2.3 Salination and desalination study

To study ionic effects, 0.5 mM and 1 mM aqueous solutions of NaCl were used instead of deionized water to make the *sacran* solution. To remove NaCl, the solution was washed by deionized water the Amicon® Ultra filter with MWCOs 100 kDa. So, the concentration of polymer could be controlled by fixed solution volume.

3.2.4 Sonication effect study

Sonication was applied using a vibra-cell ultrasonic liquid processor from sonics & materials, inc. which has processing frequency 20 kHz ± 50 Hz. The ultrasonic energy was applied 50 second on and 10 second off pulser at the amplitude 40%. The total energy input energy was treated from 200 J/mL to 1,000 J/mL using a 13 mm diameter probe to 50 mL *sacran* solution in 150 mL PYREX beaker, which was kept in an ice bath during ultrasonication to avoid overheating. The sample temperature was set at the temperatures 40 °C.

3.2.5 Microscopy observations

The *sacran* ultrasonic treated solutions (1–3 μL) were dropped onto a silicon wafer and dried at ~25°C and 1 atm. The samples were then coated with gold (Au) for 10 nm thickness. The dried particles were observed at the submicron scale with an emission scanning electron microscope (TM3030Plus, Hitachi). Scanning was performed under high vacuum at an ambient temperature (~25 °C) with a beam voltage of 10 kV. For transmission electron microscopic observation, the samples were prepared by dipping carbon coated copper grid on the particle solution then dry it. The observation was operated by Hitachi H-7650 with a voltage of 100 kV.

3.2.6 Dynamic light scattering (DLS)

The hydrodynamic diameters of *sacran* particles were performed using a Zetasizer Nano ZS90, Malvern Instruments Ltd., England. The measured scattering light intensity is displayed as photon count rate with a unit of kilo count per second (kcps). A disposable folded capillary cell (DTS1070) was used as a sample container. Zetasizer Software was used to analyze the data.

3.2.7 Gel permeation chromatography (GPC)

The GPC machine with a fused Silica column was used to analyze the molecular weight of the polymer. The mobile phase consisting of pure water and 0.100 N Sodium nitrate. The sample injection amount was typically 10 µg. The flow rate was maintained at 1 mL/min with a column temperature of 40 °C, and elution was monitored at 665 nm. The DAWN® HELEOS® II multi-angle static light scattering (MALS) detector was used to detect the molar mass and size of macromolecules in the solution.

3.2.8 Thermogravimetric analysis (TGA)

Thermal analysis and the decomposition temperature of the dried polymer were detected using Seiko Instruments SII, SSC/5200. After loading samples of the *sacran* in flat platinum pans, the measurements were taken under nitrogen at a heating rate of 5 °C/min. Thermogram was recorded from the temperature 25-400 °C.

3.2.9 Differential scanning calorimetry (DSC)

The freezable water and non-freezable bound water in the *sacran* hydrogel were measured by Seiko Instruments SII, X-DSC7000T at a scanning rate of 5 °C/min from -80 °C to 25°C under nitrogen gas. Samples were placed in a sealed aluminum pan and weighed before and after the measurements.

3.2.10 Drying behavior of the *sacran* microgels comparing with the conventional *sacran* fibers

The *sacran* died samples were prepared as 0.050 wt%. Then, the solutions (1–3 µL) were dropped onto a non-modified glass slide and dried at ~25 °C, 1 atm with the relative humidity (RH) 20-30%. The drying behavior was recoded continuously for 24 h by an optical microscope (IX73, Olympus).

3.3 Results and discussion

3.3.1 Dilution/concentration effect

Sacran is extracted from *Aphanothece sacrum*. It is a soluble polysaccharide with 10^6–10^8 g/mol molecular weight.[93] The previous report clearly indicated that *sacran* exists in water as a microfiber.[94] **Figure 3.2a and 3.2b** show optical microscopic images of dried *sacran* in different concentrations. The self-assembly/disassembly of *sacran* microfibers depends on the initial concentration of the polysaccharide. Based on illustrations from the dilution effect (**Figure 3.2a**), morphological changes of *sacran* could be discussed as a function of overlap concentration (c^*) and entanglement concentration (c_e) (**Figure 3.2c**). From the studied chain conformation of *sacran*, it indicated that c^*=0.004 wt% and c_e=0.015 wt%.[95] In a concentration of less than 0.004 wt%, the *sacran* chain will behave like an isolated negative charge polymer. As it is shown in the optical microscopic images of 0.001 wt%, no microfibers could be observed in this condition. Still, stripes with the same direction on the background of the images could be suspected as *sacran* nanofibers, which was also confirmed by the electron microscopic image on a scale of ~50 nm (**Figure 3.2d**). The concentration ranges between 0.004-0.015 wt% is in the semi-dilute unentangled state, *sacran* chain still have not shown clear microfibers assembling in the images of 0.005 wt% and 0.010 wt%. There is more possibility to overlap one another of the polymer chains at the concentration over than the c_e. The higher concentration of the polymer chain was prepared, the more interaction between fibers was created. The microfibers assembling of *sacran* were clearly observed starting from the semi-dilute entangled state as shown in the images of 0.030 wt% and 0.050 wt%. The density of fibers per unit area and the fiber length is increased depending on the increasing of *sacran* concentration. In the range of concentrations between 0.015 and 0.050 wt%,[95] *sacran* chains have many opportunities to overlap each other as a semi-rigid microfibers (**Figure 3.1, 3.2e**). The dilution and concentration effect were studied vice versa to confirm that this process

is reversible (**Figure 3.3**). The results suggested that the reversible morphological transformation of *sacran* microfibers could be proceeded by varying the initial concentration. Moreover, at the concentration under *c**, more nanofragments were observed because the polymer chain could be hydrated to dissolve more in that state (**Figure 3.2d**).

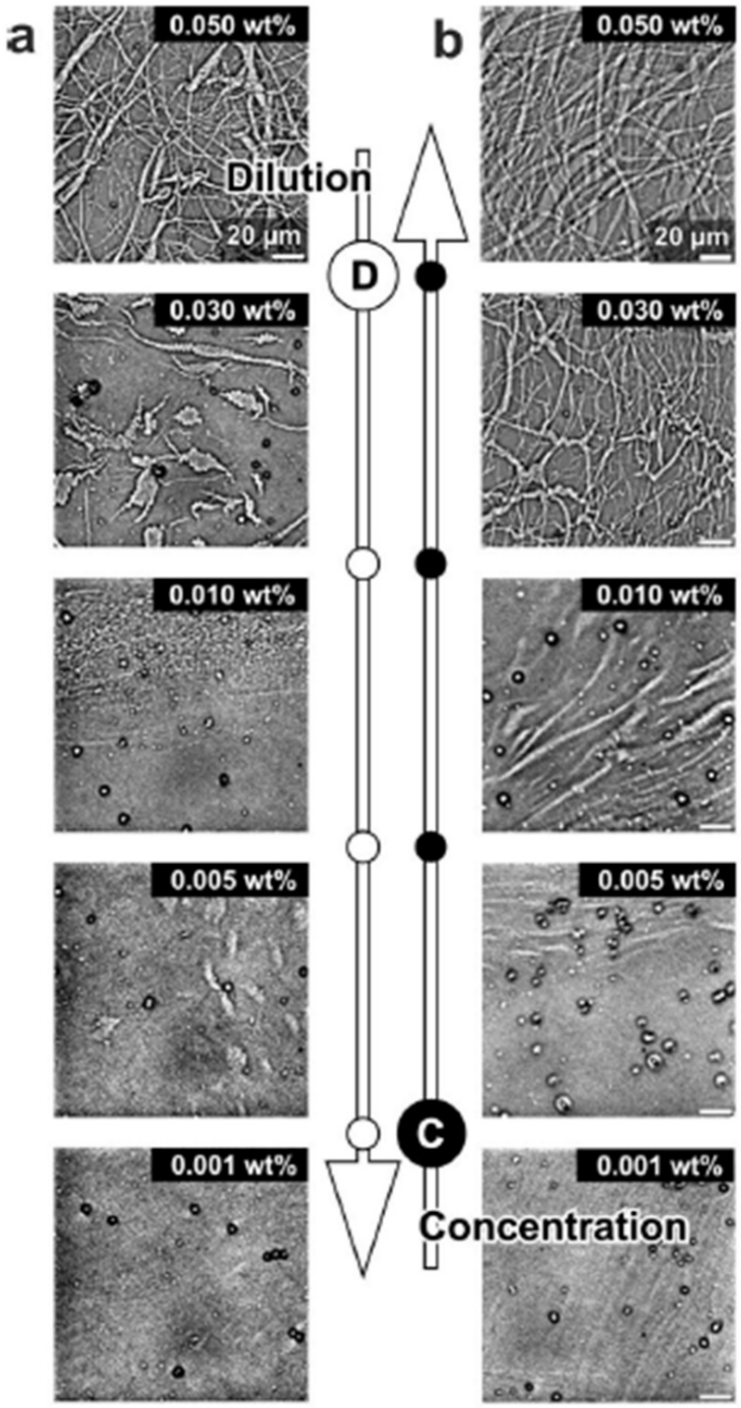

Figure 3.2 Sacran concentration effect on microfiber formation. a. Optical microscopic images of sacran for disassembled from microfibers to microparticles by dilution. **b** Optical microscopic images of sacran self-assembled from microparticles to microfibers by concentration. All scale bar = 20 μm.

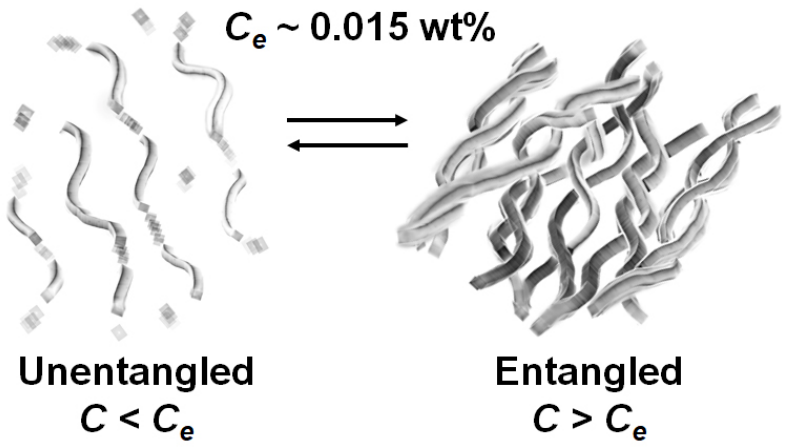

Figure 3.2c The illustration of assembly/dis-assembly mechanism of sacran microfibers and nanofragments.

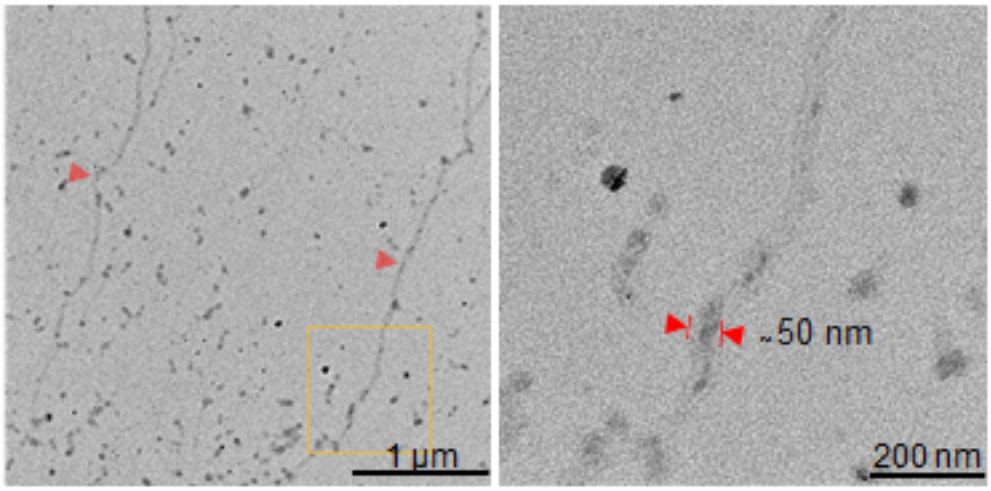

Figure 3.2d Transmission electron microscopic image of sacran at concentration 0.010 wt%.

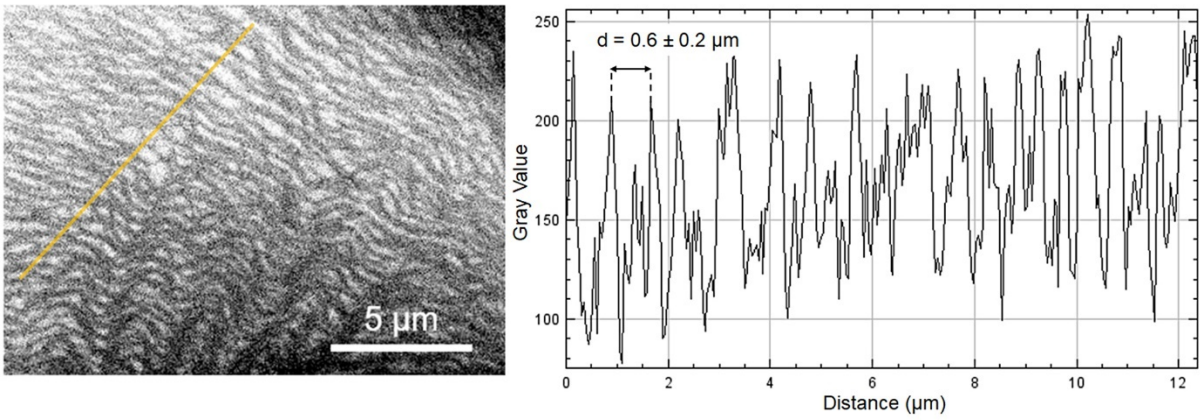

Figure 3.2e Scanning electron microscopic image of sacran at concentration 0.050 wt% and gray scale graph indicating the fiber alignment.

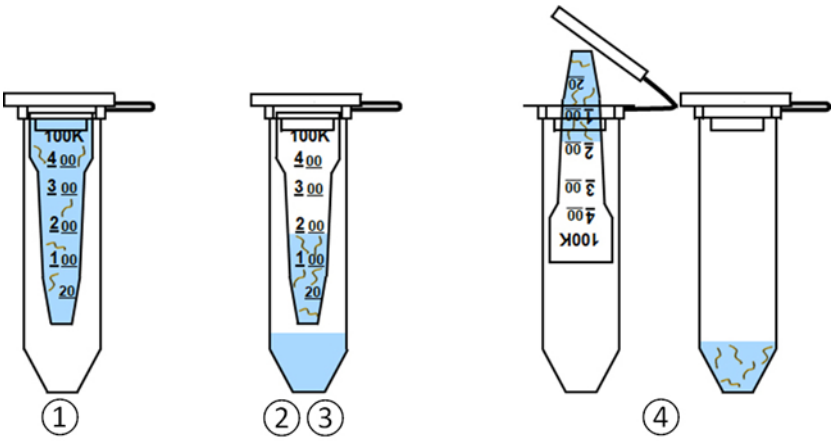

Figure 3.3 Methodology of increasing polymer concentration using ultra filter device.

1. Add 500 µL of sample to the Amicon® Ultra filter device and cap it.
2. Spin the device at 14,000 × *g* until it reaches the proper final volume.
3. Remove the filtrate solution from microcentrifuge tube.
4. Recover the concentrated solution in a clean microcentrifuge tube.

The calculation of the proper final volume for the study of concentration effect

Starting concentration; $N_1 = 0.005$ %wt

Starting volume; $V_1 = 500$ µL

Final concentration; $N_2 = 0.01$ %wt

Final volume; $V_2 = (N_1 \times V_1)/ N_2$

$= (0.005 \times 500)/ 0.01$

$= 250$ µL

3.3.2 Salination/desalination effect

Consider another factor that affects the microfiber assembling/disassembling process. The salination could disassemble the microfiber into submicrometer-scale particles. This salting effect was studied by adding different concentrations of NaCl into the *sacran* solution 0.050 wt%. To understand the effect of the salt ions on the polymer, the NaCl concentration in the aqueous mixture was determined by estimating the number of hydroxyl groups in the polymer, with one of the major side chains as the index value. As shown in the microscopy image of **Figure 3a**, the dried sample from the aqueous mixture with ~0 mM NaCl showed twisted MFs. The microscopy images of the sample from the mixture after the addition of 0.5 mM mM NaCl showed shorter MFs. Furthermore, with the addition of 1.0 mM NaCl, the MFs could not be observed. From **Figure 3.4a red arrow**, at *sacran* 0.050 wt% solutions with no NaCl added, dried *sacran* from microscopic record showed twisted microfibers with a size more than 1 μm. While the records from the solution with 0.5 mM NaCl added showed shorten microfibers. Furthermore, at 1.0 mM NaCl added none of the microfibers could be observed. The disassembly of the MFs into MPs is likely caused by the excess salt ions that lead to a decrease in hydrogen bonds among the internal structure, such as hydroxyl groups. Electrostatic free energy of the polymer was lowered by Na+ counterions, leads the increasing of the solvent activity, which resulting in higher solubility (**Figure 3.4c**). Increasing the solubility of polymer chains by added electrolyte known as a salting-in effect.[84][96][97] This is explained by the Debye–Huckel theory; the logarithm of solubility is proportional to the square root of the ionic strength.[98] The desalination process has been done to confirm that the dis-assembly microfiber from the salting effect is capable of proceeding in a reverse process. When the added NaCl was removed from the *sacran* solution (**Figure 3.6**), the microfiber could assemble as shown in the

microscopic images (**Figure 3.4a blue arrow**). In addition, the reversibility of microfiber assembly/dis-assembly was approved by the gel permeation chromatographs (**Figure 3.4b**). The chromatographs showed retention time ~15 minutes with Mw ~ 1.0×10^7 g/mol before salination. After salination, the peak split and shifted to retention time ~23 minutes with Mw ~ 1.0×10^3 g/mol (**Figure 3.5**). The salination/desalination process was reproduced several times to confirm the phenomena. The results indicated that the polymer was literally assembled/disassembled from micrometer to nanometer scale through desalination/salination effect respectively.

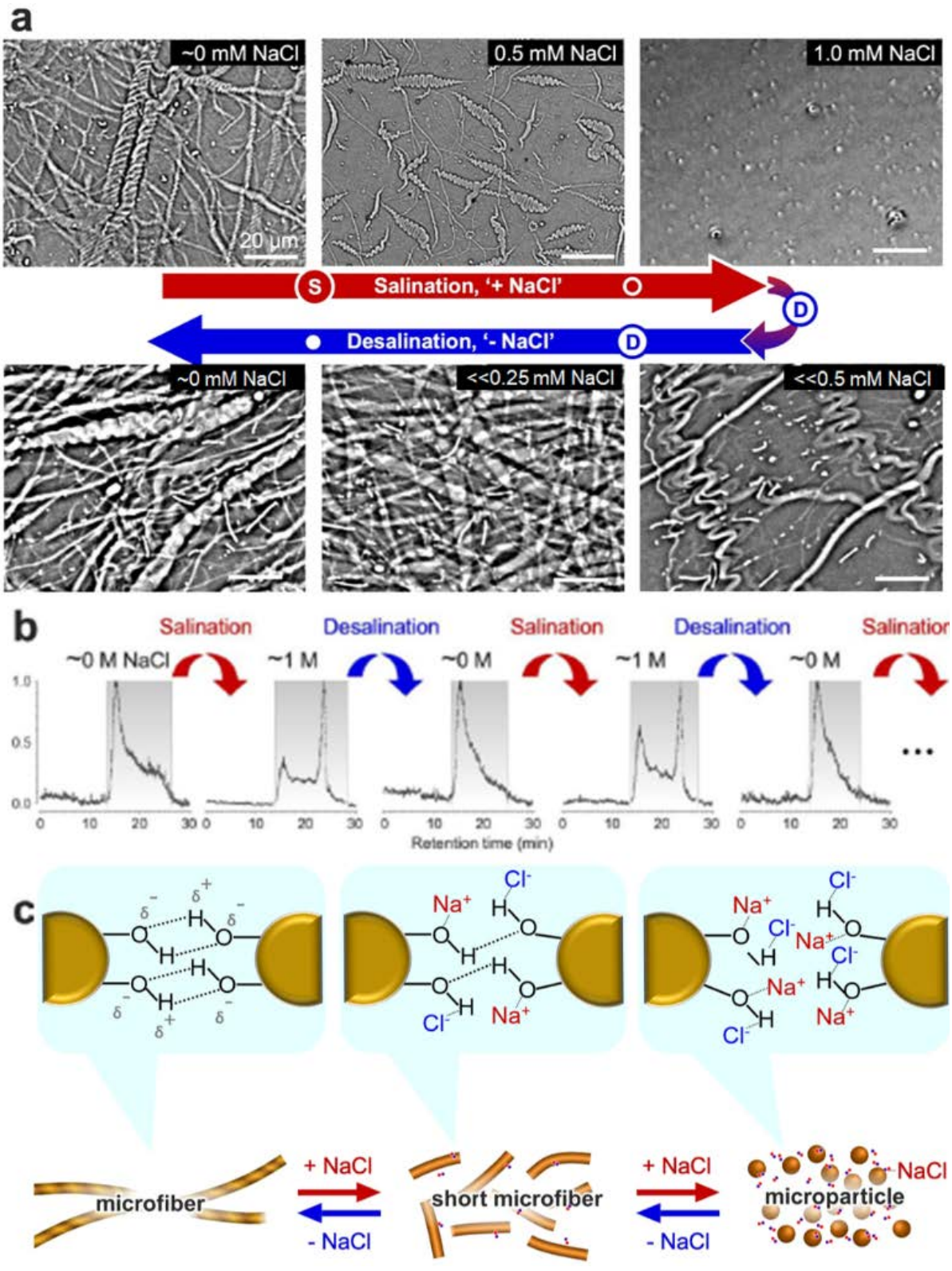

Figure 3.4 Effect of salination/desalination on *sacran* microfibers assembly/dis-assembly. a. Optical microscopic images of *sacran* salination/desalination. All scale bar = 20 μm **b.** Gel permeation chromatograph of *sacran* assembly/dis-assembly from salination/desalination process.

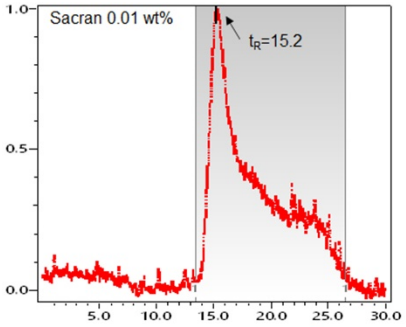

Molar mass moments (g/mol)

Mn		6.404×10^{6} (±26.187%)
Mw		1.101×10^{7} (±43.677%)

Polydispersity (Mw/Mn): 1.719 (±50.926%)

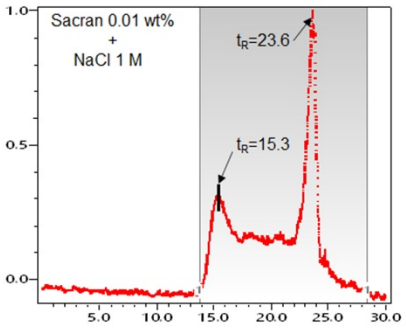

Molar mass moments (g/mol)

t_R=15.3	Mn	4.093×10^{6} (± 20.286%)
	Mw	4.463×10^{6} (± 22.652%)
t_R=23.6	Mn	3.388×10^{3} (± 20.279%)
	Mw	8.224×10^{3} (± 42.184%)
Average	Mn	3.549×10^{3} (± 21.377%)
	Mw	3.059×10^{4} (± 35.627%)

Polydispersity (Mw/Mn)

t_R=15.3	1.090 (±30.408%)
t_R=23.6	2.427 (±46.805%)
Average	8.620 (±41.548%)

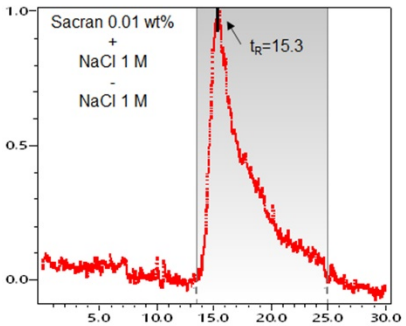

Molar mass moments (g/mol)

Mn		2.672×10^{5} (±54.992%)
Mw		4.562×10^{5} (±43.014%)

Polydispersity (Mw/Mn): 1.707 (±69.816%)

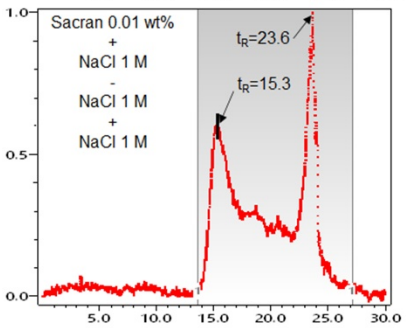

Molar mass moments (g/mol)

t_R=15.3	Mn	1.059×10^{7} (± 29.553%)
	Mw	1.179×10^{7} (± 31.130%)
t_R=23.6	Mn	6.312×10^{2} (± 59.688%)
	Mw	1.330×10^{3} (± 72.060%)
Average	Mn	1.995×10^{3} (± 50.781%)
	Mw	1.033×10^{4} (± 38.699%)

Polydispersity (Mw/Mn)

t_R=15.3	1.113 (±42.924%)
t_R=23.6	2.107 (±93.570%)
Average	5.178 (±63.846%)

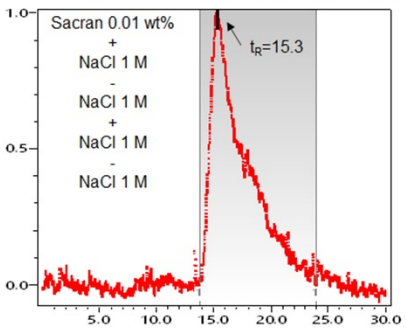

Molar mass moments (g/mol)

Mn	2.661×10^{6} (±63.663%)
Mw	3.468×10^{6} (±56.466%)

Polydispersity (Mw/Mn): 1.303 (±85.096%)

Figure 3.5 GPC results of *sacran* with salt addition showed reversible of assembling/disassembling process.

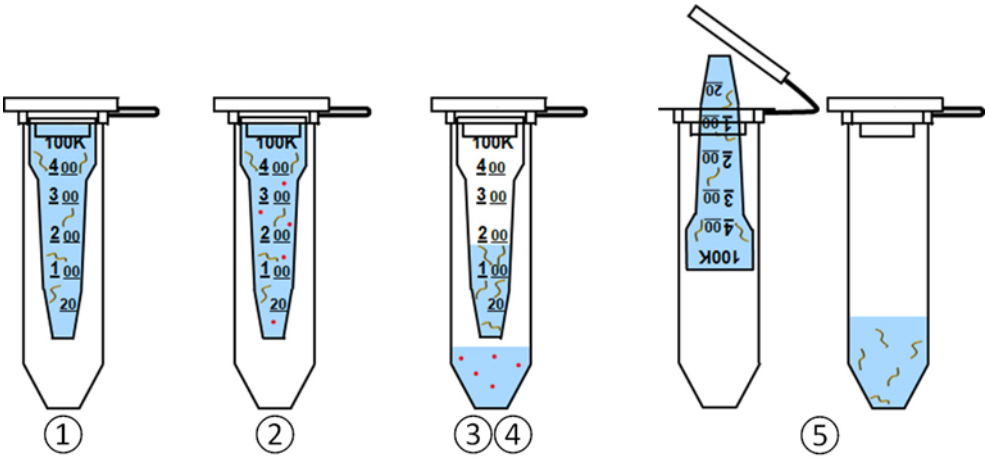

Figure 3.6 Methodology of removing salt form the solution using ultra filter device.

1. Add 500 µL of sample to the Amicon® Ultra filter device and cap it.
2. Spin the device at 14,000 × *g* until it reaches the 200 µL.
3. Remove the filtrate solution from microcentrifuge tube.
4. Add DI water 300 µL to the concentrated solution in the Amicon® Ultra filter device again.

   (Repeat step 1-4 for 10 times)
5. Recover the 500 µL of sample solution in a clean microcentrifuge tube.

As the dilution and salination effect on the microfibers' morphological change to submicron fragments, the size and shape are still uncontrollable. Accordingly, controllable morphology would be challenged in terms of a number of production perspectives. From the dynamic light scattering graph of *sacran* diluted state (0.001 wt%), a broad peak from several 10-1,000 nanometer-size particles was shown in **Figure 3.7a**. After 10 mM of NaCl was added into the solution, a minor peak appeared around 50 nm owing to higher solubility from the salting-in effect. At last, 100 mM of NaCl was added, a unimodal distribution has dominantly appeared with a very narrow size distribution (PDI = 0.053). When NaCl was excess in the system, Na^+ and Cl^- competed with the polymer molecules in binding with water. The solvation shell around polymer chains would be decreased due to a relatively more minor affinity for the solvent, resulting in less soluble of the polymer.[96][99] The effects of salt on reducing the solubility of solute commonly referred to salting-out. The addition of electrolytes on nonelectrolytes is futher complicated by the fact that different types of intermolecular alternately play the main role in different environments such as type of salt, salt concentration and, solvent etc. Water molecules were moved away from the polymer leading to less interaction between polymer-water and more interaction between polymer itself. From **Figure 3.7b**, transmission electron microscopic image of polymer at 0.001 wt% showed round particle size around 500 nm. Inside of the particle, densely packed nanoballs size around 150 nm existed. After adding high content of salt, the size distribution became noticeably narrower. This might be owing to the isolated molecules of polymer salf associated with the enhancement of the salting-out effect. In the presence of high ionic concentration, water-ion is enthalpically favorable to arrange themselves to a cage-like around the solute.[97] The less hydrophilic part of polymer molecules is thus self associated with minimizing their surface that exposed to the water as densely packed particles (crystalline part in **Figure 3.7c, 3.8**). Then, the more hydrophilic part loosely wrapped outside (amorphous part in **Figure 3.7c, 3.8**) to balance the surface energy of the particle.

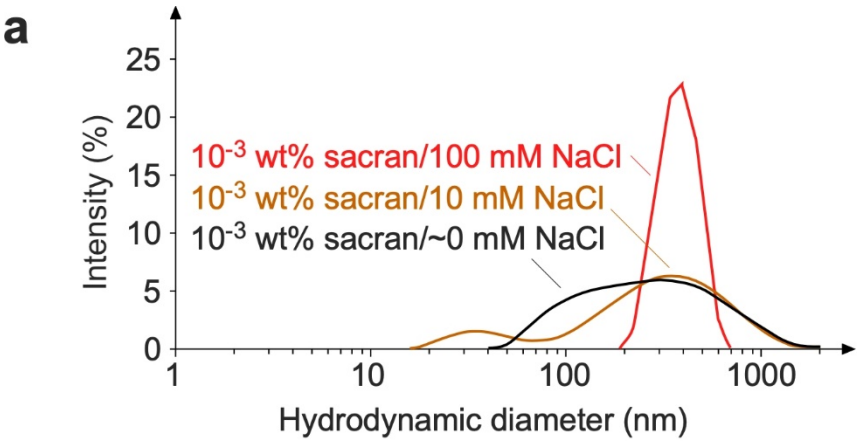

	D_h (nm)	St Dev (nm)	PDI
10^{-3} wt% sacran/~0 mM NaCl	340	262	0.597
10^{-3} wt% sacran/10 mM NaCl	396	244	0.381
10^{-3} wt% sacran/100 mM NaCl	383	88	0.053

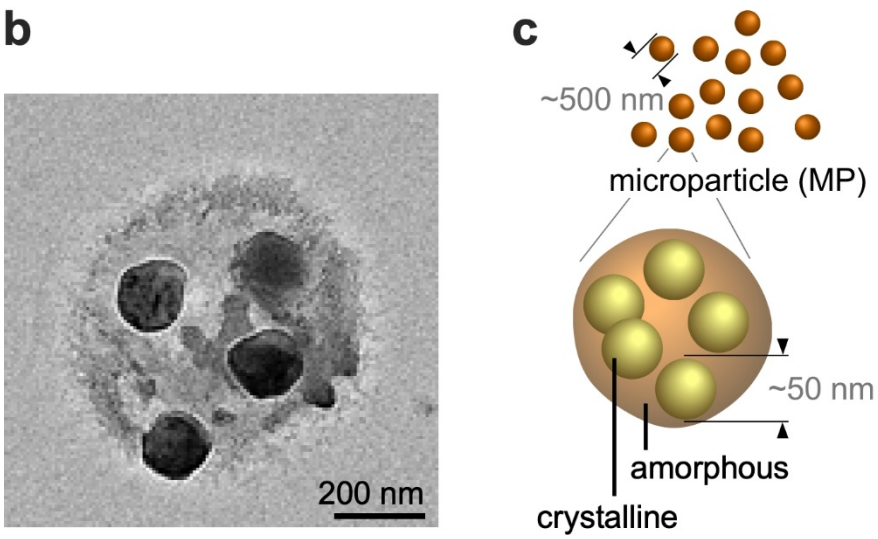

Figure 3.7 Effect of salt concentration on *sacran* microparticles formation.

a. Dynamic light scattering graph of *sacran* microparticle in different salt concentrations

b. Transmission electron microscopic image of *sacran* microparticles at *sacran* concentration 0.001 wt%.

c. Schematic illustration of *sacran* microparticles.

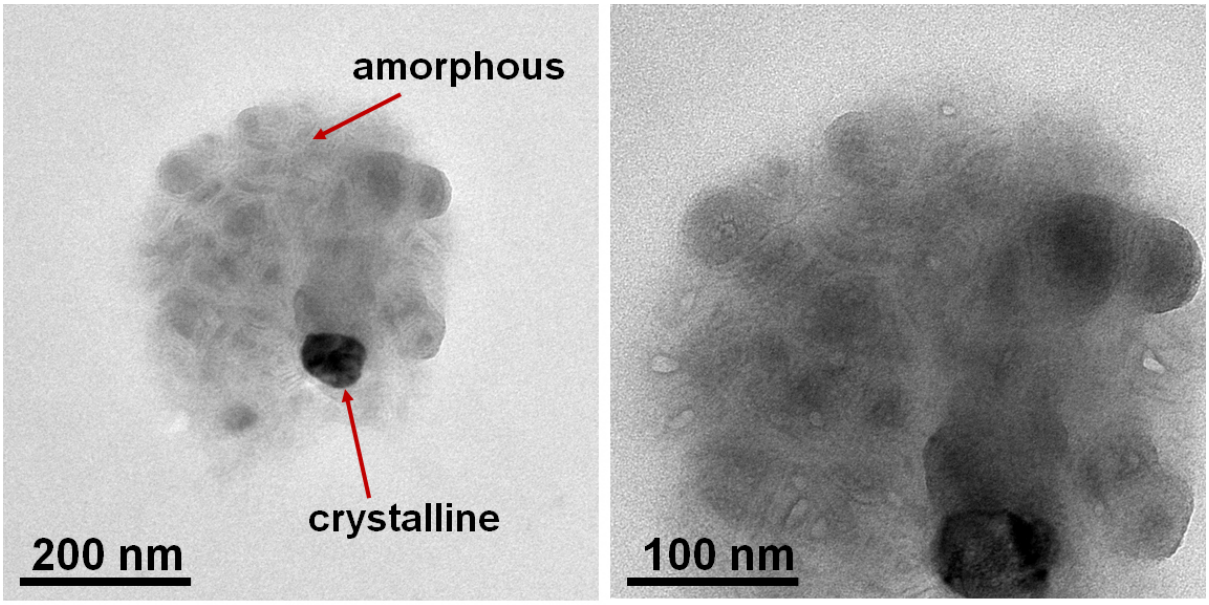

Figure 3.8 Transmission electron microscopic images of *sacran* particle showed crystalline and amorphous parts.

To study the *sacran* morphological change, the interaction between polymer chains is the most important factor. The microfibers transformed into particles by suppressing the intermolecular interaction while inducing self-association from the illustrated effect; dilution and salination. However, from the viewpoint of the quantity, a low number of qualified particles could be obtained from the above method because the particle would be formed with narrow size distribution under the isolation of a polymer chain (< 0.004 wt%) with a high concentration of salt. To overcome this problem, ultrasonication was chosen as another technique to induce the morphological transformation of *sacran* polymer.

3.3.3 Sonication effect

Ultrasonication is a facile and non-toxic technique to produce the narrow size distribution of the polymer scission caused by cavitations.[100] The polymer segments were pulled into the collapsing microbubble, which has a higher velocity than those segments further away.[101] The polymer chains become elongated and finally break apart due to high tension on the polymer backbone (**Figure 3.9a**). This process is a non-random process, as a scission generally occurs in the center of the chain.[102][103] At the concentration of 0.050 wt% (**Figure 3.10a**), after ultrasonic energy was applied for 1,000 J/mL, the polymer was cut into shortening fragments (**Figure 3.10b**) then transform into a micro ball when the energy reached 3,000 J/mL (**Figure 3.10c**). Nonetheless, at this concentration, the polymers are in an entangled state. The polymer chains are not fully stretch in that condition. It is possible that some parts are in a coil conformation. This could reflect the randomness size of cutting products, as shown in **Figure 3.10c**. To improve the size distribution issue, the appropriate concentration for this experiment was optimized at 0.010 wt%. The polymer solution was treated by ultrasonic energy from 200, 400, 600, 800 and, 1,000 J/mL. The size distribution was gradually minimized from before ultrasonication to after ultrasonication 1,000 J/mL (**Table 3.1**). Moreover, the particles size was proved by dynamic light scattering tecnique. **Figure 3.11a, b, c** showed the gradually reducing of spherical particle size from 554.9, 494.8, 392.0, 331.5 and, 303.0 nm respectively. On the acount of cavitation effect, the polymer chian scission was confirmed by gel permeation chromatography technique (**Figure 3.11d**). The molecular weight of polymer was dramatically reduced from 5.418×10^6 g/mol for initial polymer solution to 6.049×10^5 g/mol for 1,000 J/mL of ultrasonic treated solution.

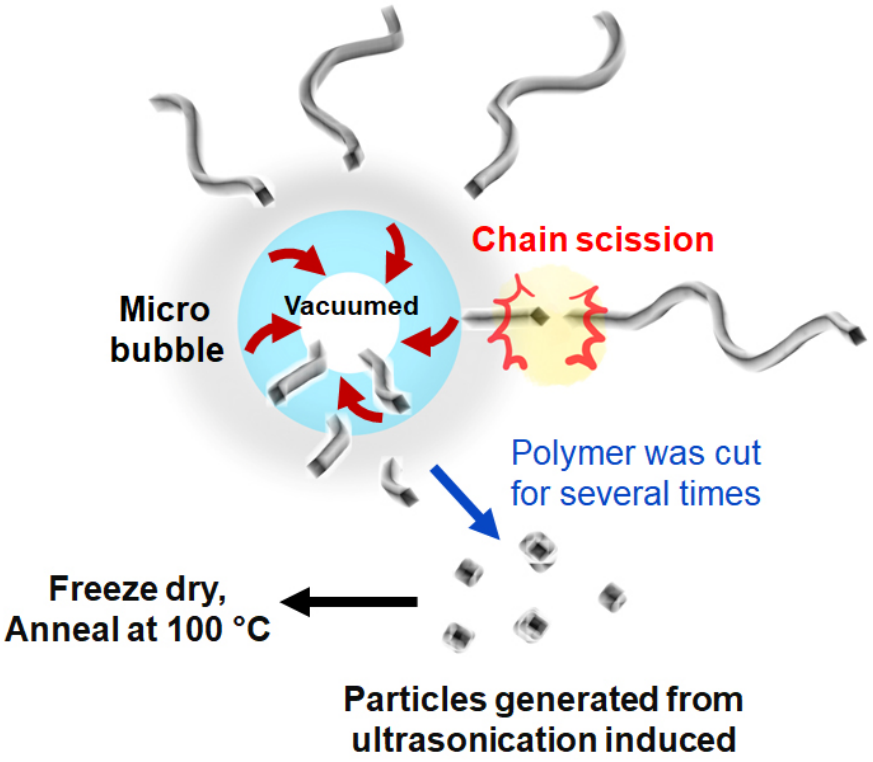

Figure 3.9 Effect of sonic energy to *sacran* particle formation.

The illustration of *sacran* sonicated annealed (SSA) preparation.

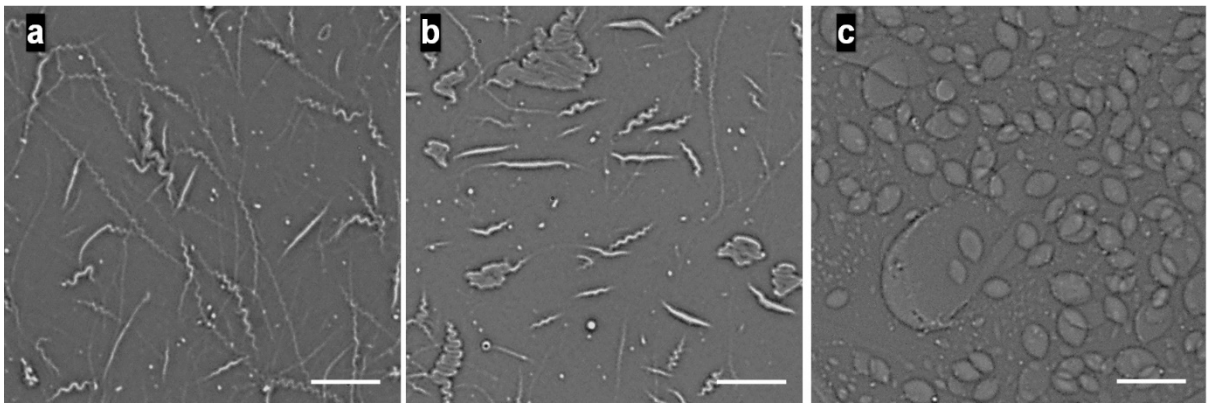

Figure 3.10 Optical microscopic images of *sacran* transformation from microfibers to micro balls induced by ultrasonication. All scale bars = 20 μm

Table 3.1 Ultrasonication effect to reduction of molecular weight and hydrodynamic size of *sacran* particles.

Energy (J/mL)	M_w (g/mol)	PDI (M_w/M_n)	D_h (d.nm)	St Dev (d.nm)	PDI $(\text{St Dev}/D_h)^2$
0	5.418×10^6	1.017	640.4	263.8	0.170
200	2.510×10^6	1.121	554.9	187.1	0.114
400	9.271×10^5	1.251	494.8	154.2	0.097
600	7.666×10^5	1.080	392.0	125.4	0.102
800	7.653×10^5	1.313	331.5	96.67	0.085
1,000	6.049×10^5	1.198	303.0	84.74	0.078

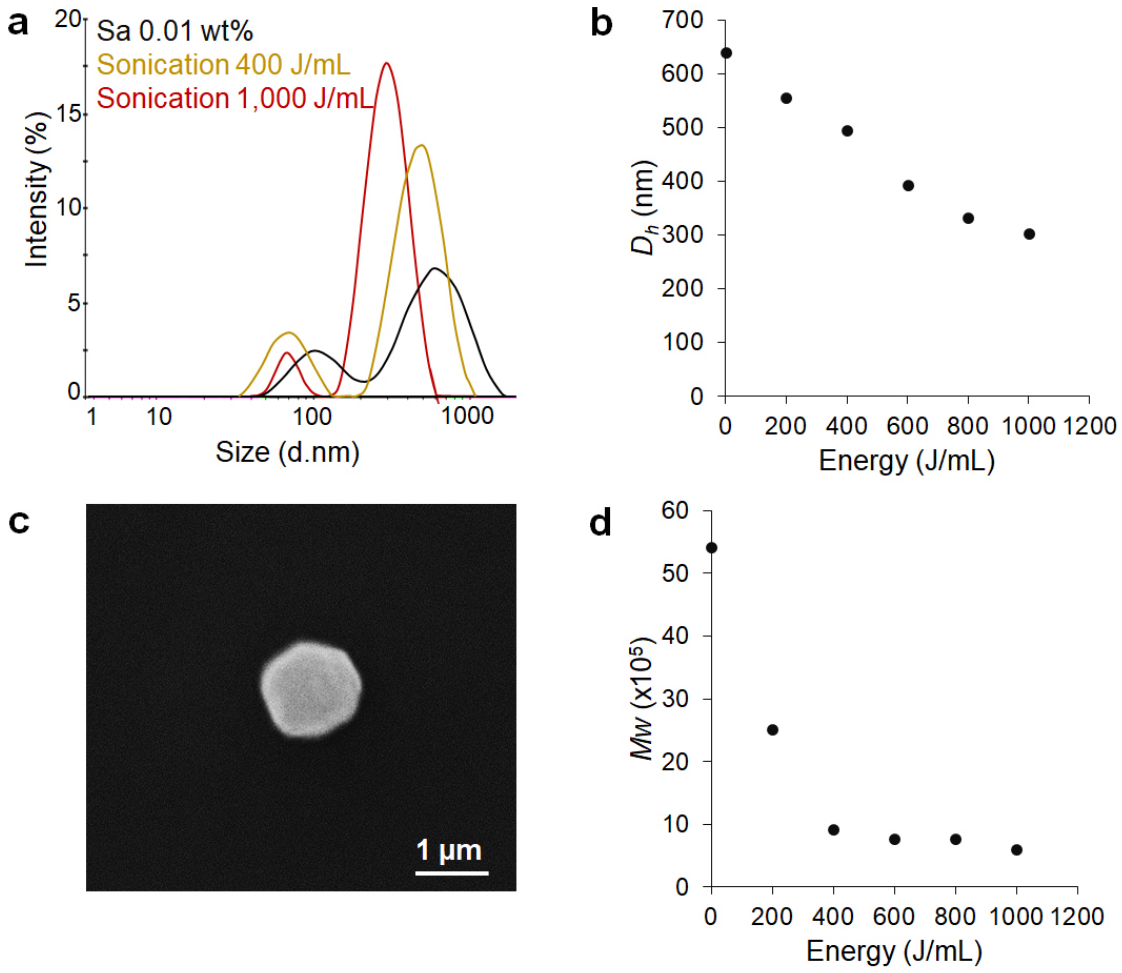

Figure 3.11 *Sacran* transformation from microfibers to microparticles induced by ultrasonication. a. Dynamic light scattering graph of *sacran* particles b. Graph relationship between ultrasonication energy treated to the polymer solution and hydrodynamic size of particle products. c. Scanning electron microscopic image of dried *sacran* 0.010 wt% treated by ultrasonication 1,000 J/mL then, annealed at 100 °C for 24 h. d. Graph relationship between ultrasonication energy treated to the polymer solution and hydrodynamic size of particle products.

Now, the condition for producing microparticles with narrow size distribution was optimized at an initial concentration of 0.010 wt% with 1,000 J/mL input energy. Focusing on the morphology of the particles, the polymer was packed densely as a spherical structure shown in **Figure 3.12a, b.** Afterward, the prepared particles were annealed at 100 °C for 24 h to perform the physical crosslinking between the polymer. **Figure 3.13** showed the overlapped thermogravimetric and the differential thermogravimetric curves of conventional *sacran* fiber, sonicated *sacran*, conventional *sacran* annealed fiber and, sonicated annealed *sacran*. The onset decomposition temperature of the conventional *sacran* fiber is at 194 °C under experimental conditions. For *sacran* sonicated sample, the onset temperature shifted to 140 °C due to its lower molecular weight. Focusing on the annealed polymer, the conventional *sacran* annealed fiber showed an onset temperature at 217 °C. Annealing induced the shift of onset decomposition temperature because of physical crosslinking between polymer chains (**Figure 3.14c**). Apart from the three samples that were mentioned above, the sonicated annealed *sacran* or the microparticles expressed differently. The two stages of weight loss were shown in the degradation pattern. The first one, which is between 160 to 240 °C is assigned to the evaporation of bound water.[104] The second decomposition temperature occurred in the range of 240 to 281 °C and, this high temperature is assigned to the decomposition of annealed *sacran* well packed structure. The annealing could be enhanced not only the thermal stability of the polymer but also be another way to reform the particle for practical application. The annealed particles were redispersed in water as microgel particles which shown fine spherical particles from scanning electron microscopic images in **Figure 3.12c**. The microgel particles exhibit well disperse in water solution, which could be the advantage for further utilization. In addition, the drying behavior of *sacran* microgel was shown outstanding water holding capacity. Comparing between sacran microgels and conventional sacran solution 0.050 wt%, 1 µL at 6 hours of drying time, the *sacran* solution was dried, the microgels still wet (**Figure 3.14a, b**).

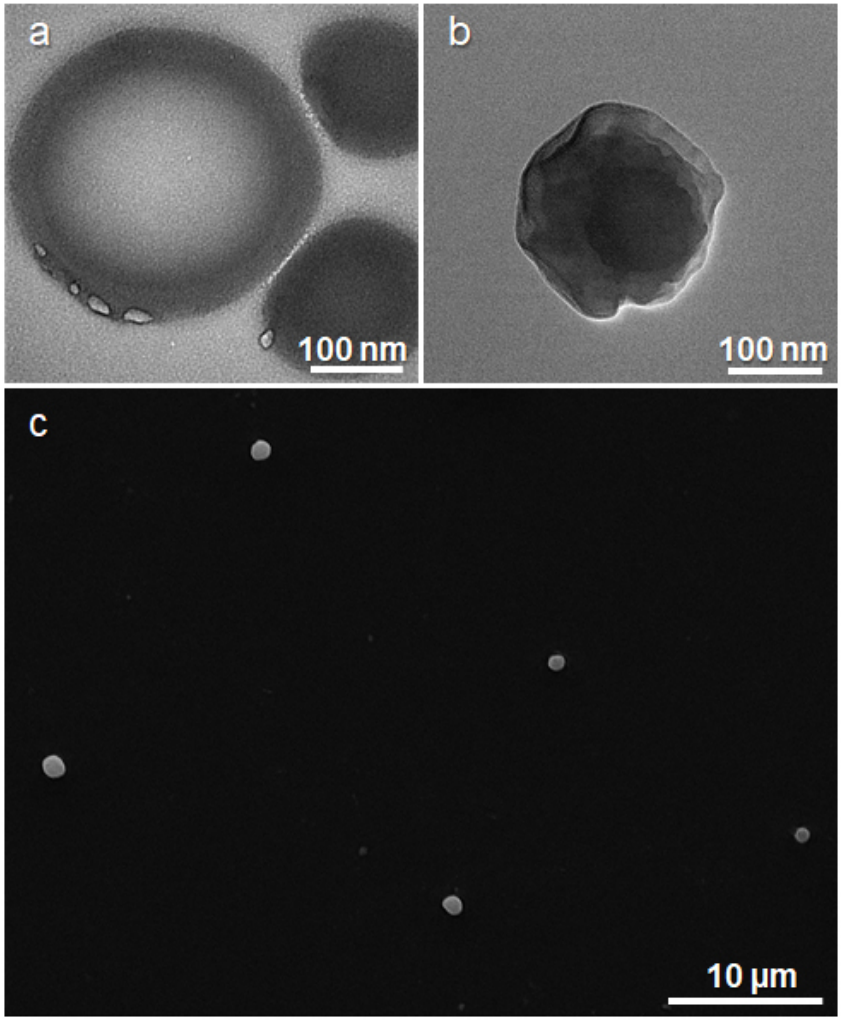

Figure 3.12 Sacran microparticles induced by ultrasonication. a. Transmission electron microscopic images of dried *sacran* 0.010 wt% treated by ultrasonication 400 J/mL before annealed. **b.** Transmission electron microscopic images of dried *sacran* 0.010 wt% treated by ultrasonication 1,000 J/mL before annealed. **c.** Scanning electron microscopic image of dried *sacran* 0.010 wt% treated by ultrasonication 1,000 J/mL then, annealed at 100 ℃ for 24 h.

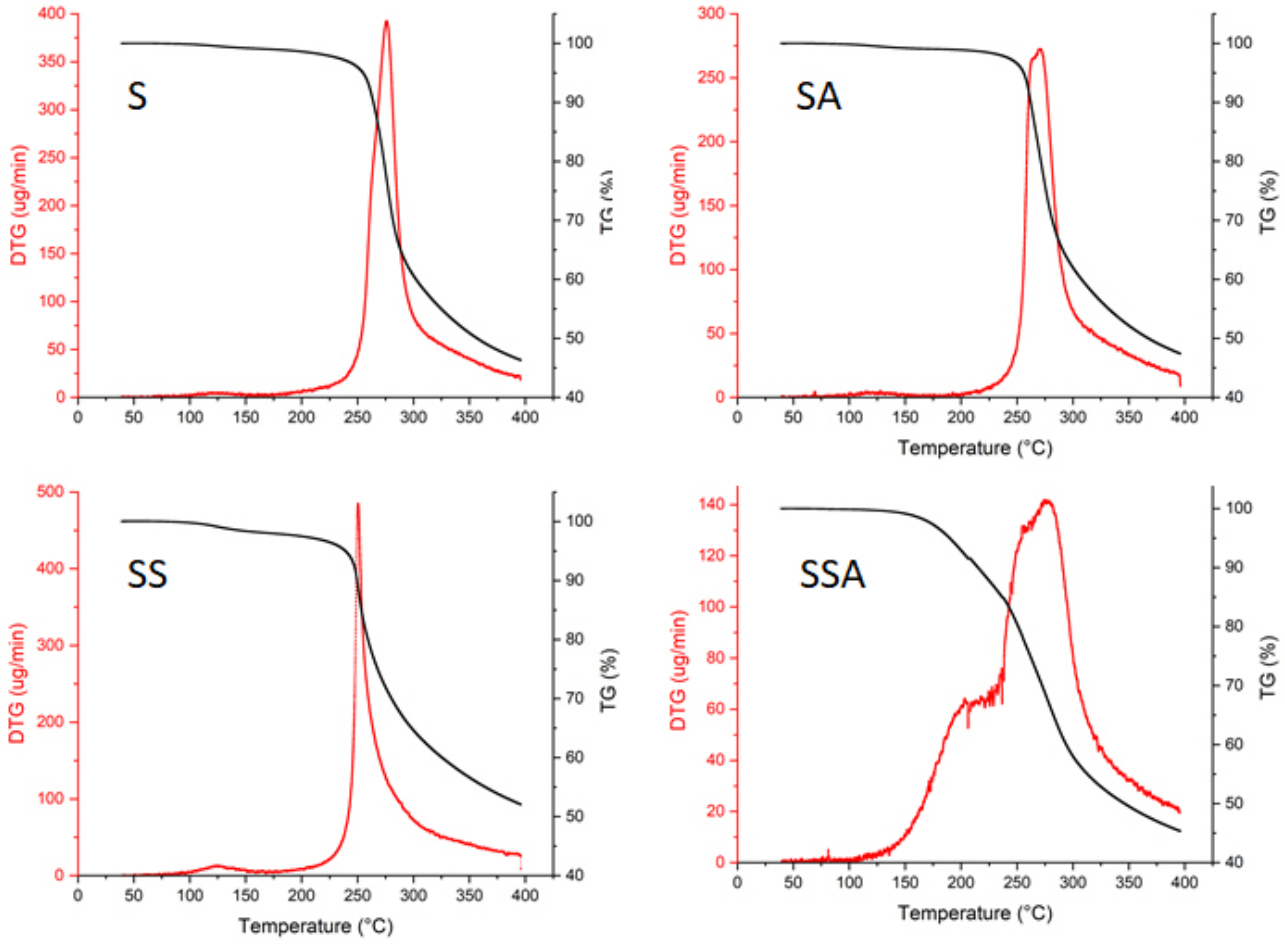

Figure 3.13 Effect of sonic energy to *sacran* particle formation. c. Thermogravimetric graph of conventional *sacran* fibers (S), conventional *sacran* fibers annealed (SA), *sacran* sonicated (SS) and, *sacran* sonicated annealed (SSA).

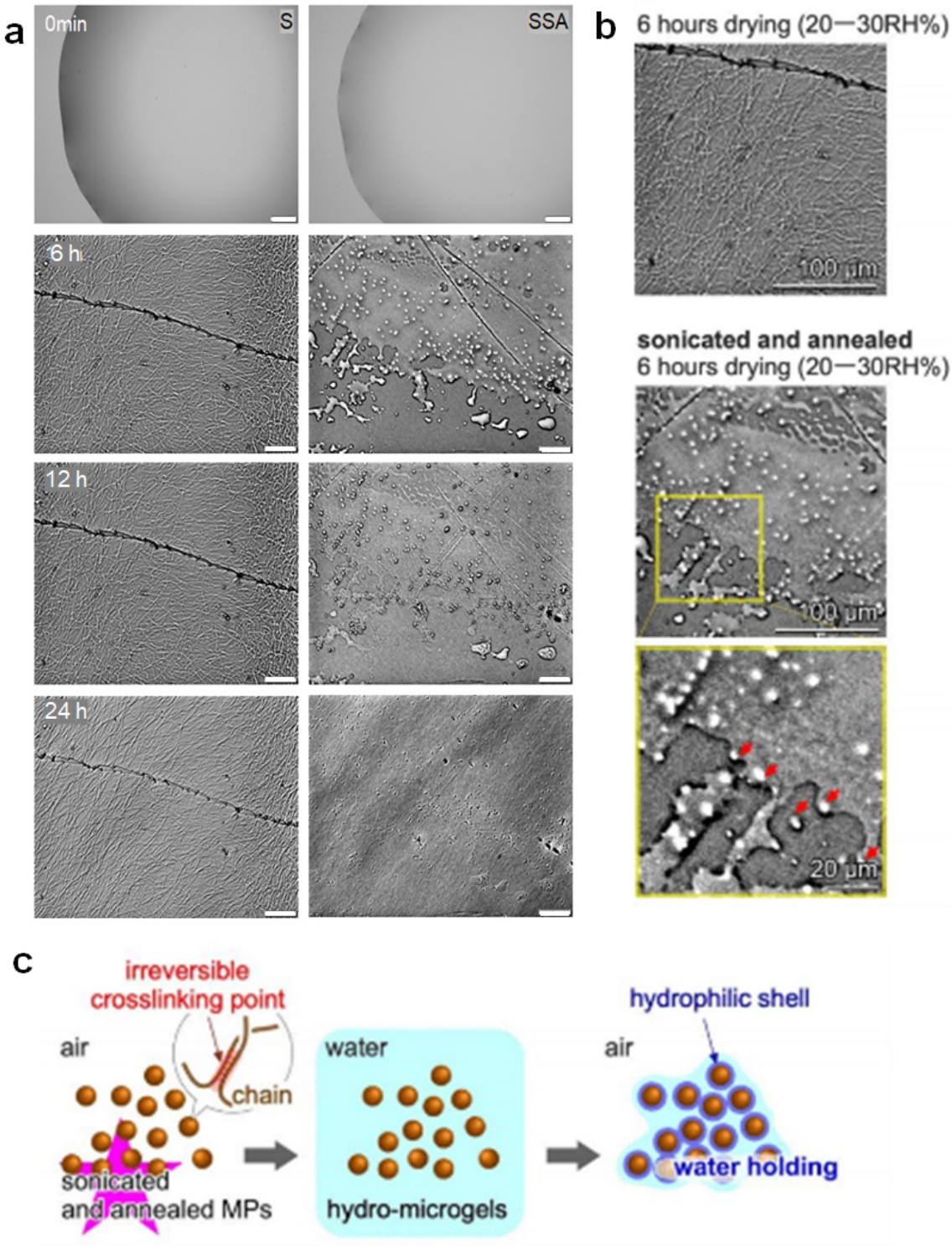

Figure 3.14 Effect of sonic energy to *sacran* particle formation. a. Microscopic records of drying behavior from 0 minute to 24 hours of *sacran* sonicated annealed (SSA) comparing with the conventional *sacran* fibers. (0 min scale bar = 200 μm, 6-24 h scale bar = 50 μm) b. Microscopic records of drying behavior of *sacran* sonicated annealed (SSA) comparing with the conventional *sacran* fibers (S) c. The illustration of *sacran* sonicated annealed interacted with water.

Generally, from the various time of drying experiments, the microgel took ~24 hours to completely dry. While the conventional *sacran* at the same condition took only ~15 minutes. The results indicated that the microgels could keep the moisture ~100 times over the conventional *sacran* in terms of evaporation rate. This could be explained by the expansion of hydrophilic surface area on the microgel that intensifies the interaction of water-polymer (**Figure 3.14c**). This explanation was supported by the results of free water and bound water that represented from differential scanning calorimetry analysis of different *sacran* samples (**Figure 3.15**). The interaction between water and polymer molecules effect phase transition behavior and, three forms of water are classified: (i) free water, (ii) freezable bound water and, (iii) non-freezable bound water. Free water and freezable bound water are able to show the phase transition by calorimetric analysis, while non-freezable water does not show the phase transition.[105][106] Deionized water was conducted as a control. The thermograms of pure water shown an endotherm with an onset temperature of ~0 °C from the heating trace, corresponding to the melting point of free water. In all compositions of *sacran* samples, melting transitions shift to temperatures lower than pure water due to the additional interaction between water-polymer or freezable bound water.[107] Noticeably, melting peak of water in sacran annealed particles 50 wt% was shown at around -20 ºC. This means all free water has interacted with polymer as bound water, including a freezable and a non-freezable bound water. For *sacran* annealed particles 80 wt%, no peak was shown in the thermogram owing to all free water was bound with polymer as a non-freezable bound water. The fusion enthalpy of ice made from the heating cycle was used to calculate the freezable water and the non-freezable bound water according to the equation explained in **Table 3.2**. Comparatively, the non-freezable bound water content in the *sacran* microgel was 12.5%, which is ~3.4 times excessive to the conventional *sacran* fiber shown the non-freezable bound water content only 3.7%. In the case of the microgels, a molar ratio between tightly bound water molecules per a sugar residue

corresponds to ~24 molecules. On the other hand, *dextran, hyaluronic acid and, Xanthan gum,* which have been extensively used in pharmaceutical and cosmetic fields, shown a lower number as 5.5, 7.5 and, 10.0 water molecules per a sugar residue respectively.[108][109] The non-freezable bound water could be observed more in *sacran* microgel might be owing to hydrophilic functional group of polymer and, well organized structure of particles.[110]

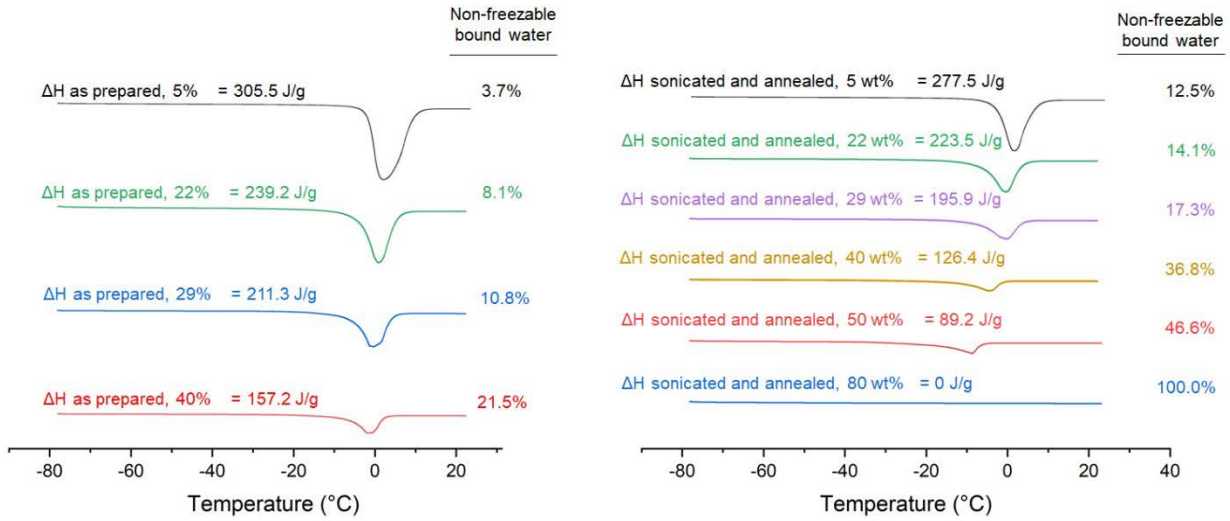

Figure 3.15 Differential scanning calorimetry graph of different types of *sacran* samples showing various values of fusion enthalpy of ice in J/g.

Table 3.2 The data of different types of *sacran* for freezable water (FW) and non-freezable bound water (NFBW) calculation.

Sample	Water content (%)	Fusion enthalpy of ice (J/g)	FW (%)	NFBW (%)
Water	-	333.8	100.0	0
Sacran as prepared 5%	95	305.5	96.3	3.7
Sacran as prepared 22%	78	239.2	91.9	8.1
Sacran as prepared 29%	71	221.9	89.2	10.8
Sacran as prepared 40%	60	157.2	78.5	21.5
Sacran sonicated 5%	95	299.7	94.4	5.6
Sacran as prepared, annealed 5%	95	292.6	92.3	7.7
Sacran sonicated, annealed 5%	95	277.5	87.5	12.5
Sacran sonicated, annealed 22%	78	223.5	85.9	14.1
Sacran sonicated, annealed 29%	71	195.9	82.7	17.3
Sacran sonicated, annealed 40%	60	126.4	63.2	36.8
Sacran sonicated, annealed 50%	50	89.2	53.4	46.6
Sacran sonicated, annealed 80%	20	0.0	0.0	100.0

The equation for non-freezable bound water (NFBW) calculation.[27][29]

$$NFBW(\%) = W(\%) + FW(\%)$$

$$FW(\%) = (\Delta H_f / \Delta H_m) \times 100$$

Where; NFBW(%) = non-freezable water content

FW(%) = freezable water content

W(%) = total water content

ΔH_f = fusion enthalpy of ice (freezable water) obtained by DSC

ΔH_m = standard fusion enthalpy of pure water 333.5 J/g.[28]

fusion enthalpy of pure water obtained by DSC 333.8 J/g

3.4 Conclusion

To study the *sacran* morphological change, the interaction between polymer chains is the most important factor. The microfibers deformed to particles by reducing the intermolecular interaction, for example the dilution and the salination. In case of decreasing concentration to the semi-diluted state ($c < c_e$ 0.015 wt%), the polymer would be in the unentangled state which is unable to form microfiber. At the concentration 0.010 wt%, the microfibers significantly deformed into the nanofibers and nanofragments. This could be the boundary concentration of nano to micro assembling process. After that, the salination effect was studied as another factor that suppresses the interaction between the polymer chains. Sacran at a diluted state (0.001 wt%) with 10 mM of NaCl added, the salting-in affected on higher solubility of polymer chains. Then, 100 mM of NaCl was added, the salt affected on less soluble of the polymer referred to the salting-out. This effect could produce the *sacran* particles with a very narrow size distribution. However, the dilution and the salination method conferred a small quantity of particles because the particle would be formed with narrow size distribution under a very low polymer concentration or with a crucial high concentration of salt. That problem could be overcome by the ultrasonication technique. At polymer concentration 0.010 wt%, the *sacran* microparticles are successfully prepared. Sonication plays an important role in polymer scission and spherical shape formation through cavitation. The overall treated ultrasonic energy directly affects the size of the particles. Consequently, the polymer particles were annealed, aiming to get microparticles gel for further applications. For instance, the *sacran* microgel represented super-moisturizing ability comparative to other currently use materials. According to the covid-19 pandemic, apart from vaccination, various kinds of treatment are on demand for the alternative option. Especially for the intranasal drug that was recently reported as an effective membrane fusion inhibitor of SARS-CoV-2.[33] The Sacran microparticles could be modified for additional application such as microgel drug carrier or intranasal spray for

moisture maintaining. Base on the outstanding properties of the prepared, this study could lead to a new material design for medical purposes in the future.

3.5 References

[79] I. Insua, A. Wilkinson, F. Fernandez-Trillo, *Eur. Polym. J.* **2016**, *81*, 198.

[80] K. Luger, A. W. Mäder, R. K. Richmond, D. F. Sargent, T. J. Richmond, *Nature* **1997**, *389*, 251.

[81] A. M. Krachler, K. Orth, *Virulence* **2013**, *4*, 284.

[82] G. Joshi, K. Okeyoshi, T. Mitsumata, T. Kaneko, *J. Colloid Interface Sci.* **2019**, *546*, 184.

[83] A. R. Paredez, C. Somerville, D. Ehrhardt, *Science.* **2006**, *312*, 1491.

[84] J. Mehringer, E. Hofmann, D. Touraud, S. Koltzenburg, M. Kellermeier, W. Kunz, *Phys. Chem. Chem. Phys.* **2021**, *23*, 1381.

[85] C. Hollitt, A. Deeb, *Determining Image Orientation Using the Hough and Fourier Transforms*, **2012**.

[86] V. Vergaro, F. Scarlino, C. Bellomo, R. Rinaldi, D. Vergara, M. Maffia, F. Baldassarre, G. Giannelli, X. Zhang, Y. M. Lvov, S. Leporatti, *Adv. Drug Deliv. Rev.* **2011**, *63*, 847.

[87] M. Müller, *Adv. Polym. Sci.* **2014**, *256*, 197.

[88] C. L. Cooper, P. L. Dubin, A. B. Kayitmazer, S. Turksen, *Curr. Opin. Colloid Interface Sci.* **2005**, *10*, 52.

[89] A. B. Kayitmazer, D. Seeman, B. B. Minsky, P. L. Dubin, Y. Xu, *Soft Matter* **2013**, *9*, 2553.

[90] C. M. Jewell, D. M. Lynn, *Adv. Drug Deliv. Rev.* **2008**, *60*, 979.

[91] H. Yin, R. L. Kanasty, A. A. Eltoukhy, A. J. Vegas, J. R. Dorkin, D. G. Anderson, *Nat. Rev. Genet.* **2014**, *15*, 541.

[92] Y. Wen, J. K. Oh, *Macromolecular Rapid Communications*, **2014**, *3*, 1819–1832.

[93] M. K. Okajima, R. Mishima, K. Amornwachirabodee, T. Mitsumata, K. Okeyoshi, T. Kaneko, *RSC Adv.* **2015**, *5*, 86723.

[94] K. Budpud, K. Okeyoshi, M. K. Okajima, T. Kaneko, *Small* **2020**, *16*, 2001993.

[95] T. Mitsumata, T. Miura, N. Takahashi, M. Kawai, M. K. Okajima, T. Kaneko, *Phys. Rev. E - Stat. Nonlinear, Soft Matter Phys.* **2013**, *87*, 1.

[96] R. Zangi, *J. Phys. Chem. B* **2010**, *114*, 643.

[97] S. Moelbert, B. Normand, P. De Los Rios, *Biophys. Chem.* **2004**, *112*, 45.

[98] R. H. Stokes, R. A. Robinson, *J. Am. Chem. Soc.* **1948**, *70*, 1870.

[99] P. K. Grover, R. L. Ryall, *Chem. Rev.* **2005**, *105*, 1.

[100] M. W. A. Kuijpers, P. D. Iedema, M. F. Kemmere, J. T. F. Keurentjes, *Polymer.* **2004**, *45*, 6461.

[101] M. M. Caruso, D. A. Davis, Q. Shen, S. A. Odom, N. R. Sottos, S. R. White, J. S. Moore, *Chem. Rev.* **2009**, *109*, 5755.

[102] G. Madras, B. J. McCoy, *AIChE J.* **2001**, *47*, 2341.

[103] T. Q. Nguyen, Q. Z. Liang, H.-H. Kausch, *Polymer.* **1997**, *38*, 3783.

[104] J. George, K. V Ramana, A. S. Bawa, Siddaramaiah, *Int. J. Biol. Macromol.* **2011**, *48*, 50.

[105] T. Hatakeyama, K. Nakamura, H. Hatakeyama, *Thermochim. Acta* **1988**, *123*, 153.

[106] S. Abasi, R. Davis, D. A. Podstawczyk, A. Guiseppi-Elie, *Polymer.* **2019**, *185*, 121978.

[107] L. Guan, H. Xu, D. Huang, *J. Polym. Res.* **2011**, *18*, 681.

[108] J. Hunger, A. Bernecker, H. J. Bakker, M. Bonn, R. P. Richter, *Biophys. J.* **2012**, *103*, 10.

[109] H. Yoshida, T. Hatakeyama, H. Hatakeyama, *Polymer.* **1990**, *31*, 693.

[110] X. Qu, A. Wirsén, A.-C. Albertsson, *Polymer.* **2000**, *41*, 4589.

[111] R. D. de Vries, K. S. Schmitz, F. T. Bovier, C. Predella, J. Khao, D. Noack, B. L. Haagmans, S. Herfst, K. N. Stearns, J. Drew-Bear, S. Biswas, B. Rockx, G. McGill, N. V. Dorrello, S. H. Gellman, C. A. Alabi, R. L. de Swart, A. Moscona, M. Porotto, *Science.* **2021**, *371*, 1379.

CHAPTER IV

GENERAL CONCLUSION

In this work, we studied the morphological change of a novel self-organized supergiant polysaccharide, *sacran*. A self-assembling/disassembling of microfiber was successfully used in the preparation of a humidity-sensitive actuator, a micropattern cell scaffold and, a super-moisturizing microparticle. Along the contact line of the evaporative air-water interface, the microfibers tended to merge into a uniaxially oriented condition. When one side of the microfibers was fixed, they morphed into 2D snaking and 3D twisted structures in a dramatic way. There are two essential factors that influence fiber deformation; 1. The initial concentration of the polymer and, 2. The evaporation rate. Multiple microfibers formed multi-twisted structures as a result of the evaporative air-water contact, demonstrating that this material exhibits self-similar nano and microstructures. The snaking and twisted fibers could show spring-like motion with millisecond-response repulsive to water vapor. It would be able to produce a variety of soft actuators responding to additional changes in the external environment, such as light, pH, and temperature, by incorporating functional molecules into the microfiber. Moreover, the micro-alignment surface was effectively prepared due to its unique capacity to generate hierarchical twisted fiber in the nano-micro scale. The results reveal that the cells could be well aligned on the scaffold. For the new material design, this could be an excellent area to start looking into cell orientation regarding the M-fibers. The interaction between polymer chains is the most essential component in studying *sacran* morphological change. Dilution and salination, for example, reduced the intermolecular connection, causing the microfibers to deform into particles. The dilution and salination, on the other hand, yielded a tiny number of particles because the particle formed with a narrow size distribution under a deficient polymer concentration or a critical high salt concentration. The

ultrasonication approach could be able to solve this problem. The *sacran* microparticles have been prepared successfully. Through cavitation, sonication plays a crucial role in polymer scission and spherical shape development. The size of the particles is directly affected by the overall treated ultrasonic energy. As a result, the polymer particles were annealed with the goal of obtaining microparticles gel for potential upgrades. The microgel performed admirably in terms of moisturizing compared to other extensively used polysaccharides. This would be a significant investigation of a new polysaccharide particle due to its simple and non-organic solvent preparation process. The *sacran* microparticles could be further modified for use as a microgel drug carrier or an intranasal spray to keep the throat moist. Based on the superior properties of the *sacran* morphological changeable, this research could lead to a unique material design for medical or biological uses in the future.

LIST OF PUBLICATIONS

Journals:

First author:

- K. Budpud, K. Okeyoshi, M. K. Okajima, T. Kaneko, *Small*. **2020**, *16(29)*, 2001993.
- Chapter III : under the preparation to submit.

Co-author:

- D. Takahashi, A. V Sainath, J. Ikeda, K. Budpud, T. Kaneko, M. Kawai, T. Mitsumata, *Polym.* **2021**, *13*.
- K. Okeyoshi, M. Yamashita, K. Budpud, G. Joshi, T. Kaneko, *Sci. Rep.* **2021**, *11*, 767.
- K. Okeyoshi, M. Yamashita, T. Sakaguchi, K. Budpud, G. Joshi, T. Kaneko, *Adv. Mater. Interfaces.* **2019**, 1900855.
- K. Okeyoshi, T. Shinhama, K. Budpud, G. Joshi, M. K. Okajima, T. Kaneko, *Langmuir.* **2018**, *34(46)*, 13965.

Conferences:

1. Poster “Snaking/twisting fibers formation of cyanobacterial supra-polysaccharides in drying process” Kulisara Budpud, Kosuke Okeyoshi, Maiko Okajima, and Tatsuo Kaneko. JAIST Japan-India Symposium on Advanced Science 2019. JAIST Hi-tech center, Nomi, Ishikawa. March 7, 2019.

2. Oral “Snaking/twisting fibers formation of cyanobacterial supra-polysaccharides in drying process” Kulisara Budpud, Kosuke Okeyoshi, Maiko Okajima, and Tatsuo Kaneko. Spring 2019 ACS National Meeting & Exposition. Orlando, Florida, USA. March 31 – April 4, 2019.

3. Oral and poster “Humidity responsive polysaccharide film composed of snaking/twisting fiber networks” Kulisara Budpud, Kosuke Okeyoshi, Maiko Okajima, and Tatsuo Kaneko. 68th symposium on macromolecules 2019 and gel symposium, (SPSJ). Fukui University, Fukui. September 25-28, 2019.

4. Oral “Snaking/twisting fibers formation of supra-polysaccharides for humidity responsive application” Kulisara Budpud, Kosuke Okeyoshi, Maiko Okajima, and Tatsuo Kaneko. 第 8 回日本バイオマテリアル学会　北信越ブロック若手研究発表会. JAIST Hi-tech center, Nomi, Ishikawa. December 6, 2019.